An Accessible Architecture for Affordable Access to Space

by

James Kendall Villarreal

A Dissertation Presented in Partial Fulfillment
of the Requirements for the Degree
Doctor of Philosophy

Approved November 2011 by the
Graduate Supervisory Committee:

Kyle Squires, Chair
Taewoo Lee
Praveen Shankar
Thomas Sharp
Valana Wells

ARIZONA STATE UNIVERSITY

December 2011

ABSTRACT

A design methodology for a new breed of launch vehicle capable of lofting small satellites to orbit is discussed. The growing need for such a rocket is great: the United States has no capabilities in place to quickly launch and reconstitute satellite constellations. A loss of just one satellite, natural or induced, could significantly degrade or entirely eliminate critical space-based assets which would need to be quickly replaced. Furthermore a rocket capable of meeting the requirements for operationally responsive space missions would be an ideal launch platform for small commercial satellites. The proposed architecture to alleviate this lack of an affordable dedicated small-satellite launch vehicle relies upon a combination of expendable medium-range military surplus solid rocket motor assets. The dissertation discusses in detail the current operational capabilities of these military boosters and provides an outline for necessary refurbishments required to successfully place a small payload in orbit. A custom 3DOF trajectory script is used to evaluate the performance of these designs. Concurrently, a parametric cost-mass-performance response surface methodology is employed as an optimization tool to minimize life cycle costs of the proposed vehicles. This optimization scheme is centered on reducing life cycle costs per payload mass delivered rather than raw performance increases. Lastly, a novel upper-stage engine configuration using Hydroxlammonium Nitrate (HAN) is introduced and experimentally static test fired to illustrate the inherent simplicity and high performance of

this high density, nontoxic propellant. The motor was operated in both pulse and small duration tests using a newly developed proprietary mixture that is hypergolic with HAN upon contact. This new propellant is demonstrated as a favorable replacement for current space vehicles relying on the heritage use of hydrazine. The end result is a preliminary design of a vehicle built from demilitarized booster assets that complements, rather than replaces, traditional space launch vehicles. This dissertation proves that such capabilities exist and more importantly that the resulting architecture can serve as a viable platform for immediate and affordable access to low Earth orbit.

To my many teachers: this work is dedicated directly to you.

And to my students during my instructor teaching stint of MAE465/598 *Rocket Propulsion* and MAE460 *Space Systems Design* at Arizona State University. Your persistent questions and fervent demand for answers has forever altered my perspective, for the better.

To my understanding family: Thomas Wylie, Mary Frances, Michael Angelo, and of course Kelly Marie, for their seemingly unending support.

Lastly (but not *leastly*) to Kelly Susan Mahon, for her sound-boarding and proofreading assistance with this dissertation, but more specifically her love and support throughout our shared graduate career.

ACKNOWLEDGEMENTS

I gratefully acknowledge the advice, mentoring and engineering support from Rick Loehr of Raytheon Missile Systems.

I would also like to recognize the *Daedalus Astronautics* student rocketry group for greatly enhancing my engineering experience and opening doors for the better part of a decade. Also to Lenny Bucholz and Andre Magdelano in the student machine shop for their help with the design and fabrication of the HAN-Solo v.1 monopropellant thruster.

This effort was sponsored in part by a NASA Space Grant Graduate Fellowship.

TABLE OF CONTENTS

Page

LIST OF FIGURES

Figure Page

Figure Page

Figure Page

Figure Page

LIST OF TABLES

NOMENCLATURE

3DoF	=	three degrees of freedom
α	=	angle of attack, Lagrange multipler
β	=	partial regression coefficients
δ	=	latitude
ε	=	structural coefficient
γ	=	ratio of specific heats
λ	=	payload ratio; longitude
μ	=	gravitational parameter [m^3 sec^{-2}]
Φ	=	flight path angle [degrees]
ρ	=	density [kg m^{-3}]
ω_E	=	angular velocity of Earth, $7.27*10^{-5}$ [rad/sec]
A	=	velocity azimuth angle [degrees]
C_D	=	drag coefficient
CER	=	cost estimating relationship
COTS	=	commercial off the shelf
DDT&E	=	design, development, testing and evaluation
DoD	=	Department of Defense
e	=	eccentricity of orbit
G	=	gravitational constant, $6.67428*10^{-11}$ [m^3 kg^{-1} sec^{-2}]
g	=	gravity [m sec^{-2}]
GTO	=	geosynchronous/geostationary transit orbit
f_i	=	inert mass fraction
H2O2	=	hydrogen peroxide
HAN	=	hydroxyl ammonium nitrate
ICBM	=	intercontinental ballistic missile
I_{SP}	=	specific impulse [sec]
J_n	=	Jeffery's spherical harmonic constants
L*	=	characteristic length
LCC	=	life cycle cost

LEO	=	low Earth orbit
M	=	Mach number
m*	=	payload mass [kg]
$m_{f,i}$	=	final mass of stage number i [kg]
$m_{o,i}$	=	initial mass of stage number i [kg]
m_p	=	propellant mass [kg]
MR	=	mass ratio
MRE	=	mass estimating relationship
m_s	=	structural or inert mass [kg]
n	=	solid rocket motor regression rate exponent
O&M	=	operations and management
ORS	=	Operationally Responsive Space
p_o	=	rocket engine stagnation pressure [Pa, psi]
p_e	=	nozzle exhaust pressure [Pa, psi]
p_a	=	ambient pressure [Pa, psi]
R	=	specific gas constant [J kg^{-1} K^{-1}]
r	=	radial distance [m]
r_E	=	radius of Earth; 6,378,140 [m]
r_p	=	radius of perigee [m]
RCS	=	reaction control system
RSM	=	response surface methodology
SM	=	Standard Missile line of missiles
SRM	=	solid rocket motor
t	=	time [sec]
TVC	=	thrust vector control
U_e	=	effective exhaust velocity [m/s]
u_e	=	actual exhaust velocity [m/s]
Δv	=	change in velocity [m/s]

1. Introduction

"The Earth is the cradle of humanity, but one cannot eternally live in a cradle."

-Konstantin Tsiolkovsky (1857 to 1935),

Father of Astronautics and Rocketry

Necessity for Affordable Access to Space

The critical problem facing the 21st century of space flight is immediate and low cost access to low Earth orbit (LEO). An inherent difficulty in escaping Earth's gravitational influence to establish a circular or elliptical orbit about Earth, even at low altitudes, is the genesis of this problem. The vast amount of energy necessary to perform this task requires that space launch vehicles, using the current proven technology developed over the past 100 years, be powered by chemical rocket engines using enormous quantities of propellant. Often times upwards of 90% (or more!) of the gross mass of any orbit-bound rocket is entirely propellant. However, once a stable orbit has been attained about Earth the laws of orbital mechanics illustrate that travel to other bodies in our solar system (the Moon, Mars and beyond) use significantly smaller percentages of the total propellant mass used to get to LEO. Or as the famed author Robert Heinlein succinctly described: *once you get to Earth orbit, you are halfway to anywhere in the solar system*. Indeed this is not far from the truth.

Cost has always been the general frustration. Though there are a myriad of applications that access to space provides the space community, generally the only ones that can afford such space assets are large businesses interested in telecommunication satellites or government agencies sponsoring science missions or military satellites. Of the entire constellation of artificial satellites nearly fifty percent of them are in LEO defined as 160 to 2,000 kilometers above the Earth's surface. On the contrary the most lucrative of satellite launches are comprised of launching to a geostationary or geosynchronous transit orbit (GTO) which corresponds to an altitude of nearly 36,000 kilometers above the surface of the Earth.

Regrettably a very minimal amount of launches to LEO and beyond are used to conduct meaningful science or exploration, the exceptions being such landmark missions as the Hubble Space Telescope or the International Space Station. This shortcoming is born out of the inherent limitations of chemical rocket propulsion, specifically solid rocket motors and liquid rocket engines, which when coupled with the need for very lightweight structures translates to only a small percentage of final payload mass lofted to orbit. A new frontier of significantly increased space activity may be traversed if propulsion technologies are advanced to a sufficient point or launch vehicles, staged or single stage to orbit, are developed to take advantage of economies of scale. Until such time, interplanetary probes, robotic missions to other planets, and even manned space flight

are effectively limited to the small-term given the current impracticality of affordable access to space.

Many potential solutions have been proposed to alleviate our inability to access space at a reasonable cost. The driving notion behind such ventures is “build it and they will come.” In other words affordable access to space will act as a catalyst for future commercial and scientific activities. As an example, the United States Space Shuttle fleet was originally projected to launch upwards of 60 flights per year for the five original Orbiters. However the largest value ever reached were nine (9) total flights in 1985 for the entire fleet. Despite promises of reusability the Space Shuttle has been marred by difficulties, remains expensive to maintain and was never able to reduce launch costs. A potential shuttle replacement, the *X33* or its commercial equivalent *name VentureStar*, was a single stage to orbit commercial concept developed by Lockheed Martin that held numerous advantages over the NASA Orbiter design. Unfortunately, the realization of single stage to orbit was hindered by technological hurdles that the developers were not able to overcome at the time.

In the unmanned sector several relatively new companies have made strides to lower the cost to LEO, but as of yet their ambitions are unrealized. Much of the problem stems from the design philosophy followed by rocket designers for decades: rockets must rely on high technology lightweight structures and propulsion systems, hence high

cost, to loft a payload of any size to orbit.[1] This driver of "performance at all costs" is born out of the 1950s era intercontinental ballistic missile (ICBM) program and almost all modern day launch vehicles are built accordingly. It could be said that rockets have changed very little in fifty years of advancement with only a few notable exceptions. Instead, the priority should shift away from increasing performance specifications to reducing overall launch costs.

The fundamental goal to achieve future uninhibited access to space is the development of a space launch platform that can significantly lower the current $10,000/lb launch costs to LEO. Secondary to this, the launch vehicle should provide operational flexibility to achieve a range of orbits and meet a variety of differing government agencies and commercial market demands.

It should also be stated that the vehicle is not required to loft a large tonnage to LEO. The recent AIAA Space 2009 Conference has forecast an increase in "cheapsat" use (satellites costing less than $2.5 million) for both military and civilian purposes, including: pico, nano, micro and mini satellites, compared in Figure 1. The future use of cheapsats is an endeavor driven by the miniaturization of electronics where small satellites, upwards of only 500 kilograms, can perform the existing duties of larger satellites currently in use. Many U.S. government agencies have taken note of these new classes of satellites and have gone so far as to give them specific names dependent upon the sponsoring agency:

LightSats by the U.S. Defense Advanced Research Projects Agency (DARPA), Single Purpose Inexpensive Satellite Systems or *SPINSats* by the U.S. Naval Space Command and Tactical Satellites or *TACSats* by the U.S. Air Force. Regardless of the name, much of the interest in this these smaller breeds of satellites is generated by the growing necessity of responsive access to space, namely for high profile military missions.

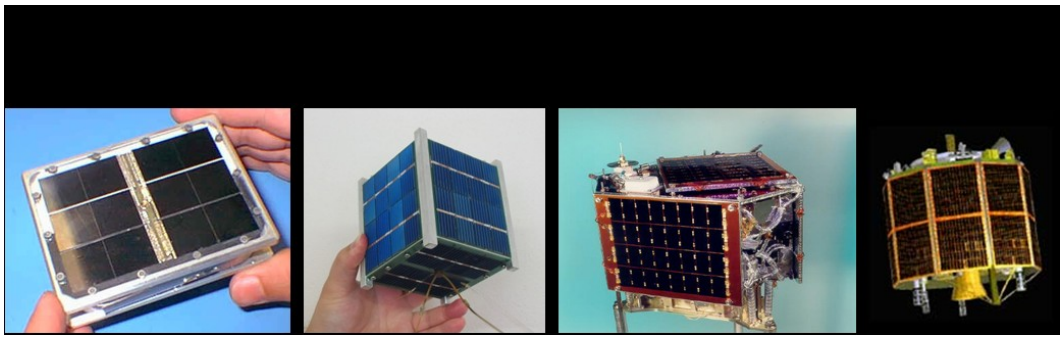

Figure 1: Examples of small satellites under 500kg. From left to right: Pico, Nano, Micro and Mini-Satellites.

The emergence of small satellites, driven by the high cost per pound to LEO, must be matched by appropriate launch vehicles capabilities. Following suit, many startup companies have been developing new rockets to meet these demands. Such rockets, capable of carrying singular or clustered satellites, cheapsats or otherwise, might well open the door to affordable access to space. The resultant explosion of new product offerings, scientific missions and inherent discoveries has the potential to spawn a secondary space age limited not only to competing governments and corporate behemoths, but also to smaller civilian

exploration or educational research agencies. Such a new market obviates the need for an affordable space launch vehicle platform.

Operationally Responsive Space

The United States' Office of Operationally Responsive Space (ORS) is a prime motivator for affordable and quick access to space. ORS exists to very quickly accommodate a variety of high profile missions necessary to the well being or security of the United States. Current Department of Defense (DoD) space policies have identified uninhibited access to, and use of, space as a critical strategic enabler of US military and peacekeeping power. An Air Force white paper *The Aerospace Force: Defending America in the 21st Century*[2] succinctly defines the growing necessity for quick access to space:

> *"The country's growing investment in, and reliance on, space-based capabilities that support the national information and commercial infrastructure are creating an economic and military center of gravity – a vulnerability that, if exploited, could adversely affect the nation."*

A loss of just one satellite (natural or induced) could therefore significantly degrade or entirely eliminate critical space-based assets, which would need to be quickly replaced.[3] Such responsive space missions include: surveillance, wind and weather, communications, and reconstitution of on-orbit assets which fail for any reason.[4] Unfortunately, the ORS has a severe lack of affordable, robust, responsive access to

space[3] with current systems often taking months of preparation and months or even years to place, or replace, a satellite into orbit. Therefore, the ORS needs a solution to achieve an Earth-centered orbit within days, if not hours, of an incident and specifically requires four (4) key capabilities:

1. On-demand satellite deployment,
2. launch to sustain required constellations and for peacetime operations,
3. recoverable, rapid-response transport to, through, and from space, and
4. integrated space operations mission planning.[3]

The establishment of ORS is motivated by the very real threat of annihilation of key strategic military and civilian satellites by enemy ground-to-air missiles or co-orbital anti-satellites. In effect, the battlefield of future wars involving space-faring nations will extend into space.[5] The reasoning for this is quite simple in context: a nation's military is heavily dependent, if not completely reliant, upon satellites held in LEO and Geostationary transit orbits (GTO) for the fundamental roles of communications and reconnaissance. This problem is exacerbated by the reality that such space-based assets are relatively unprotected beyond the inherent technological difficulty of sending up a "kill" vehicle into a co-orbital position to destroy a satellite. Less sophisticated methods involve

using nuclear warheads to detonate in the vicinity of the targeted satellite where either the blast radius or the subsequent electromagnetic pulse will destroy or effectively neutralize the satellite as well as any unlucky neighboring satellites. Moreover, no known (or published) countermeasures exist other than attempting to swiftly shift satellites out of position prior to impact or destroying the launch vehicle or kill vehicle en route to the target satellite.

Destroying a satellite even by means of a direct kinetic interception is not in the realm of science fiction. Such was demonstrated in the 1980s by both the United States and the Soviet Union. However, a more recent demonstration was displayed in January 2007 when China launched a missile that successfully destroyed an aging weather satellite in LEO. In a frightening throwback to the Cold War Era this act caused international concern as China's test definitively demonstrated their growing capability for military acts in space.[6] This prompted a similar display by the United States in February 2008 when Raytheon Missiles Systems augmented a Standard Missile – 3 (SM-3) to destroy a non-functioning satellite in danger of de-orbiting that carried a large supply of hydrazine, a propellant known to be extremely toxic to humans. The mention of SM-3 is an important ancillary to the present discussion as this dissertation endeavors to convince the reader that use of such demilitarized missiles can be used to launch small satellites, civilian or otherwise, into LEO, in addition to their destructive roles. Furthermore, a novel replacement propellant and

engine configuration will be proposed as a substitute for hydrazine, a popular but inherently dangerous in-space propellant.

The very real scenario of satellite vulnerability sanctions the demand for a launch vehicle capable of meeting the requirements of ORS. Specifically, the United States Strategic Command (USSTRATCOM) mandates three (3) essential desires for such ORS capabilities:

1. to rapidly exploit and infuse space technological or operational innovations,
2. to rapidly adapt or augment existing space capabilities when needed to expand operational capability and
3. to rapidly reconstitute or replenish critical space capabilities to preserve operational capability.[3]

Small Satellite Roles – Military, Commercial and Civilian Uses

Small satellites emerged out of the necessity for reducing satellite weight such that smaller and therefore less expensive launch vehicles could be used; though, there is of course a bottom line as to how small an orbit-capable space vehicle can be cost effectively operated. The miniaturization of electronics has further accelerated this process and new breeds of satellites are beginning to take form. These small satellites are designed such that they display a similar operational capability to their more massive ancestors.

Continuing with the discussion of military intentions, a project undertaken by Goodrich and ATK is currently in development to support urgent electro-optical needs available straight to tactical commanders in a theater of war. This new small satellite, aptly named *ORS-1* has a mass of 450 kilograms and a goal to have it operational in 24 months which is actually a very short lead time in comparison to traditional satellites. However, *ORS-1* has a requirement to stay in orbit for one year, but the design includes a propulsion module that could effectively increase its lifespan upwards of four years.[7] Additional smaller satellites are under development including a notable example by IntelliTech Microsystems for a constellation of microsatellites called *Kestrel Eye*. Similar to ORS-1, this satellite will provide instant access to warfighters on the ground, though it will rely on a constellation of 30 satellites in LEO to provide global coverage at all times with a cost of only $1million per satellite.[8]

There are of course competitors in the small satellite technology sector, with China leading the progression. The final Chinese launch in 2009 was a small 50 kilogram Earth Monitoring Satellite which experts have agreed is actually a reconnaissance micro-satellite.[9] In addition to their proven capability of attacking an in-orbit satellite (joining the ranks of the U.S. and Russia with such capabilities), China is also developing co-orbital satellites that have "the intent to catch up to and destroy or jam another satellite".[6] Other nations are seeking such capabilities as well. A 2003 Iranian paper[10] suggests use of Orbital Science's *Pegasus* vehicle to

launch Iranian spy microsatellites within Iran's airspace and mitigate forbidden flight zones of their Eastern neighbors.

An unlikely example of small military satellites in use has been the U.S. Air Force Academy which builds rapid, low-cost satellites as a platform for Department of Defense space research and development payloads and their own student-built payloads.[11] Multiple small satellites, called *FalconSAT*s as shown in Figure 2, have been built and flown. The foundation of this program, and the reason it is an interesting endeavor, is that the Academy leverages commercial off the shelf (COTS) hardware and existing modular commercial satellite framework developed by Surrey Satellite Technology Limited. Surrey intends to build small satellites, some less than 10kg, designed and built to standardized payload interfaces with the aim of "sending small satellites into space longer, more successfully and more economically than anyone else in the world".[12] However, Surrey realizes that the driving issue withholding major implementation of small satellites is the lack of available launch capacity. Most current small satellites simply piggyback onto larger satellites being launched, but the company stresses its demand for a dedicated launcher for small satellites.

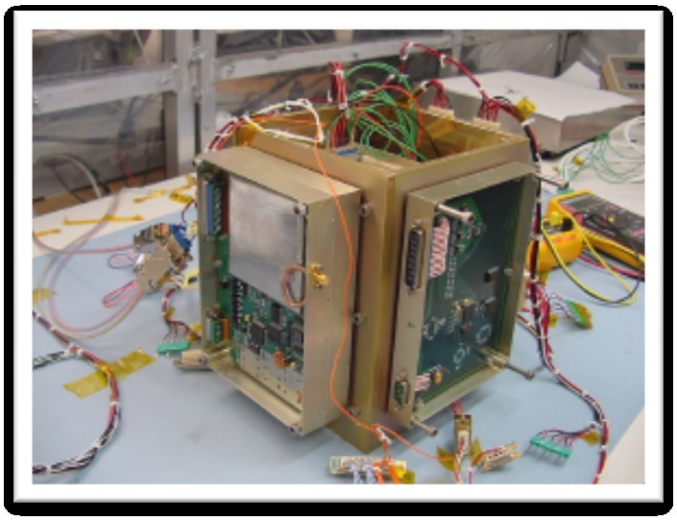

Figure 2: *FalconSAT-2* spacecraft architecture making use of SNAP standardized mechanical and electrical interface modules.[11]

This category of “plug & play” space-proven hardware might well prove to be the baseline architecture for future small satellite development. Current research also delves into the commercial uses for such small satellites with an emphasis on precision formation arrangement and alignment for arrayed satellites used for science or communication missions. A recent article is *Space News* highlights the growing market with a recent contract award worth $75 million given to Orbital Sciences by DARPA for the design of clusters of small wirelessly connected modules. These small satellites are “designed to perform tasks once reserved for large, traditional spacecraft while providing the same overall mission capability”.[13]

The civilian possibilities are also exciting. A notable example includes the implementation of radio or telescope interferometric

observation platforms with clusters of wirelessly connected small-satellites in formations as large as kilometers in diameter.[14] Spectral imaging observations would also enable major breakthrough in the understanding of the universe if the technology is sufficiently developed. In addition to the NASA sparse array, other uses for small satellites, and therefore a launch capable of delivering small satellites to LEO, include more affordable options for civilian communications, Earth monitoring, and science and exploration missions by companies and research institutions alike. Additional needs by the emerging Indian and Chinese civilian space markets will continue to motivate larger growth out of this specific industry in the years to come.[15] However, no launch system yet exists to provide individual services to these customers. Such a substantial increase in market size dictates the need for an affordable launch solution. A vehicle capable of meeting the ORS requirements to augment or reconstitute space based assets could also be used for civilian launch purposes with little to no change in design philosophy.

This specific dissertation topic began as a simple thought-problem suggested by a senior engineer at Raytheon Missile Systems: *could a combination of demilitarized rocket motors be used in conjunction to loft a small payload to the Moon?* The question of carrying a payload to the Moon was prompted by the Google Lunar X-Prize. This competitive prize is comparable to the Ansari X-Prize where $10 million was offered to the first non-government organization that could launch a reusable manned

spacecraft into a sub-orbital trajectory twice within two weeks. The Ansari X-prize was claimed in late 2004 by Burt Rutan's (owner and founder of the aerospace company Scaled Composites) *SpaceShipOne*, a spacecraft sponsored by Microsoft co-founder Paul Allen. Since that time Scaled Composites has been in close collaboration with Sir Richard Branson's Virgin group to build larger suborbital spacecraft capable of ferrying tourists to the edge of space for a cost of $200,000 per flight. Thus the X-Prize, itself akin to the Orteig prize that prompted the first trans-Atlantic flight claimed by Lindbergh in 1927, is a proven motivator for space progress in the last ten years.

Three other X-prizes have since been founded; the Archon X-Prize in genomics, the Progressive Insurance Automotive X-Prize, and finally the Google Lunar X-Prize. The latter is a $30 million international competition to safely land a robot on the surface of the Moon and perform specified tasks. Again, the aim of the original question posed was whether or not such a launch vehicle could be built out of surplus military rockets. The inherent rationale is that a custom launch vehicle would circumvent the need for a costly commercial launch vehicle whose purchase alone would be over the Lunar Google X-prize winning purse.

The first intended mission, after the proposed launch vehicle has successfully achieved orbit, is to loft a payload of minimal mass and impact the Moon. Though the premise is simple, such a mission represents a significant technical challenge. Later missions could

potentially focus on precision orbital maneuvers intended to put the spacecraft into a stable orbit around the Moon. Further launches would then concentrate on providing a soft touch-down on the surface of the Moon to allow a small rover to carry out said tasks pursuant to the rules of the Google Lunar X-Prize. But the original question still stands: *can it be done with refurbished military missiles?* It is the purpose of this dissertation to prove that such capabilities exist and more importantly that the resulting architecture can serve as a viable platform for immediate and affordable access to low Earth orbit.

Comparable Existing Architectures

Prior to beginning a preliminary design of a new launch vehicle it is prudent to begin the discussion with a historical perspective on existing space launch platforms. As previously mentioned, almost all modern day launch vehicles are derivatives of ICBMs. However, some ICBMs have been directly converted to launch vehicles and have been used or are still in use today. These include the U.S. *Titan 2* ICBM, U.S. *Minuteman* ICBM, Russian Submarine missiles, Russian *SS-25* ICBM and Russian *Tsyklon* ICBM to name a few. Though such ICBMs number in the thousands, the Strategic Arms Reduction Treaty (START) which is a bilateral agreement by both the U.S. and Russia, has slowly motivated the dwindling such stockpiles. Thus, while the prospect of using demilitarized ICBMs can be argued as a significant cost-saving measure and a fitting use of former

weapons of mass destruction, it is not a wholly sustainable business plan. Instead businesses must develop new space capable launch vehicles, derivatives of ICBMs or otherwise. To this end, three (3) separate options exist to satisfy the requirements of the ORS and a commercially-viable venture:

1. A new system specifically designed,
2. evolution of current expendable or reusable launch systems,
3. or commercially provided launch services.[3]

The intended focus of the following competitive analysis is to identify the current strengths and weaknesses of a listing of market competitors. Companies such as United Launch Alliance, Orbital Sciences, SpaceX, and Arianspace currently provide launch services for large satellites, but negate the needs of the smaller satellite market due to the inherently high cost of their launch vehicles. To quantify the strengths and weaknesses of competitors an examination of each company with regards to their capabilities for affordable access to space for small payload quantities is first required. The most noteworthy are:

Orbital Sciences, whose manufacturing facility is in Chandler, AZ, was started by three Harvard Business School graduate entrepreneurs and is a prime example of the evolution of current expendable or reusable launch systems from military uses over to civilian applications. This concept very closely matches the proposed architecture with the exception of the scale and type of the demilitarized boosters. Much of Orbital

Science's space launch business has been derived from use of large decommissioned ICBMs. A recent noteworthy example of this type of booster was the *Minotaur* space mission that launched the Arizona State University CubeSAT as a piggyback on a larger satellite headed to orbit. Nevertheless, these large boosters take months or years to prepare for a launch and are deemed unsuitable for solely small satellite or operationally responsive space mission needs.

Orbital Sciences' *Pegasus XL* is also worth mentioning as it is currently the most active small launch vehicle used by the United States. The *Pegasus* is noteworthy for its uncommon "air-launch" from a converted L-1011 aircraft. The *Pegasus*, which is powered by three solid rocket motors, can loft a payload of 1,015 lbs (460 kg) to LEO. This vehicle has flown 40 times since 1990, with a maximum of six in one year launch in 1998. However, the *Pegasus* costs anywhere from 12 to upwards of 30 million per launch, for a total cost to LEO of approximately $12,000 to $30,000 per pound of payload.[16]

Figure 3: Orbital Sciences *Minotaur* large booster launch.

The company ***Microcosm*** is a notable example of building a rocket specifically to service the small satellite market and government needs for quick responsive access to space. Over the past ten years they have spent over $50 million dollars, funded mostly through government or SBIR sources, to develop such a launcher, named *Scorpius*, and have succeeded in only two suborbital launches. In spite of this progress, they still project costs to be around $4,000/lb of payload to LEO, not including the cost of inventory currently projected at 0.75% of the vehicle cost per month,[24] which would significantly increase their sale costs. While this signifies a cost cutting method of approximately half the current market the company has yet to provide a workable orbital vehicle.

A similar company using start up funds by the Army Space and Missile Defense Command is ***Orion Propulsion*** based out of Huntsville, AL. Similarly, they are designing a new class of rocket from scratch to provide responsive launch capability to the military for approximately $1

million per launch. This program is very much in its infancy with their first hot fire of a 2,500 lbf nitrous oxide / ethane fuel completed just recently.[17]

The last company under evaluation is ***SpaceX***. This company was built from the ground up by *PayPal*™ inventor Elon Musk over the past 8 years and has since been very popular in the news because they promise to substantially reduce costs to LEO. Financed almost exclusively by Musk's own personal wealth, the company's initial rocket *Falcon I* can launch several hundred kilograms to LEO. The development of this rocket has been off to a shaky start, with three (3) of the four (4) launches ending in disaster. The most recent *Falcon I* launch did manage to reach orbit and more launches are scheduled. SpaceX also captured the NASA Commercial Orbital Transportation Services contract worth $800M to provide services to the International Space Station, but these missions will be performed with their new much larger rocket called *Falcon 9*.

Figure 4: SpaceX *Falcon I* launch of a small satellite.

After reviewing the above companies (and other somewhat similar business strategies) it is apparent that the vehicles are all derivatives of 1950s era large intercontinental ballistic missiles and are not optimized for small satellite launches, with the exception of perhaps the SpaceX *Falcon I* which is still in its infancy. In fact, many small satellites simply piggyback on a larger satellite launch vehicle and are appropriately jettisoned into orbit after the main insertion burn. Furthermore, the companies that build new vehicles from scratch, such as SpaceX, Microcosm and Orion Propulsion are engaged in very long lead times (10years+) until they have a workable vehicle capable of making any profit. Even then the vehicles are only produced on an as-needed basis.

The reason for the high cost of current expendable launch vehicles is their unwavering reliance on state of the art technologies such as lightweight structures and high-performance engines in order to maximize payload and range, resulting in large and very expensive vehicles.[1] In the past such large vehicles were necessary to lift large satellites to geosynchronous orbits, but large launch vehicles are quickly becoming obsolete in the small-satellite to LEO market. The main differentiation of the proposed solution to this immediate problem is that to offset the high cost of vehicle manufacture the vehicle will instead use medium range surface to air military surplus missiles. These residual rocket motors, which number in the thousands, are available at low cost and will be

refurbished and retrofitted to meet the performance requirements to launch small payloads to LEO.

Proposed Solution and Contributions of Study

The proposed design methodology for a dedicated small-satellite launch vehicle relies upon using a combination of expendable medium-range military surplus (or retired) booster and sustainer solid rocket motor assets. This methodology is similar in concept to refurbishment of ICBMs for commercial uses, as originally mandated by the Office of the President in 1988,[18] but differs in the type of assets used as well as overall scale.

Such architectures have been proposed before. As early as 1957, the U.S. investigated the use of small, low weight and inexpensive military derived orbital-capable solid rocket fueled rockets called Solid Controlled Orbital Utility Test or *Scout*. Several variances existed throughout the 1960s, but it remained the first solid-fuel launch vehicle to achieve orbit, and remains the only U.S. orbital launch vehicle powered solely by solid rocket motors. However the payload capability was very small, on the order of 100 kilograms or less with its four stages, all of which were scavenged from three (3) separate earlier programs: the Navy *Polaris*, Army MGM-29 *Sergeant* and the Navy *Vanguard*.[19] However, 100 kilograms of payload proved hardly acceptable for the low technology satellites of that time. The program was abandoned after nearly three decades of service with a 95% success rate on over 100 launches of scientific experiments when the Shuttle came into service.

Figure 5: Scout vehicle composed of four solid rocket motors. Image Source: NASA, [*http://lisar.larc.nasa.gov/IMAGES-/SMALL/EL-1996-00116.jpeg*]

With the recent emergence of small satellites with similar operating capabilities compared to larger traditional satellites, the launch manifest of the *Scout* rocket would be in high demand. In fact the *Scout* system would provide a near optimal solution to the current problem defined by the Office of ORS. Sadly, the *Scout* rocket cannot be resurrected because all of the rocket motors were comprised from existing off-the-shelf components that are no longer available for purchase. As such, these payloads can only be exclusively launched by the Orbital *Taurus*, *Minotaur* or *Pegasus*, though all are quite expensive and have capabilities more suited for 500+ kg of payload. No other country maintains a similar rocket

with any success rate capable of launching *small* payloads to orbit. China, Iran, South Korea, North Korea, Brazil and soon Indonesia[20] have all tested and to some extents flown (almost always in failure) several such rockets. But their future, like that of SpaceX *Falcon I*, is as of yet unknown.

The intended focus then inevitably shifts to what arrangement of solid rocket motors will suite the purposes for an ORS capable rocket. An ideal choice would be a rocket motor or rocket motor combination that exists in high quantities and has a long successful track record. Moreover, the rocket motor should be accessible to a company interested in purchasing a high volume or have surplus stores available and should be easily retrofitted or refurbished to meet new design constraints. For the purposes of this dissertation, the Mk70 booster and Mk30 sustainer have been selected for reasons to be discussed later. However, the Mk70, used in a variety of missile systems throughout several decades, has also been retrofitted to serve as an ideal booster platform for testing new technologies. An example is the Orbital Science's *Coyote* supersonic test cruise missile. The *Coyote*, shown in Figure 6, can operate only at high velocities due to its oxidizer-lean propellant combination, consequently the Mk70 was used to accelerate the test missile to the appropriate velocity.

Figure 6: Orbital Sciences' GQM-163A *Coyote* Supersonic Sea Skimming Target using a residual Mk70 solid rocket motor booster.[21]

The remainder of the dissertation will show that a combination of Mk70 and Mk30 solid rocket motors, illustrated assembled in Figure 7, can indeed provide the necessary energy required to rapidly place a small satellite into LEO. This novel idea differs from use of ICBMs in that the smaller military boosters, namely tactical missiles are:

- Produced in mass quantities for volume of purchase at low cost with superb quality control,[22]
- engineered for long shelf-lives with no servicing required,
- make use of solid rocket motors which do not require fueling prior to launch,
- can be launched from existing military platforms around the world,

- are designed to be ready to launch within minutes of need,
- are readily available at little to no cost from the U.S. military surplus,[23]
- require only minimal extra support equipment and services,
- can be easily shipped and stored,
- are very easily serviceable and augmented,
- and can be arranged to meet the requirements of different mission profiles.

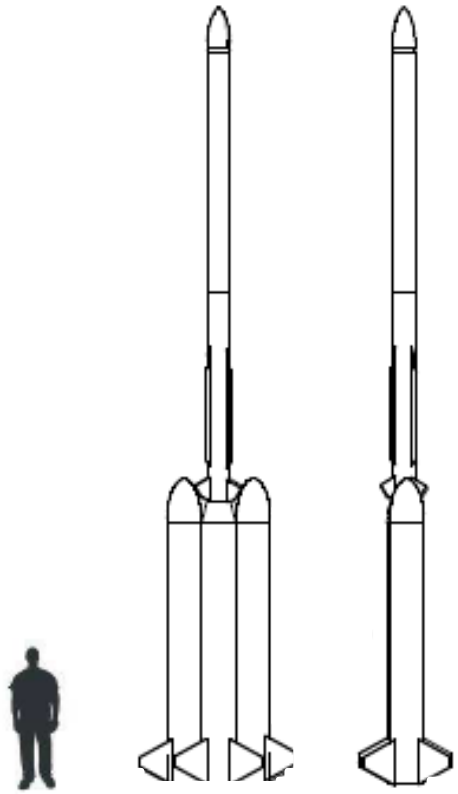

Figure 7: Rendering (to-scale) of the proposed small satellite launch vehicle exhibiting significant decrease in overall size and mass compared to existing orbital launch vehicles.

The chief disadvantages of the proposed architecture are (1) the limited amount of payload that can be brought to LEO, (2) the need to build additional fairings and couplers for the payload and stage integration, (3) a need for development of an advanced upper stage involving a liquid rocket engine and reaction control systems (RCS), (4) a requirement to provide integrated space operations mission planning for a variety of launch sites,[3] and (5) the regulatory, philosophical and cultural hurdles to quickly launch a rocket that has been created over time.[24] The latter includes range certification, FAA approval processes, flight safety requirements (including flight termination implementation), and payload processing that will hamper the ability to rapidly launch a payload on a moment's notice.

System level design for new space launch vehicles[25] recommends that the aim of the new launch vehicle be to alleviate the common problems prevalent amongst current launch vehicles. This dissertation focuses on addressing these four items as the drivers for the successful implementation of such a rocket.

1. *Reduce launch system complexity by reducing the number and complexity of tasks required by human intervention.* Therefore it is advisable to include a high degree of commonality between differing stages as well as simplified payload launcher interfaces. Using decommissioned military

missiles for the various stages certainly accomplishes these recommendations.

2. *Increase subsystem accessibility as a driver for system maintainability.* Such missiles are not necessarily designed for such quick access, but are instead designed such that maintenance is not required. However, fluid and mechanical systems designed for the launcher should provide for accessibility as they are often the culprit for required internal tests.[26]
3. *Make payload interfaces independent of the launcher, with standardized interfaces*. Payload integration constitutes a major fraction of the cost of launch operations. Therefore payloads should be designed as independent of the launch vehicle as possible.[26]
4. *Use less toxic propellants.* Although hydrazine is an optimal candidate for in-space missions, launch personnel must wear hazard suits to protect themselves from the carcinogenic or corrosive materials. Use of a new propellant comparable to hydrazine will be examined in this dissertation to eliminate a significant amount of ground processing which has been shown to provide economic benefits.[27]

As the dissertation will discuss there are many barriers and constraints that act on a rocket. The report narrates a step-by-step

approach to evaluating the utility of the rocket architecture with a Matlab trajectory and cost-mass-performance optimization code in addition to detailing the design of a new breed of rocket engine to act as the final orbital stage. The engine is designed for ease of use but differs starkly from the current state of the art by utilizing a new environmentally benign propellant combination with performance traits similar to traditional space propellants. Lastly, the dissertation centers on meeting the objectives of the Office of Operationally Responsive space but moreover focuses on the development of a vehicle that will complement, rather than replace, traditional launch vehicle product offerings from existing space program companies.

2. Flight Profile

"When once you have tasted flight, you will forever walk the earth with your eyes turned skyward, for there you have been, and there you will long to return."

-Leonardo da Vinci (1452 to 1519)

Inventor, Scientist, Engineer and Artist

The first step towards realizing the potential of the proposed architecture is to evaluate the capabilities that such a system can provide. To this end, an adequate flight simulation program capable of assessing the true capabilities must be developed. This program will be required to take into account not only the thrusting vectors and subsequent trajectories of a rocket in multiple dimensions, but also such influential terms as gravity, drag and steering.

Fundamentals of Rocket Momentum Exchange

It is sensible to begin with a simple derivation that introduces the fundamental equations used to predict the amount of propellant required for a given mission. Coupled with known technology factors, these equations will drive the entire vehicle design and sizing requirements. In the same scope, these equations can easily be used to evaluate existing systems and examine their usefulness as potential rocket motor stages for the proposed LEO achievable rocket launch vehicle.

Modern rockets function through the expulsion of high velocity gases generated via chemical reactions, also known as "chemical

rockets". These include solid rocket motors, hybrid rocket motors and liquid rocket engines. Each genre signifies the method in which the required propellant is stored and will be covered more thoroughly throughout the dissertation. Additionally, these propulsion types each operate at high operating pressures and temperatures inside of their respective combustion chambers. Combustion gases are subsequently expanded through a converging-diverging nozzle which converts the hot, high pressure stagnation gas into useable kinetic energy through enthalpy expansion. The gas that exits the nozzle leaves at a very high speed known as the "exhaust velocity", u_e, which can be just over 4,500 meters per second (about 10,000 miles an hour) for a liquid rocket engine. The exhaust velocity is a function of the propulsion type with lighter, hotter gasses being the most effective and is directly derived from the fundamental enthalpy equation $h_o = h_e + u_e^2 / 2$ and isentropic relations as:

$$u_e = \sqrt{\frac{2\gamma R T_o}{\gamma - 1}\left[1 - \left(\frac{p_e}{p_o}\right)^{\frac{\gamma-1}{\gamma}}\right]} \qquad (1)$$

where R is the specific gas constant of the combustion products, T_o is the stagnation temperature in the combustion chamber, γ is the ratio of specific heats, p_o is stagnation pressure, p_e is exit pressure out of the exit plane of the nozzle.

It is common knowledge that the exhaust velocity will change for changing exit conditions, i.e. the flow will be under-expanded or over-

expanded depending on the altitude and hence ambient pressure conditions. Such expansion is a function of exit Mach number which is related to the pressure ratios again via isentropic relations. However, for the following derivation the exhaust velocity is assumed constant since in actuality it does not detract much from the overall performance.

The following analysis now considers a rocket before and after a thrusting period. This fictional rocket of mass “m” is displayed below in Figure 8 moving at an initial velocity “v” at the start time “t”.

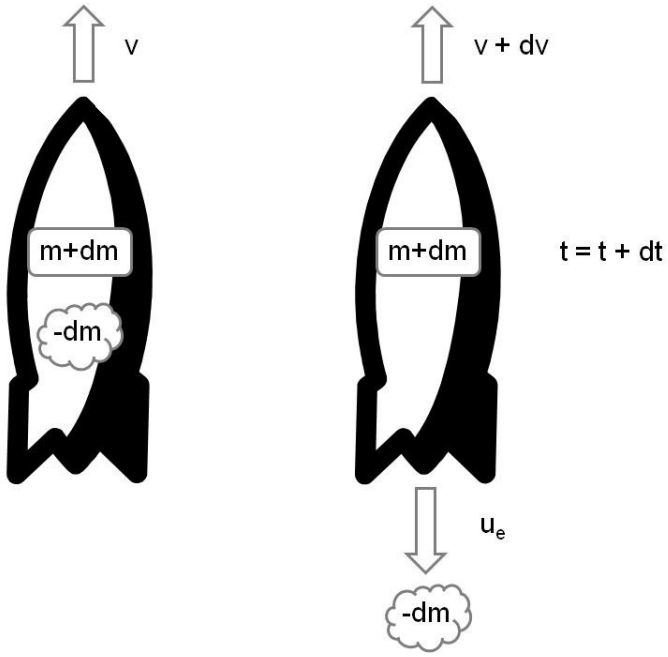

Figure 8: A rocket before and after a thrusting period.

Using an absolute frame of reference the total momentum, p after thrusting can be compared to determine the net change in momentum. This is given by: $p = (m + dm)(V + dv) + (-dm)(v - u_e)$, which after expansion of the terms yields: $p = mv + m\,dv + u_e\,dm$. Applying Newton’s second law and neglecting, for the time being, the effects of gravity and

the drag force yields the quantity “mv” as a constant. Hence: m dv = $-u_e$ dm . Integration of linear velocity from zero to some total change in velocity, Δv and rocket mass from an initial starting mass, m_o to a final mass, m_f equals:

$$\int_0^{\Delta v} dv = -u_e \int_{m_o}^{m_f} \frac{dm}{m} \quad \Rightarrow \quad \frac{m_f}{m_o} = \exp^{-\frac{\Delta v}{u_e}} \tag{2}$$

However, Equation 2 can be further expanded to include the widely used “specific impulse” term defined as $I_{sp} = u_e/g_0$ where g_0 is the gravity of Earth, 9.807 m/sec^2. This equation, in its final form, is called the *Ideal Rocket Equation*:

$$\frac{m_f}{m_o} = \exp^{-\frac{\Delta v}{I_{sp} \cdot g_o}} \tag{3}$$

Specific impulse has units of seconds and is a measure of how much thrust is gained per weight-flow-rate of propellant. Therefore propulsion systems with higher I_{sp} utilize propellant mass more efficiently and can provide more total change in velocity for significantly less fuel (note the exponential relationship in Equation 3) than other less efficient propulsion systems. Typical values of I_{sp} for a chemical engine can be as high as 460 seconds for liquid rocket engines. Solid rocket motors peak at approximately 280 seconds. Equation 3 shows that to maximize the m_f/m_o ratio, also called the mass ratio or simply “MR”, the I_{sp} should be as high as possible. Maximizing the MR will allow the vehicle to carry more

effective payload mass, m* to its final destination or use more structural weight, i.e. higher factor of safety, heavier materials, etc.

Another important quantity in the Ideal Rocket Equation is the total change in velocity required or Δv, pronounced “delta V”. The Δv characterizes the requirements of the vehicle to reach a prescribed destination and is determined through the mission profile. For example, the velocity required to maintain a stable circular orbit of 250 kilometers above the surface of the Earth is 7,755 m/sec and is found easily through the expression derived from the astrodynamic *vis viva* equation (or orbital energy conservation equation) and specific angular momentum:

$$v_c = \sqrt{\frac{\mu_E}{r}} \tag{4}$$

where μ_E is the gravitational parameter for Earth and r is the radial distance of the satellite from the center of Earth.

However, the velocity required to reach that same orbit is slightly higher, about 9,000 m/sec when real-world variables are factored appropriately. The most significant of these real world affects are losses due to the gravitational pull while within the sphere of influence of a planet’s gravity given by the fundamental gravity equation. These losses may be approximated according to the equation:

$$\Delta v_{grav} = \int_0^t g \cdot cos(\varphi) dt \tag{5}$$

For a sounding rocket on a perfectly vertical trajectory, the Δv_{grav} losses are simply $\Delta v_{grav} = g_0 t$ or approximately 1,178 m/s after two minutes

of flight. Of course with a change in flight path angle (Φ) delta v will reduce according to the cosine of the angle. This is called a “gravity turn” maneuver, an integral part to the launch sequence as will be discussed later. Once the vehicle has successfully turned from a Φ of zero degrees (vertical) to a flight path angle of 90 degrees the vehicle will no longer be subject to a ∆v gravity loss. At that point Earth’s gravity is helping the satellite maintain a stable orbit about the Earth if the satellite has sufficient tangential velocity.

Other ∆v losses include drag, ∆v changes due to the Earth’s rotation and steering losses incurred from thrust vectoring of the rocket nozzle(s). These losses must be added to the total change in velocity required to reach the orbital velocity at a given altitude. When the aforementioned factors are all accounted for, this net change in velocity is the final amount the vehicle will have to produce in order to establish the required orbit at the proper flight path angle. Typical values for these losses are collated in Table 1.

Table 1: Velocity Budgets to LEO[28]

Launch Vehicle	$\mathbf{v_{LEO}}$	$\mathbf{\Delta v_{gravity}}$	$\mathbf{\Delta v_{drag}}$	$\mathbf{\Delta v_{steering}}$	$\mathbf{\Delta v_{rot}}$	$\mathbf{\Sigma \Delta v = \Delta v_{prop}}$
Ariane A-44L	7,802	1,576	135	38	−413	9,138
Atlas I	7,946	1,395	110	167	−375	9,243
Delta 7925	7,842	1,150	136	33	−347	8,814
Space Shuttle	7,794	1,222	107	358	−395	9,086
Saturn V	7,798	1,534	40	243	−348	9,267
Titan IV/ Centaur	7,896	1,442	156	65	−352	9,207

Note that the rotation of the Earth provides a negative ∆v component. This negative translates to a gain in net velocity owing to the Earth's rotation if the launch vehicle launches in an Easterly direction. Of course, satellites can also be launched in a Westerly direction, called retrograde satellites, but they will not benefit from the gain in velocity. Moreover, launches at lower latitudes provide even more velocity gain according to the equation:

$$\Delta v_{rot} = \omega_E r_E cos(\delta) \cdot cos(i) \quad \textbf{(6)}$$

Where ω_E is the angular velocity of Earth ($7.27*10^{-5}$ rad/sec), r_E is the radius of Earth, δ is the launch latitude and *i* is the launch inclination destination. It is important to observe that launches at lower latitudes (closer to the equator) and due East provide the highest benefit: a maximum of 463 m/s.

Thus the final equation for calculating the required ∆v for the propulsive effort is additive:

$$\Delta V_{prop} = V_{LEO} + \Delta V_{gravity} + \Delta V_{drag} + \Delta V_{steering} - \Delta V_{rot} \quad \textbf{(7)}$$

Equation 7 is not exhaustive. Other factors may contribute to increase or even decrease the amount of propulsive ∆v required. Examples of methods used to decrease the ∆v required are gravity assists, such as gravity slingshots, and in-situ propellant utilization.

Another way to effectively increase the ∆v that a rocket provides is to utilize staging, defined as discarding unused rocket mass after the propellant has been expended. In practice, staging is used often and

remains the ideal method for launching payloads to LEO and beyond. Referring back to the Ideal Rocket Equation, the total Δv produced from a staged rocket is additive for each stage.

$$\Delta v_T = \sum_j^n \Delta v_j = \sum_j^n \left[I_{SP\,j} \cdot g_0 \cdot \ln\left(\frac{1}{MR}\right)\right] \qquad (8)$$

Where MR is the mass ratio, defined as $MR=m_f/m_o$. A high MR therefore signifies a rocket with low structural mass capable of carrying a larger amount of payload, or a higher payload fraction $\lambda = m^*/m_o$.

Before proceeding further it is essential to note the nomenclature for staged rockets. Stages are numbered j = 0,1,….,n with the zeroth stage denoting strap-on side boosters. Referring to Figure 9 for a two stage rocket the individual stage initial and final masses are defined by Equation 9 where m_s, m_p and m^* are the structural, propellant and payload masses, respectively.

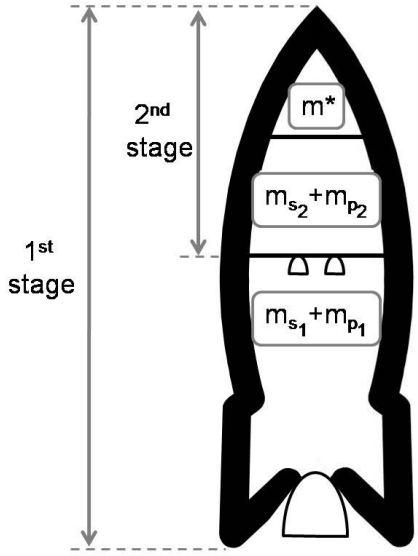

Figure 9: Nomenclature for a two-stage rocket.

$$
\begin{aligned}
m_{o_1} &= m_{s_1} + m_{p_1} + m_{s_2} + m_{p_2} + m^* \\
m_{f_1} &= \left(m_{o_1} - m_{p_1}\right) = m_{s_1} + m_{s_2} + m_{p_2} + m^* \\
m_{o_2} &= m_{s_2} + m_{p_2} + m^* \qquad \left(m_{f_1} \neq m_{o_2}\right) \\
m_{f_2} &= \left(m_{0_2} - m_{p_2}\right) = m_{s_2} + m^*
\end{aligned}
\tag{9}
$$

If the effective exhaust velocities are the same for all stages, $U_e^1 = U_e^2 = \ldots U_e^j$ then by the natural log product rule:

$$
\Delta v_T = U_e \cdot \ln \prod_j^n \left(\frac{1}{MR_j} \right) \tag{10}
$$

Extending this analysis further, for a rocket that also has stages of identical mass ratios, $MR_1 = MR_2 = \ldots MR_j$, and specific impulses or exhaust velocities that are still the same, $I_{sp}^1 = I_{sp}^2 = \ldots I_{sp}^j$, this function simplifies to:

$$\Delta v_T = n \cdot U_e \cdot \ln\left(\frac{1}{MR}\right) \quad (11)$$

The significance of this example is that if you double stages "n" you double the Δv of the rocket! Thus, it is advisable to stage a rocket that is required to exert a high Δv. For instance, if a single stage rocket is required to go to orbit, the limit of current technology will allow only 3% of its gross lift-off weight (GLOW) as useable payload weight to orbit.[29] Additional stages should be added to increase the payload fraction, λ as illustrated in the equation below:

$$\lambda_T = \prod_j^n \lambda_j = \left(MR_j - \eta_j\right) \cdot \left(MR_{j+1} - \eta_{j+1}\right) \cdot \ldots \cdot \left(MR_n - \eta_n\right) \quad (12)$$

As a word of caution it should be stated that there exists a point of diminishing returns for stage additions. Adding an additional stage is not always the optimal solution beyond a certain amount of stages. In these situations a higher total payload fraction can be achieved by instead adding more propellant mass to the bottom stage(s). This trend is demonstrated in Figure 10.

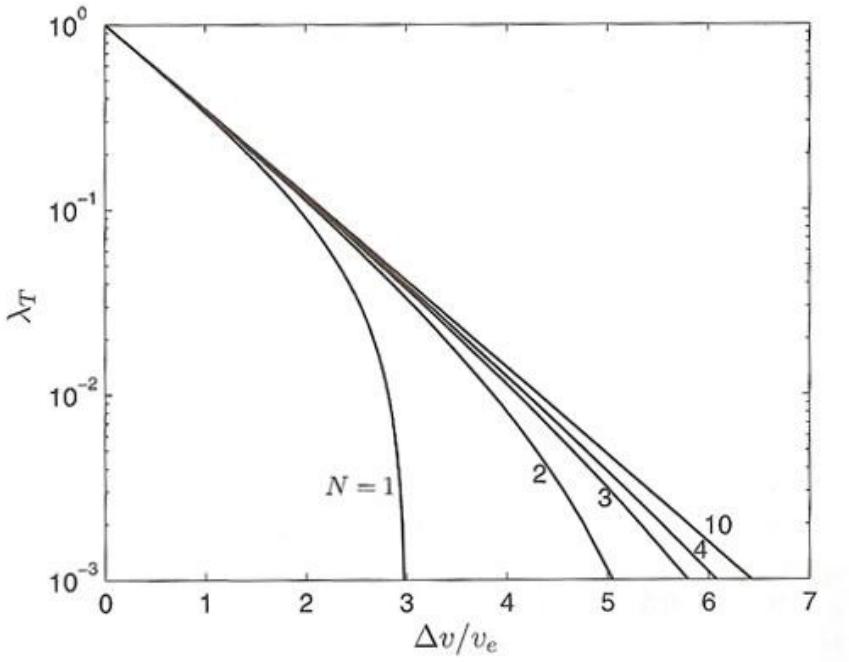

Figure 10: Variation of total payload ratio of a multi-stage rocket with performance parameter $\Delta v/u_e$.[31]

It is therefore important to maximize the velocity ratios of all stages such that final payload is maximized. There are various methods to perform such a maximization, the most straightforward of which is the brute force method: an iterative solution that converges on the highest payload ratio. An additional technique of calculus of variations is outlined in Hill and Peterson[30]. This method makes use of an undetermined constant α, a Lagrange multiplier used to maximize the mass ratio according to the below equation, hence maximizing the payload ratio of each stage.

$$\Delta v_n = \sum_j^n u_{ei} \ln \frac{\alpha \cdot u_{e_j} + 1}{\alpha \cdot \varepsilon_j \cdot u_{e_j}} \quad (13)$$

Where ε_j is the structural coefficient of each individual stage given by the equation $\varepsilon_j = m_s/(m_s+m_p)$.

The Lagrange multiplier is then set such that the addition of the each stage velocity contribution is equal to the total velocity required for the mission, including Δv losses incurred from gravity, drag, etc. Once obtained, the final mass ratio of each stage can be calculated by the following equation:

$$MR_j = \frac{\alpha \cdot \varepsilon_j \cdot u_{e_j}}{\alpha \cdot u_{e_j} + 1} \quad (14)$$

This then leads to direct calculation of the payload ratio for each individual stage according to the equation listed below. Stages are then sized relative to one another accordingly. Similar structural coefficients ε_j and engines types, u_{ej}, further simplify the process.

$$\lambda_j = \frac{\varepsilon_j - MR_j}{MR_j - 1} \quad (15)$$

An additional computational method is described by Tewari[31] with supplementary capabilities for zeroth stage booster configurations. However, the optimization does not always tend towards realistic solutions so care must be taken when evaluating the outputs and as such a familiarity with realistic numerical values is absolutely essential. A different

tool utilizing response surface methodology is discussed in a later section that serves as a better model for comparison.

Regardless of the analysis method the result is the same: rockets should be designed “bottom heavy” with larger stages comprising the base of the rocket and utilizing lower specific impulses.[1,32] The end result is that higher specific impulse engines, which are likely to be much more costly, should instead be reserved for the latter stages and will nominally provide more of the total Δv.[33] An additional benefit from this architecture is that the bottom stages are more insensitive to weight gain. As an example, adding a kilogram to the bottom stage might only diminish the payload weight by one tenth of a kilogram, as opposed to adding a kilogram to the uppermost stage which will instead effectively take away one useable kilogram of payload weight.[29] Consequently, the bottom stages can be manufactured with more cost effective materials or higher factors of safety. To this end, utilizing surplus military missiles is advantage, and the resulting optimization studies should focus on the size of the additional stages.

Three Degree of Freedom Trajectory Program

With a sound understanding of the fundamental equations and optimization schemes, a trajectory code can be written to explore the interdependence of the many variables and arrive at an optimum solution for the given constraints and conditions. A higher fidelity modeling

program must incorporate the many factors listed above including modules for calculation of drag, gravity, and the rotational effects that Earth has on a spacecraft. Moreover, such a program requires numerical integration of the equations of motions, listed below, which do not have closed-form solutions.[28] A three (3) degree of freedom (3DOF) point-mass modeling effort for conceptual design is adequate[34] for these evaluation purposes. A future 6DOF model may be required to include the three aerodynamic forces (normal, axial and side forces) and the three aerodynamic moments (pitch, roll and yaw moments) once thrust vector control and/or aerodynamic steering are taken into account, but this is reserved for a more detailed analysis of the guidance and control system. Additionally, the rocket is assumed “stiff” and as such aeroelasticity effects are ignored.

Having chosen a 3DOF model, the position and velocity vectors must be determined at each time instance. This will require a numerical integration scheme of the equations of motion. The reference frame for these equations is Earth-fixed or “relative”, see Figure 11, for reasons of taking the Earth’s rotation into account. Subsequent transformation to the spacecraft inertial frame will later be required to determine pertinent orbital characteristics following successful orbit attainment.

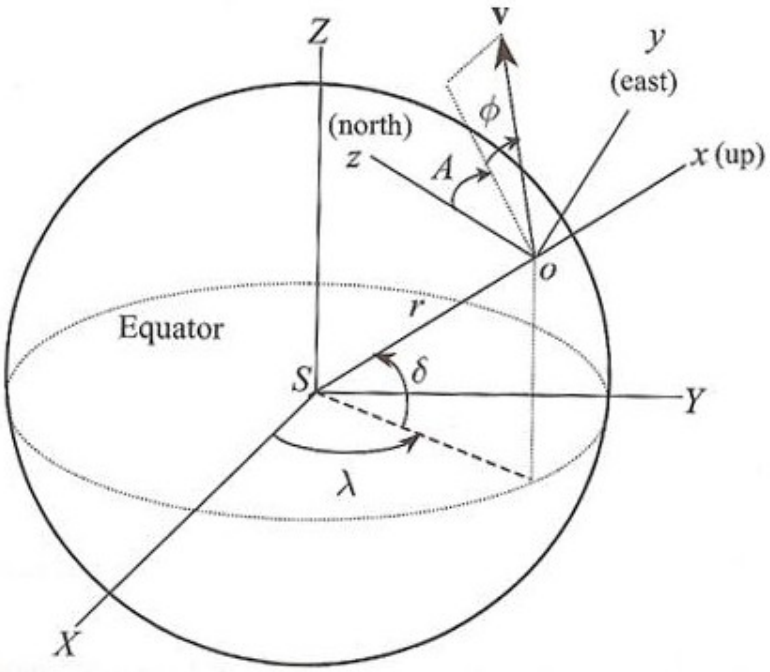

Figure 11: Earth-fixed relative frame denoting position and velocity vectors.[31]

The kinematic equations relative to a rotating planet are expressed by the relative position vector given in spherical coordinates by a radial distance r, the latitude δ and the longitude λ. These are related to the inertial velocity vector **v** = v(sinΦ**i** + cosΦsinA**j** + cosΦcosA**k**) where Φ is the relative flight path angle and A is the relative flight azimuth angle. When transformed to the Earth-rotating frame by inclusion of the inertial acceleration, the kinematic equations are:

$$\dot{r} = v \cdot sin(\theta) \tag{16}$$

$$\dot{\delta} = \frac{v}{r}\cos(\phi)\cdot\cos(A) \quad \left(\frac{d}{dt}\ latitude\right) \tag{17}$$

$$\dot{\lambda} = \frac{v \cdot \cos(\phi) \cdot \sin(A)}{r \cdot \cos(\delta)} \quad \left(\frac{d}{dt} \; longitude \right) \tag{18}$$

The above equations yield the position vector, once the dynamic equations (next) are solved to give the relative velocity vector [v, Φ, A]. Expressed in terms of spherical coordinates, the relative velocity vector components are derived[31] with knowledge of the aerodynamic force vector (i.e. lift and drag, D), the thrust f_t and the gravity force g.

$$\begin{aligned} m \cdot \dot{v} = {} & f_t \cdot \cos(\varepsilon) \cdot \cos(\mu) - D - m \cdot g_c \cdot \sin(\phi) + m \cdot g_\delta \cdot \cos(\phi) \cdot \cos(A) \\ & - m \cdot \omega^2 \cdot r \cdot \cos(\delta) \cdot [\cos(\phi) \cdot \cos(A) \cdot \sin(\delta) - \sin(\phi) \cdot \cos(\delta)] \end{aligned} \tag{19}$$

$$\begin{aligned} m \cdot v \cdot \cos(\phi) \cdot \dot{A} = {} & m \frac{v^2}{r} \cdot \cos^2(\phi) \cdot \sin(A) \cdot \tan(\delta) + f_t \cdot \sin(\mu) + f_y - m \cdot g_\delta \cdot \sin(A) \\ & + m \cdot \omega^2 \cdot r \cdot \sin(A) \cdot \sin(\delta) \cdot \cos(\delta) \\ & - 2 \cdot m \cdot \omega \cdot v \cdot [\sin(\phi) \cdot \cos(A) \cdot \cos(\delta) - \cos(\phi) \cdot \sin(\delta)] \end{aligned} \tag{20}$$

$$\begin{aligned} m \cdot v \cdot \dot{\phi} = {} & m \frac{v^2}{r} \cdot \cos(\phi) + f_t \cdot \sin(\varepsilon) \cdot \cos(\mu) + L - m \cdot g_c \cdot \cos(\phi) - m \cdot g_\delta \cdot \sin(\phi) \cdot \cos(A) \\ & + m \cdot \omega^2 \cdot r \cdot \cos(\delta) \cdot [\sin(\phi) \cdot \cos(A) \cdot \sin(\delta) - \cos(\phi) \cdot \cos(\delta)] \\ & - 2 \cdot m \cdot \omega \cdot v \cdot \sin(A) \cdot \cos(\delta) \end{aligned} \tag{21}$$

Though these ordinary differential equations are coupled, they are in fact nonlinear and require a numerical integration scheme such as Runge-Kutta. Such solvers are built-in functions in Matlab and are used accordingly with initial conditions given for the [r,δ, λ, v, Φ,A] values to

yield the time dependant solution vector. Initialization of the first the solver requires knowledge of the thrust, drag and gravity forces, all of which are a function of time. Such values for thrust can be input as a thrust histogram, or thrust curve. More simple analyses would make use of a constant thrust curve given assumed values for the specific impulse of the motors being used. Of course the mass, m(t), of the rocket is required and is heavily dependent on the burn time of the individual propulsive engines for each stage. Staging must also be factored in to appropriately solve for the reduction of mass as the propellant of a stage has been extinguished. Likewise, coasting periods can be input as well as changes to the flight path angle and azimuth angle accounting for any required trajectory changes mid-flight.

Drag Prediction

Of the forces and moments acting on a missile or a rocket body, drag is the most difficult to predict or measure accurately.[35] It is of course important to minimize the drag else useful kinetic energy produced from the propellant mass expulsion is instead dissipated to thermal energy. The drag force is defined by:

$$D = \frac{1}{2}\rho \cdot v^2 \cdot C_D \cdot S \qquad (22)$$

Where ρ is the density of air at the appropriate altitude, C_D is the non-dimensional drag coefficient and S is the reference area taken as the cross sectional area of the rocket.

The drag coefficient is an especially difficult number to predict accurately because it is a function of the non-dimensional Mach, Reynolds and Knudsen numbers As such it is a function of time as the rocket progresses through different velocity values and atmospheric conditions. The drag coefficient is normally approximated until experimental wind tunnel tests or actual flight trials can be carried out. Therefore, it is sufficient to assume, for reasonable Mach numbers, that the drag coefficient is solely a function of Mach number for rockets of similar geometry. This drag coefficient will then account for the rocket skin friction, pressure drag and compressibility drag assuming a comparable rocket exists. Fortunately, a wealth of information regarding the drag coefficient for rockets has been collated since the 1950s using sounding rockets traveling at high speeds through the lower atmosphere. Figure 12 is an example of such measurements,[36] derived from the Terrapin second stage rocket launched in 1956.

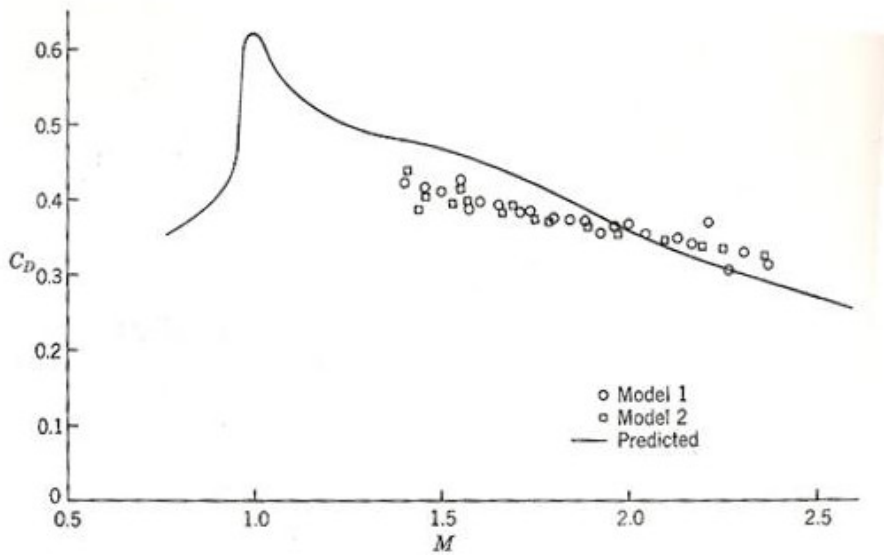

Figure 12: Drag coefficient prediction and experimental determination as function of Mach number for the *Terrapin* sounding rocket.[36]

The model used for determination of the density and other pertinent atmospheric values is based off of the 1976 U.S. Standard Atmosphere[37] compilation upwards of 86 kilometers in altitude, with a notable addition by Tewari[31] to include the 1962 U.S. Standard Atmosphere[38] that more accurately models the atmosphere in 21 layers up to 2,000 kilometers. The atmosphere model by Tewari also includes other useful parameters such as the speed of sound, Mach number, dynamic viscosity, Prandtl number, Knudsen number and Reynolds number. Velocities are solved from the solution of the inertial kinematic and dynamic equation and the reference area is an input based on the cross sectional area of each individual stage.

Gravity Calculation of a Nonspherical Earth

The Earth, flattened at its poles, deviates somewhat from a perfect sphere and needs to be modeled accordingly. The present model assumes symmetry only about the polar axis, which is true for most planets (not asteroids though), and as such we neglect longitudinal asymmetry. Then the oblateness and any other such abnormalities of Earth can be modeled by spherical harmonics for the radial gravity, g_r and the small but real g_Φ which is the transverse component due to a non-axisymmetric body.

$$g_r = -\frac{GM}{r^2}\left[\begin{array}{l} 1-3\cdot J_2\left(\frac{r_e}{r}\right)^2\cdot P_2\cos(\phi)-4\cdot J_3\left(\frac{r_e}{r}\right)^3\cdot P_3\cos(\phi) \\ -5\cdot J_4\left(\frac{r_e}{r}\right)^4\cdot P_4\cos(\phi) \end{array}\right] \quad (23)$$

$$g_\phi = -\frac{3GM}{r^2}\left(\frac{r_e}{r}\right)^2\cdot\sin(\phi)\cos(\phi)\left[\begin{array}{l} J2+\frac{1}{2}J_3\left(\frac{r_e}{r}\right)\sec(\phi)\cdot\left(5\cdot\cos^2(\phi)-1\right) \\ +\frac{5}{6}J_4\left(\frac{r_e}{r}\right)^2\left(7\cdot\cos^2(\phi)-1\right) \end{array}\right] \quad (24)$$

Where P_n denotes Legrendre polynomials and J_n are Jeffery's constants for the planet Earth, collated in Table 2.

Table 2: Jeffery's spherical harmonic values for measuring Earth's oblateness.

Jeffery's Constants	Values	Purpose
J_2	0.00108263	measures ellipticity or oblateness
J_3	−0.000002532153	pear − shaped; triangular Harmonic
J_4	−0.0000016109876	square Harmonic component

It is important to model gravity to the above indicated level of accuracy. As the results will show, the gravity turn can have a significant velocity impact on the spacecraft, not to mention the necessity of the gravity calculations in determination of the relative dynamic equations to solve the velocity vector.

Orbital Mechanics

In addition to actually launching the rocket it is necessary to derive the subsequent orbital parameters dictating where the rocket is headed, i.e. what kind of orbit it has achieved. Namely, conversion from relative coordinate frame to the spacecraft inertial frame is required. Also, there are a variety of factors that limit the type of orbit achieved. The first such limitation is the initial orbital inclination. Rockets cannot launch into inclinations lower than the launch latitude since the spacecraft must revolve around the planet center of mass, or more appropriately the barycenter. This in turn will dictate what the initial Earth-relative launch azimuth angle, A, will be to best take advantage of the Earth's rotational energy. The relation is prescribed by:

$$\sin(A) = \frac{\cos(i)}{\cos(\delta)} \tag{25}$$

Where again *i* is the intended orbit inclination, ranging from -90° to 90° for prograde orbits, 90° defined as a polar orbit and δ is the spaceport launch latitude.

A coordinate transformation is required to gain an understanding of the end results of the orbital parameters of the lofted payload or spacecraft. This transformation from the Earth fixed frame, rotating at angular speed $\omega_{E,}$ to the inertial spacecraft frame is necessary to calculate the inertial velocity, launch azimuth and flight path angle, denoted by v*, A* and Φ* respectively, relative to the celestial frame of the spacecraft. These spherical coordinate transformations, given by the relationship, $v^* = v + (\omega \times r)$, are collated below:

$$\tan(A) = \tan(A^*) - \frac{\omega_E \cdot r \cdot \cos(\delta)}{v \cdot \cos(\phi) \cdot \cos(A^*)} \quad (26)$$

$$\tan(\phi) = \tan(\phi^*) - \frac{\cos(A)}{\cos(A^*)} \quad (27)$$

$$v = v^* \cdot \frac{\sin(\phi^*)}{\sin(\phi)} \quad (28)$$

and must be appropriately solved for the inertial conditions. The solution to Equation 26 reduces to:

$$\frac{1}{\cos(A^*)}\left[\sin(A^*) - \frac{\omega_E \cdot r \cdot \cos(\delta)}{v \cdot \cos(\phi)}\right] - \tan(A) = 0 \quad (29)$$

which is an implicit function for A* and can only be determined using a root finding method. Care must be taken though to assume that the correct root is calculated as several solutions exist for the range of reasonable azimuth angles and the function is asymptotic in nature. A good initial guess for the location of the inertial velocity azimuth angle is the relative velocity azimuth angle. Once the value is calculated, the

inertial flight path angle and inertial velocities are easily found through the preceding equations.

Knowledge of the inertial coordinates allows for subsequent calculation of the orbital parameters, namely in this case the eccentricity, *e*, which is a measurement of the non-circularity of an orbit. The eccentricity has values between zero and one for orbits about the Earth; zero referring to a perfectly circular orbit and values other than zero but below one defining elliptical orbits. An eccentricity of exactly one is a parabolic orbit; the spacecraft having reached just enough kinetic energy to move outside of the Earth's gravity well and placing the spacecraft into a heliocentric orbit just outside of Earth's own orbit about the Sun. An eccentricity greater than one translates to a hyperbolic or escape orbit with some excess velocity. Such values are necessary to travel to other planets in the solar system, though an eccentricity of over one is not necessarily required for travel to our own Moon.

The relationship between circular, elliptical, parabolic and hyperbolic orbits can be derived from the trajectory equation and knowledge of the specific mechanical energy, E:

$$E = \frac{v^2}{2} - \frac{\mu}{r} \tag{30}$$

In this case the velocity "v" refers to the inertial velocity v*. The relates the kinetic energy of the spacecraft, given on the left hand side, and the potential energy of the planet. Hence if the kinetic energy is larger

than the potential energy, the spacecraft will have enough energy to successfully escape the gravitational well of the planet and excess kinetic energy to travel beyond. When used in conjunction with the specific angular momentum equation the eccentricity can be found through: $e = \sqrt{1 + \left(\frac{2 \cdot E \cdot h^2}{\mu^2} \right)}$ where $h = r \cdot v \cdot \cos(\gamma)$ again using inertial values. However, it is more telling to instead use a different equation that relates the eccentricity to the inertial flight path angle and a new variable, $\lambda_{KtoP,}$ defined as twice the ratio of kinetic energy to potential energy: $\lambda_{KtoE} = \frac{v^2}{\mu / r}$.

By substitution we obtain:

$$e = \left(\lambda_{KtoE} - 1\right)^2 \cdot \cos^2(\gamma) + \sin^2(\gamma) \quad \textbf{(31)}$$

Consequently the orbit at burnout can be determined knowing only the inertial flight path angle and the parameter $\lambda_{KtoP.}$ The importance therein signifies that for values of λ_{KtoP} = 2, the spacecraft has attained a hyperbolic exit orbit so long as the orbital path does not intersect the Earth, or more appropriately that radius of perigee r_p is greater than the radius of Earth, r_E. Thus, regardless of the flight path angle, the spacecraft has reached escape velocity.[39]

Examination of the preceding equations governing the launch and subsequent orbital trajectories over Earth shows a relationship between

the final parameters and the rotation of Earth. This link demonstrates the importance of including such effects in any robust trajectory code and can, as was explained in earlier sections, decrease the necessary Δv_T required to reach a prograde orbit. To gain the Δv_{ROT} benefit, launch vehicles must be turned into a proper Eastward direction immediately after launch. Nonetheless these trajectories have constraints. For instance, Israeli based rockets are required to launch in an inefficient retrograde orbit such that the launch vehicles do not pass over neighboring countries such as Iran. In this manner the orbital stages will instead fall to the Mediterranean Sea. Iran has a similar problem,[10] and both countries have launched or proposed the launch of spy microsatellites and would benefit from the proposed architecture.

Similar problems of launching over land are also present for other countries, even the United States. A discussion with officials from Spaceport America in New Mexico expressed major concerns over the launch of the proposed architecture in an Eastward direction. Though it would of course be more efficient to launch in this manner, having turned abruptly after liftoff, the spaceport seeks to limit this maneuver in order to mitigate the problems arising from dropping unused stage masses over their Eastern neighboring states, namely Texas. Such maneuvers are discussed in the next section including a novel compromise orbit that may be more suitable.

Gravity Turns and Attaining Orbit

Modern day launch vehicle flight profiles follow the general trajectory illustrated in Figure 13 with a few small amendments. Ordinarily rockets will fly in a nearly vertical trajectory for a matter of seconds to clear the launch rail then begin a constant flight path angle change to initiate a gravity turn. In fact, it is best to attain a low circular orbit, i.e. $\Phi=0°$, to reduce gravity losses then use the upper stage engines to increase the velocity of the orbit until a higher orbit is attained.[40] This is called a *super-orbit*, where an initial circular orbit of low altitude is attained, and then subsequent acceleration will raise the spacecraft to a higher orbit. Reaching a low initial orbit has its limits. It is not possible to attain a very low initial orbit without incurring a substantial amount of Δv_{DRAG} losses as a result of flying quickly through the thickest part of the atmosphere. More importantly, flying at high orbital velocities through the Earth's atmosphere is not feasible due to high dynamic loads and aerothermal heating.

Though a gravity turn is used in most cases the change to the flight path angle of zero can be subtle, having reached the intended orbit after minutes of flight at every decreasing values of Φ^*.

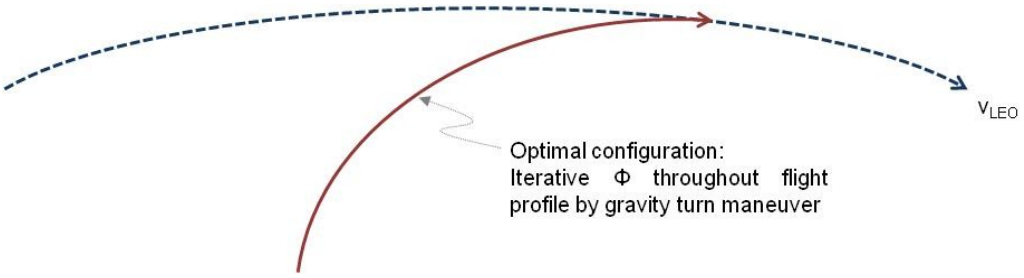

Figure 13: Illustration (not to scale) of optimal launch trajectory to stable LEO.

A gravity turn includes the combined effects from gravity and the rotation of the Earth to minimize the $\Delta_{gravity}$ losses by steering the velocity vector in line with the vehicles longitudinal axis prescribed by:

$$d\gamma = -\frac{g\cos(\gamma)}{v} \tag{32}$$

Gravity turns from a rocket attitude adjustment or initial flight path angle are including in the previous set of equations of motion for the rocket. Likely a gravity turn maneuver does not work well enough, or minimize the $\Delta v_{gravity}$ losses enough alone. Instead steering the vehicle into a linear-tangent, or ramped angle of attack often works well once the rocket has reached an altitude commensurate with minimal drag losses.[28]

However, if a long land track over the surface of the Earth whilst in the atmosphere is not desirable, then the rocket could make use of a nearly vertical trajectory and force a flight path angle of zero when it reaches the destination orbit. This scheme is illustrated in Figure 14.

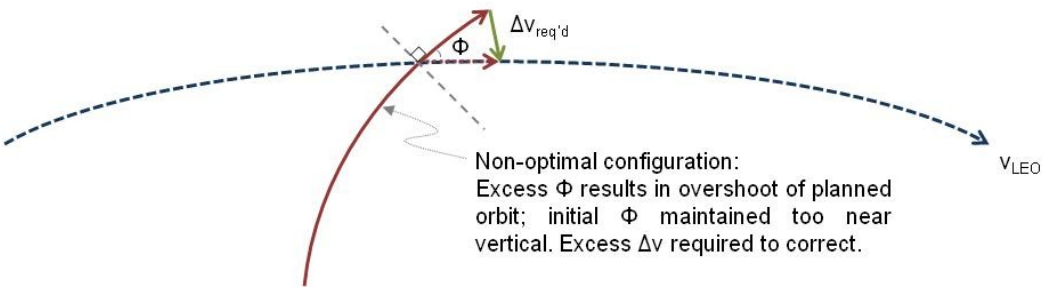

Figure 14: Illustration (not to scale) of non-optimal launch trajectory to LEO with initial flight path angle maintained throughout majority of flight.

Of course this abrupt change in velocity, which can be considered impulsive, would be quite expensive in terms of Δv losses if the flight path angle relative to the horizon is large. Smaller changes in flight path angle would subsequently be smaller according to the law of cosines:

$$\Delta v_{\Delta\phi} = \sqrt{(v^*)^2 + (v_{LEO})^2 - 2 \cdot v^* \cdot v_{LEO} \cdot \cos(\phi)} \qquad (33)$$

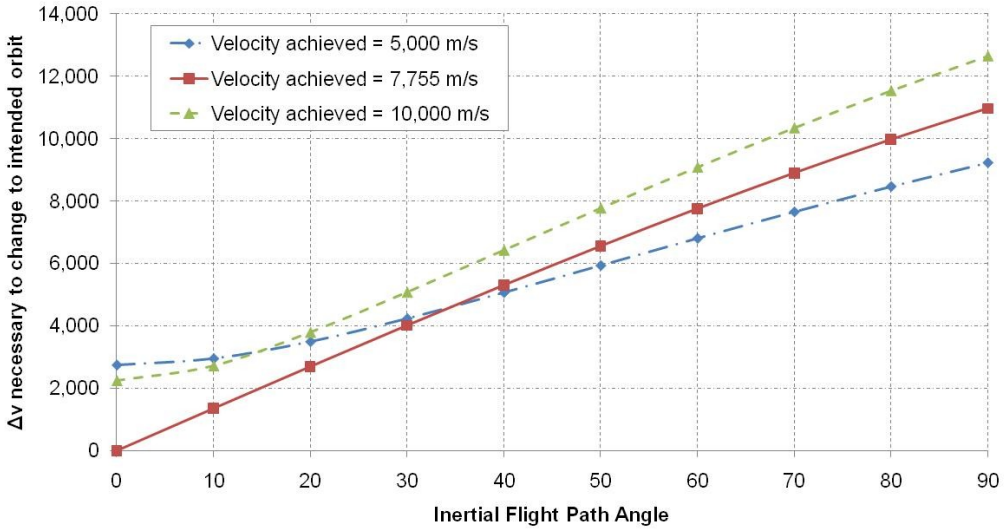

Figure 15: Δv required for impulsive change to an orbit of 250km, v_{LEO}=7,755 m/s for differing excess velocities.

This type of impulsive maneuver for small changes could also be used to change the ellipticity of an orbit, though as the equation describes should be completed if possible when the velocity of the intended orbit is small, i.e. at the point of apogee for a non-circular orbit.

A potential compromise is to (1) limit the $\Delta v_{gravity}$ losses while still (2) transverse over a minimum amount of land, specifically during the initial boost phase. In essence the rocket would only travel in a vertical trajectory for as long as the initial boosters are thrusting. This concept is illustrated by Figure 16. After the zeroth and first stage burnout the stages would still be at a position nearly above the launch site or appropriately launched to a position where they would fall in a controlled area near the launch site. These boosters would either tumble to their demise or deploy parachutes such that they could be refurbished and possibly reused at a later date.

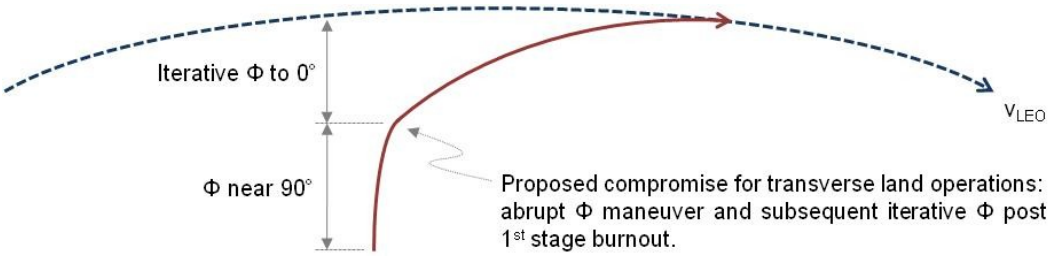

Figure 16: Proposed launch trajectory to minimize travel over populated land masses until stage separation. Results in reduced final payload mass to orbit.

While literature describes this type of maneuver, studies have shown that the payload mass might be decreased as much as 70%

through by this method. However, another study showed that this shortcoming could be alleviated by properly selecting the staging ratios and that the payload might then only be reduced by one third. [29] It is one of the purposes of this dissertation to further define this maneuver as an accessible means of safely entering LEO transverse to populated land masses.

3. Vehicle Design and Performance

Performance of Standalone Booster Configuration

It is instructive to begin the design process with a validation case comparing the performance of the trajectory code verses analytical expressions and empirical data. An ideal case might start with an assumed one-dimensional rocket launch, though such an analysis could not include more complicated functions such as gravity turns. However, it would suffice to compare these quantities to empirical data derived from previous launch vehicles and validate the individual components, e.g. percentages of velocity lost due to gravity, drag, etc. This design exercise will show the magnitudes of such contributions and identify the limitations of analytic computations.

With some foreknowledge of the ideal configuration, this design exercise will entail a three (3) stage rocket design complete with two (2) zeroth stage parallel boosters. The motors chosen are Mk70 boosters and Mk30 sustainers; both using solid rocket motors and which can be obtained from military surplus. These rocket motors were used on the Standard Missile-2 (SM-2), pictured in Figure 17, built by Raytheon Missile Systems to serve as the U.S. Navy's surface to air missile by the Aegis combat system. The SM class of missiles has been used by the U.S. armed forces since the late 1960s, and continues today as different block designs, with the new SM-3 class having anti-ballistic missile and anti-satellite capabilities. Furthermore, the Mk70 booster is a direct derivative

of the older Terrier class missiles and is sometimes referred to as a *terrier* booster. Thousands of such missiles have been manufactured, many of which have been retired after reaching their long shelf-life. However, these motors can still be considered for use after a series of refurbishments. This process is described in the next section.

Figure 17: A Standard Missile 2 (SM-2) composed of a Mk70 booster and a Mk30 sustainer is launched from a U.S. Navy Aegis Combat System Destroyer.[41]

The motivation hereafter is to build off the successful history of the SM family of surface to air missiles and retrofit or refurbish them such that they can loft a small payload to orbit about the Earth. The proposed architecture is modeled in Figure 18. This design configuration illustration will not change drastically for the following designs. The external geometries remain largely unchanged, only the operating and trajectory

characteristics, adjustments to the nozzles, and addition of a fourth stage for orbital maneuvering encompass the bulk of the required changes.

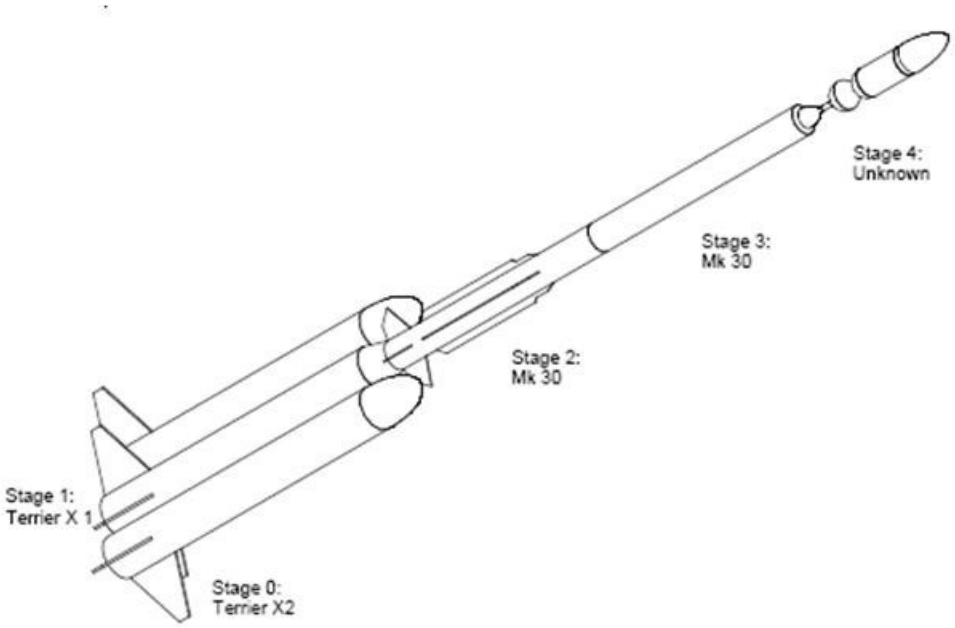

Figure 18: Proposed launch configuration utilizing demilitarized and refurbished Mk70 and Mk30 solid rocket motors and fuselages.

Other variations are of course possible. In addition to differing staging schemes (more/fewer stages) there exists a large assortment of different existing baseline solid rocket motors to use that would fit the profile well. The exercise here was to limit the development of new motors, possibly only a re-qualification of existing motors to the different operating conditions and require nozzle refurbishments. This would be in the form of a small re-qual program including updated thermal conditioning, launch and transportation shock and vibration at their current aging status. A robust concept selection method should be employed to arrive at the optimal configuration for a given mission. However, lacking

mission constraints, the above figure shows a suitable concept that can indeed loft significant amounts of payload to LEO at a total payload fraction, m^*/m_o, of 2.8%. Reference 42 gives an excellent example of a concept selection to better suit the mission profile, namely launching from the current U.S. Navy Mk-41 Vertical Launch System (VLS). In this case the entire launch vehicle must be shorter to fit within the limited constraints of the launcher (266 inches in length with each cell capable of holding up to 22 inches in diameter). However, it is not the purpose of this dissertation to optimize the final configuration, but rather to show steps that can be taken once a mission profile has been given and a suitable base design is selected.

Next, the discussion proceeds with a design example to demonstrate the capabilities of the boosters in a stand-alone configuration launching a 50 kilogram payload in a sounding rocket trajectory. That is to say, what is the result if the motors were simply stacked one upon another and fired as-is, no changes to motor characteristics or steering added. The listed values in Table 3 do not necessarily represent the actual motor performance characteristics of the motors as such numbers are proprietary, but they do provide rough estimates and are suitable for preliminary designs.

Table 3: Pertinent Operating Characteristics of Standalone Configuration; no Refurbishments Performed to Motors or Trajectory.

Stage #	Type	m_o [kg]	m_p [kg]	t_b [s]	I_{sp} [s]	Thrust [N]
Stage 0	2 x Mk70	1,909	1636	6.2	260	698,863
Stage 1	Mk70	991[1]	818	6.2	260	349,431
Stage 2	Mk30	373	296	32	260	23,542
Stage 3	Mk30	373	296	32	260	23,542
Payload	m *	50	n/a	n/a	n/a	n/a
Total:		3,696	3,046		Total impulse:	8MN

A statement of the initial conditions for the launch is required such that the Runge-Kutta solver can solve the coupled set of kinematic and dynamic equations of motion governing the rocket flight through the atmosphere and continuing into space. The initial launch position, used throughout the remaining launch configurations, is that of the new *Spaceport America* launch complex in New Mexico. Initial starting values are listed in Table 4 and the graphical results follow, starting with the three dimensional trajectory plot, Figure 19.

Table 4: Initial Conditions for Standalone Boosters Trajectory

Initial Condition	Variable Symbol	Value	Units
Longitude	λ	-106.9574	degrees
Latitude	δ	33.060241	degrees
Radial Distance	r	6,378,140	m
Velocity	v	0	m/s
Flight Path Angle	Φ	90 (vertical)	degrees
Velocity Azimuth Angle	A	90 (East)	degrees

[1] Includes weight of coupler for Mk30 sustainer estimated at 80lbs or 36.4 kg.

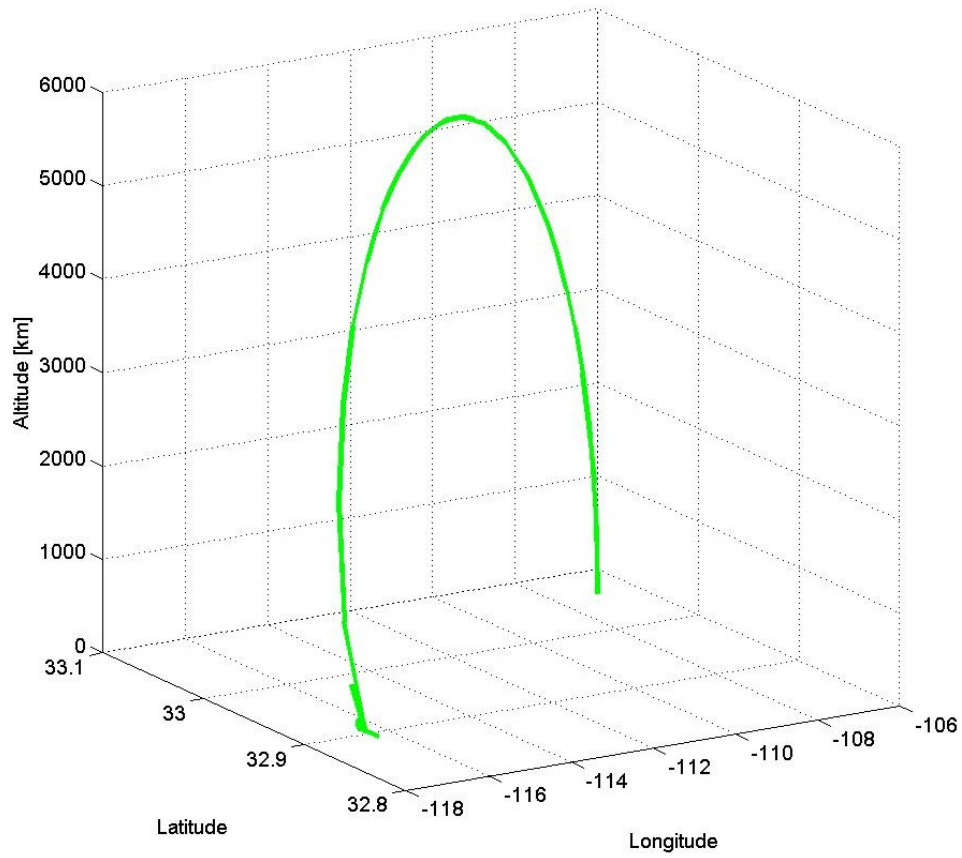

Figure 19: Trajectory trace for Mk70/Mk30 stand-alone booster configuration case with 50 [kg] payload. Axes not to scale.

As might be expected the rocket is a on a suborbital trajectory, that is to say that the final stage of the rocket reaches a maximum altitude, 5,661 kilometers, then returns to Earth approximately one hour after its departure. The final leg of reentry is not accurate as it does not include the aerothermal effects acting on the reentry vehicle. Note in Figure 19 that the trajectory (1) hardly deviates in the latitude (North-South) direction due to the chosen flight azimuth angle of 90°, and (2) the rocket has a

Westerly travel. Recall that this ground track is relative to a rotating Earth, and therefore is different than the inertial orbital projection. Following this plot would lead one to believe that the rocket moves about 10° of longitude to the West (landing in the Pacific Ocean just south of California) though it is a small displacement compared to the nearly 6,000 kilometers of vertical travel above the Earth's surface. Transformation to the inertial frame would instead reveal an Eastward travel of $\omega_E * t_b$, or nearly 16.5° change in latitude from the relative position, or 6.5° to the East: firmly in the state of Texas.

This reentry is further shown by examining the relative flight path angle which will not change substantially for inertial coordinates. Figure 20 shows the initial flight path angle of 90° change as it reaches the apogee of its trajectory, eventually reversing 180° in the inertial frame to 270° in the Earth-relative frame. The rocket will stay on this flight path angle up until it impacts the Earth. In contrast, the azimuth angle does not change until the point of impact which explains the very small change in the latitude trace of Figure 19.

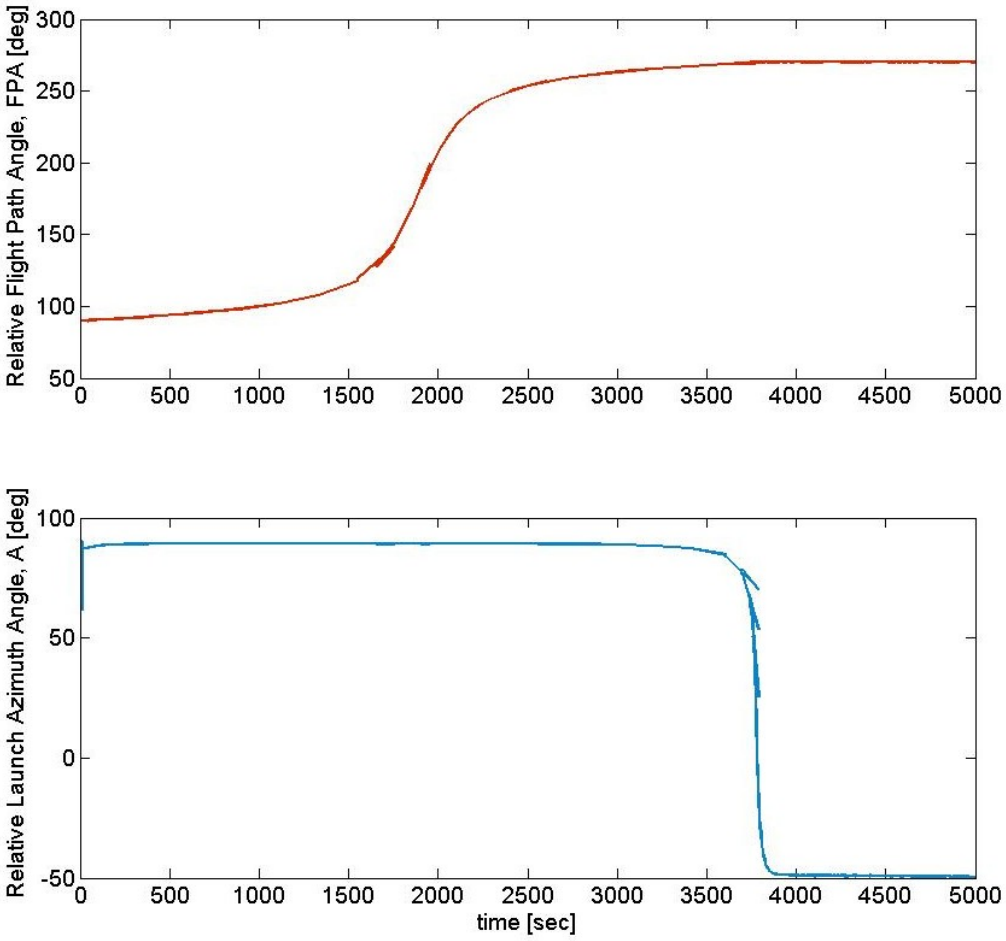

Figure 20: Relative flight path and launch azimuth angles for stand-alone booster configuration with 50 [kg] payload.

Through further examination of the velocity during the boost phase, Figure 21 reveals the potential for orbital attainment of the rocket configuration.

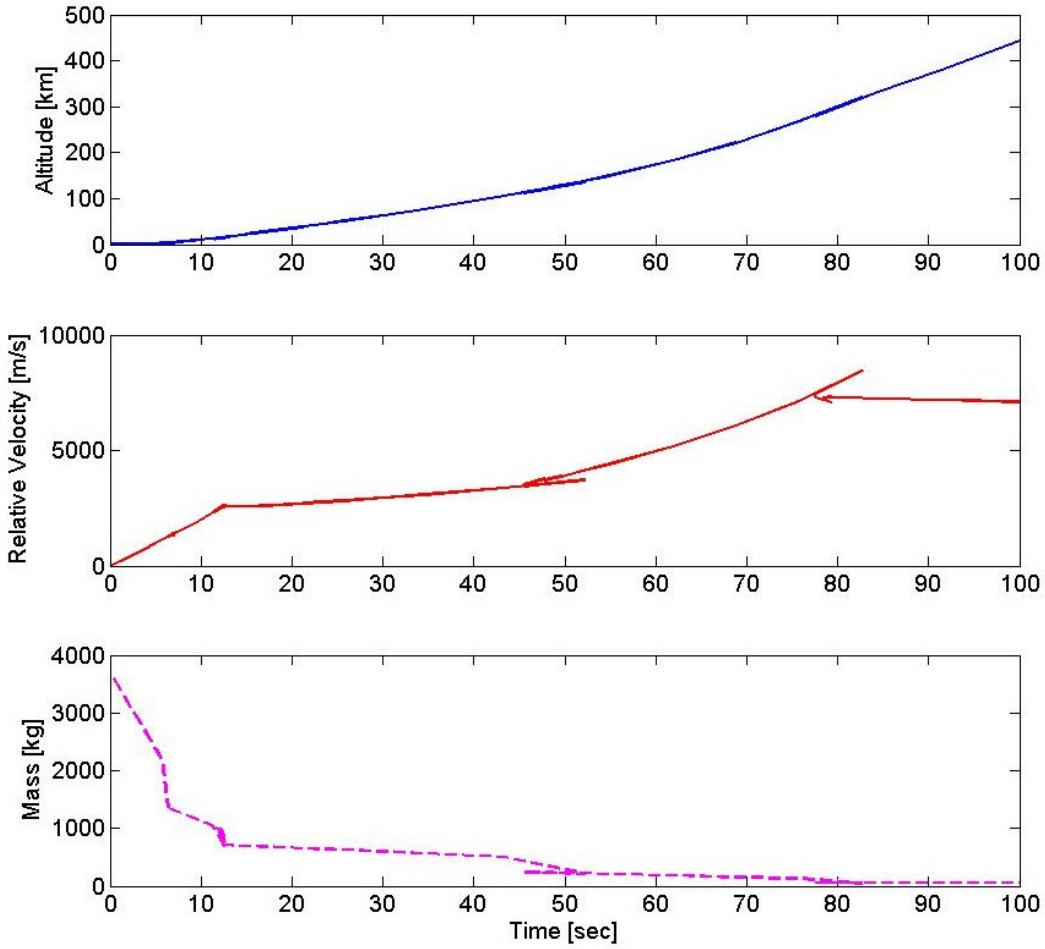

Figure 21: Altitude, relative velocity and rocket mass during boost phases for stand-alone booster configuration with 50 [kg] of payload.

At burnout, the rocket's relative velocity is 7,314 m/s, though if transformed to its inertial velocity of the final stage, is 7,329 m/s showing negligible gain from any small gravity turn up to that point. Even after only 80 seconds of flight this rocket has already covered over 250 kilometers (267.8 km) in altitude. At this altitude the velocity required to maintain a stable orbit is approximately 7,755 m/sec. Thus it demonstrates that the configuration is capable of reaching orbital velocities at altitudes

commensurate with LEO satellites. However, for this suborbital case the flight path angle is nearly 90°, meaning that an orbital change to the proper orientation would be very costly; refer to Figure 14 and associated discussion. At the minimum this rocket requires an iterative turning maneuver including the use of a gravity turn to place any appreciable payload into orbit.

Furthermore if the eccentricity of this orbit is examined, it is apparent that it approaches 0.9. This is a highly elliptical orbit with a radius of perigee smaller than the radius of Earth, thus it intersects the Earth as illustrated in the above figures. Such a high eccentricity hints at the possible capability of hyperbolic orbits, i.e. a rocket capable of leaving Earth's gravitational influence, and is discussed in a later configuration of the vehicle.

For comparison purposes it is prudent to examine the velocity losses of the rocket to assess the functionality of the trajectory code verses known values. These values are collated as such:

Table 5: Velocity budget for stand-alone booster configuration.

Change in Velocity	Value (m/s)
$V_{obtained}$	7,329
$\Delta v_{gravity}$	604
Δv_{drag}	817
$\Delta v_{rotation}$	15
ΣV_{TOT}	8,765

Examining the losses due to gravity up to the end of the boost segment from all stages is approximately 8% of the Δv obtained, which is in good agreement with similar launch vehicles. As an estimate, the $\Delta v_{gravity}$ can be approximated by $\Delta v_{gravity}=g_o*t_b$, or 755 m/s for a rocket with a straight vertical component. The discrepancy between these two values accounts for the change in gravity during the flight up to the final burn out altitude of 267.8 kilometers as well as the small change in flight path angle. Both will effectively reduce the $\Delta v_{gravity}$ losses, thus it is suggested to start the gravity turn close to the start of the initial takeoff. Though flight path angle changes will invariably increase the travel time to orbit and thus invoke additional gravity losses. Losses due to drag however are higher than normal, nearly five times as much. The reason for this is shown below in Figure 22:

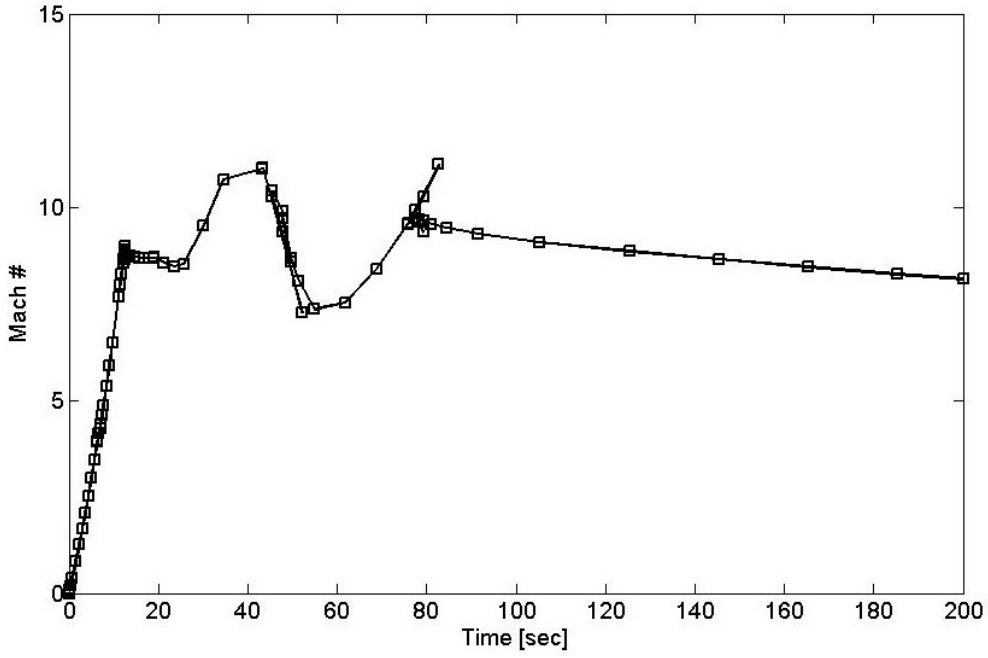

Figure 22: Mach number verses time for stand-alone booster configuration with 50 [kg] payload. Mach number in excess of 10 during flight through lower atmosphere.

As shown in the above figure, the rocket approaches a Mach number of 10 prior to 20 seconds into the burn. The altitude covered during this span is only 32 kilometers. Therefore, the rocket is accelerating substantially through the thickest part of the atmosphere and according to the drag equation the drag force goes as the square of velocity. The rocket is therefore accruing considerable dynamic pressures and aerodynamic heating well beyond the design capabilities of the Mk70 and Mk30 missiles. This problem is attributed to the fast burn times of the Mk70 motor, approximately 6.2 seconds in its current configuration.

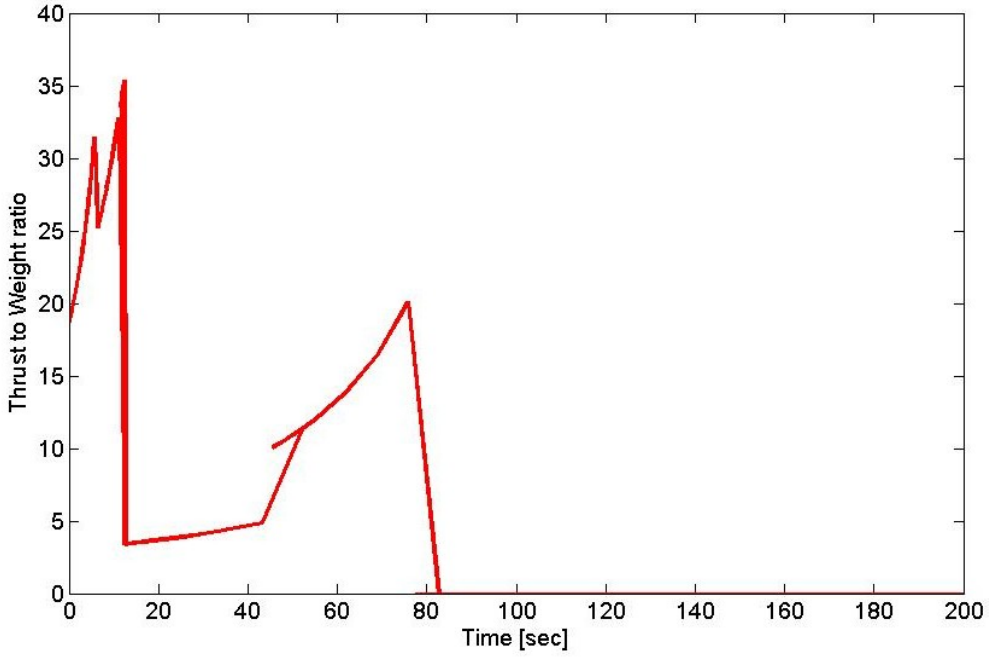

Figure 23: Rocket thrust to weight ratio verses time for stand-alone booster configuration with 50 [kg] payload. T/W ratio peaks at 35; highly undesirable.

Furthermore, Figure 23 illustrates the subsequent thrust to weight ratios of such a design. Similar to the Mach number plot, these values are in excess of the design constraints of the existing motors. Values at least below 20 would be structurally manageable. To alleviate both of these issues a reduction in motor burn times is required.

Required Refurbishments / Refitting

Before the analysis can proceed with additional flight profiles it is appropriate to address the necessary modifications and additions to the existing Mk70 and Mk30 surplus military missiles. As discussed

previously, the aim of the new launch vehicle should be to alleviate the common problems amongst current space launch vehicles, namely:

1. *Reduce launch system complexity by reducing the number and complexity of tasks required by human intervention.* Therefore it is advisable to include a high degree of commonality between differing stages as well as simplified payload launcher interfaces. Using decommissioned military missiles for the various stages certainly accomplishes these recommendations.
2. *Increase subsystem accessibility as a driver for system maintainability.* Such missiles are not necessarily designed for such quick access, but are instead designed such that such maintenance is not required. However, fluid and mechanical systems designed for the launcher should include such accessibility as they are often the culprit for required internal tests.[26]
3. *Make payload interfaces independent of the launcher, with standardized interfaces*. Payload integration constitutes a major fraction of the cost of launch operations. Therefore payloads should be designed as independent of the launch vehicle as possible.[26]
4. *Use less toxic propellants.* Although hydrazine is an optimal candidate for in-space missions, launch personnel must

wear hazard suits to protect themselves from the carcinogenic or corrosive materials. Use of a new propellant comparable to hydrazine will be examined in this dissertation to eliminate a significant amount of ground processing which has been shown to provide economic benefits.[27]

As addressed in the prior section, the most necessary change to the design system is that of burn times. There are multiple reasons for this:

(1) Shorter burn times are required to limit the velocity while the rocket travels through the lower atmosphere, thereby reducing drag and associated aerothermal heating issues and structural loads.

(2) In addition, the thrust to weight ratio is excessive without reductions in burn time.

(3) And use of older residual military boosters that are past their shelf life will likely lead to some degradation of the propellant by means of crack formation.

While the first two are pivotal to the immediate design exercise, without which the mission would be unrealistic, the third bullet is key to maintaining sufficient cost margin to make the mission ultimately financially viable. The reasoning for this is quite apparent when evaluating the cost of newly manufactured rocket motors. Mk70 boosters (and their

kinematic upgrades, Mk72) cost well in excess of $100,000. For example, the SM2 all up round as seen in Figure 17 costs over $400,000 whereas the upgraded SM3 costs in the range of $9 to 24 million.[43] On the other hand, decommissioned motors can be purchased for significantly lower prices, one example citing only $15,000 for the Mk70 booster (including fins) for use on NASA Black Brandt XI and XII sounding rockets launched from WSMR.[44] Therefore, in the interest of significantly lowering launch costs it would be highly desirable, where possible, to refurbish and reuse existing stockpiles of decommissioned rocket motor hardware.

Though the cost benefits are enormous, the use of decommissioned rocket motors is generally done on a limited basis; mostly for research endeavors. The reason for this, as alluded to in the previous paragraph, is that rocket motors generally suffer from deterioration when subjected to a number of stimuli over their lifetime. Figure 24 illustrates an example of a hypothetical motor undergoing the myriad of adverse stimuli and its associated cumulative damage. Though cumulative damage is easy to illustrate in this figure (both the level and its bounds), it is quite difficult to measure. Usually aging surveillance would relate not to the damage, but to allowable limits of its propellant modulus (effective or relaxation). Real-time aging of solid rocket motors, especially in-service motors, is not easily calculated as it can be greatly extended or degraded by exposure to a number of stimuli which are different for each motor/propellant combination. In general, age prediction of the non-linear

viscoelastic composite propellants normally found in solid rocket motors relies on these three features [Ref. 28]:

- Induced loads from transportation and handling such as temperature, humidity, shock, vibration, accelerations, pressure and gravity.
- Mechanical properties of the material (material response and failure). These include relaxation modulus, poisson ratio, coefficient of thermal expansion, etc.
- Chemical properties which drive the natural aging and damage response of the propellant. These are mainly driven by migration and diffusion of different chemical specific through materials over extended periods of time.

Of these, temperature and humidity are particularly well-known culprits in advanced aging of propellants. Many motors undergo accelerated aging using these two factors as prime variables, as seen in the Arrhenius equation.[45] For well sealed motors, the temperature usually dominates the aging mechanism, namely cross-linking between the oxidizer (e.g. Ammonium Perchlorate) and polymeric binder (e.g. HTPB).[46] To some extent this can be mitigated by good choices in regards to bonding agents, etc. but generally they are to the detriment of performance. For example, more binder percentage often increases the mechanical properties,[28] but leaves less volume for energetic materials, i.e. lower propellant solids loading.

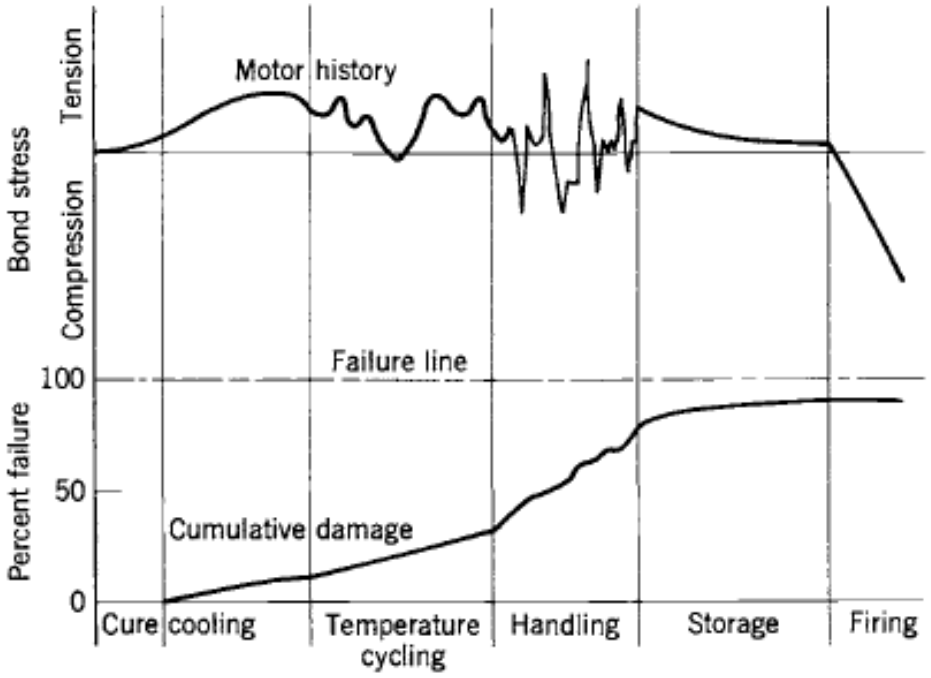

Figure 24: Hypothetical stress history and associated cumulative damage of a solid rocket motor over its lifetime.[66]

Rocket motor composite propellant aging manifests itself as a number of failure modes including, but not limited to: propellant deformation or cracking, propellant voids, and insulator cracking and debonding. A known reason for this is that while a motor ages and goes through thermal cycling, the motor bore is hardened and is therefore more susceptible to damage.[47] Over time or with a rapid pressure rise this can lead to cracking of the rubbery propellant.

A key concern with motor aging is that when the motor fails it will likely be catastrophic, not only resulting in a mission failure, but also a possibility for loss of life. A known failure mode is attributed to grain damage upon ignition, where the transient pressures from start-up are

very large. This large rise in axial pressure distribution can end in grain breakup if the propellant modulus cannot withstand the flux, resulting in significantly higher surface area (which drives pressure and thrust, adding to runaway pressure buildup) and possibly ending in catastrophic failure. This is compounded by the fact that if the motor explodes on start-up, it is in close proximity to the launch area, normally a ship, aircraft, or ground crew. Such unpredicted failure risks are not taken lightly, so rocket motor munitions are often given a short life span and retired or de-militarized thereafter.

With those risks known, it has still been estimated from the Naval Surface Warfare Center at Indian Head that for one type of missile "98% of its missiles taken out of service are actually viable and removed from service prematurely".[48] The need for rocket motor prognostics and health management (PHM) is therefore great. However, many programs do not pursue predictive aging, the most common of which is expensive destructive testing at staged intervals in the rocket motor lot's lifetime.[49] Even then, the lifetime of tactical motors is rarely extended. This is due to the lack of data surrounding its load and environmental history and a lack of a satisfactory technique that could predict the cumulative damage and yield a service life extension. Yet another reason for this is motor-to-motor variability as each motor experiences a different load and environmental history. Thus taking a small sampling at a specified aging point for one motor is not enough evidence to provide service life extension for the

entire lot, even if it was mixed from the same propellant batch. A number of efforts have been ongoing for the past several decades to provide rocket motor prognostics and health monitoring. This is achieved by either active techniques such as temperature, humidity and pressure data logging or more direct methods employing small sensors to directly measure the stress field.[50] Such methods are currently being deployed on a limited number of live rocket motors for field testing and surveillance.[51] Both rocket motor suppliers[49] and government laboratories[48] are amendable to such sensing techniques and have researched and endorsed differing methods over the years.

With regards to propellant aging it is apparent that higher pressures during ignition transient and following through to stable combustion, are a detriment to aged motors. Thus it is wise to limit these pressure extremes to mitigate initial propellant cracking and limit burning of additional surface caused by small aged cracks or propellant voids. In a likewise fashion these smaller chamber pressures would lead to increased burn times which is a benefit to the proposed architecture. According to the fundamental equation for regression rate of a solid rocket motor, these shorter burn times can be set by increasing the nozzle throat size to reduce the chamber pressure.

$$\frac{dr}{dt} = \dot{r} = a \cdot {p_o}^n \tag{34}$$

Where *a* and *n* are regression rate coefficient and exponent, respectively. Such numbers are derived empirically for each unique propellant combination through small scale burn rate tests and can be assumed constant for a large range of motor operating pressures.

A decrease in chamber pressure will result in a lower solid rocket motor regression rate. This regression rate is directly proportional to the mass flow rate of the rocket motor by the following equation:

$$\dot{m} = \rho \cdot \dot{r} \cdot A_b = \frac{p_o \cdot A^*}{c^*} = fn(p_o) \quad \textbf{(35)}$$

Which is of course related to the total thrust of the rocket motor by the following equation, hence it will take more time for the propellant to be extinguished by changing one of these key variables, in this case the throat area, A*.

$$F = \dot{m} \cdot Isp^{eff} \cdot g_o = p_o \cdot A^* \cdot C_F = fn(p_o) \quad \textbf{(36)}$$

Tactical solid rocket motors operate at high operating pressures, so the increase of the nozzle throat can effectively drop the operating pressures in the range of 500 to 600psi, where the specific impulse will decrease only slightly. Additionally, since the area goes as the radius squared, even small changes to the throat geometry can have the desired effect.

As an example the author has experience with custom solid rocket motor propellant mixing and changing the nozzles to achieve drastic

changes in operating pressure. In addition to propellant strand testing in a Crawford Bomb[52] at multiple pressures, the empirical “a” and “n” values from the regression rate equation can be found by operating a propellant at a minimum of two different pressures, or two different nozzle throat areas. One such example is cited in Reference 53, whereas a new propellant formulation (5% aluminum, 83% solids loading with dual AP particle sizes) was found to have an “a” and “n” value of 0.0012 (in/a*PSI^n) and 0.8857, respectively. This “n” value is quite high, by design, meaning even a small change in pressure can have a large effect on the burning surface rate.

In this specific example, the ratio of the burning surface area of the propellant to the nozzle throat area (this ratio is known as the “Kn” value) were 197 and 280 for the larger and smaller nozzle throats, respectively. This lead to a difference of operating pressures from an average of 800psi to over 2,200psi for the large and smaller nozzle throats, respectively. The burn times thusly changed from 1.2 seconds to 0.4, meaning that a 40% change in Kn dropped the pressure by 50% but decreased the burn time by 300%.

It should be said that most production mixes only go up to a combustion index “n” of approximately 0.6. For the purposes on this dissertation topic it is beneficial to have larger indexes as that would limit the amount of nozzle refurbishments to smaller increases in diameter. Of

course, this burning rate is also dependant on the chemical makeup of the propellant. A large range of regression rates are available:

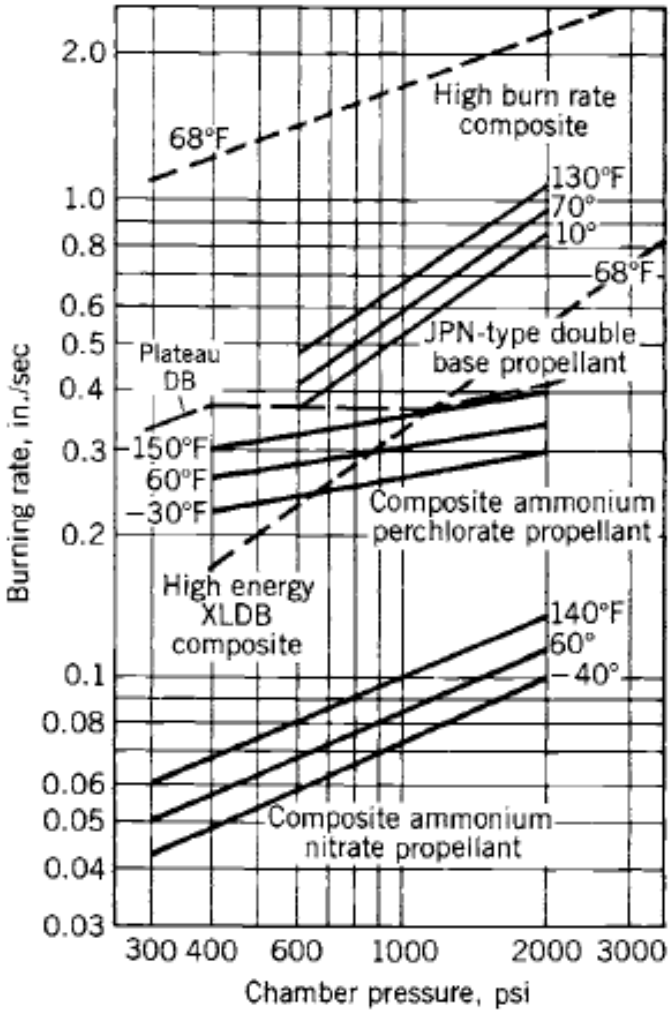

Figure 25: Plot of burning rates as a function of typical propellant type, chamber pressure, and ambient temperature.[66]

As an added caveat, removal and subsequent replacement of a new nozzle affords the opportunity to optimize the nozzle further for the new mission. This would be accomplished by replacing the Mk70 and

Mk30 nozzles, which are expanded to very low comparative altitudes, with a higher expansion ratio nozzle to increase the thrust coefficient (recall $F = p_o A^* C_F$) of the motor beyond the factory installation. This would be more pronounced for the Mk30 motors since they will be operating at much higher altitudes with lower ambient pressures. The gains are clear, as shown in Figure 26, with changes from an expansion ratio of 6 to 10 or even 20 increasing the Isp a factor upwards of 15%! For the final stage motor design a more appropriate value of 50+ should be chosen for a C_F over 1.7.

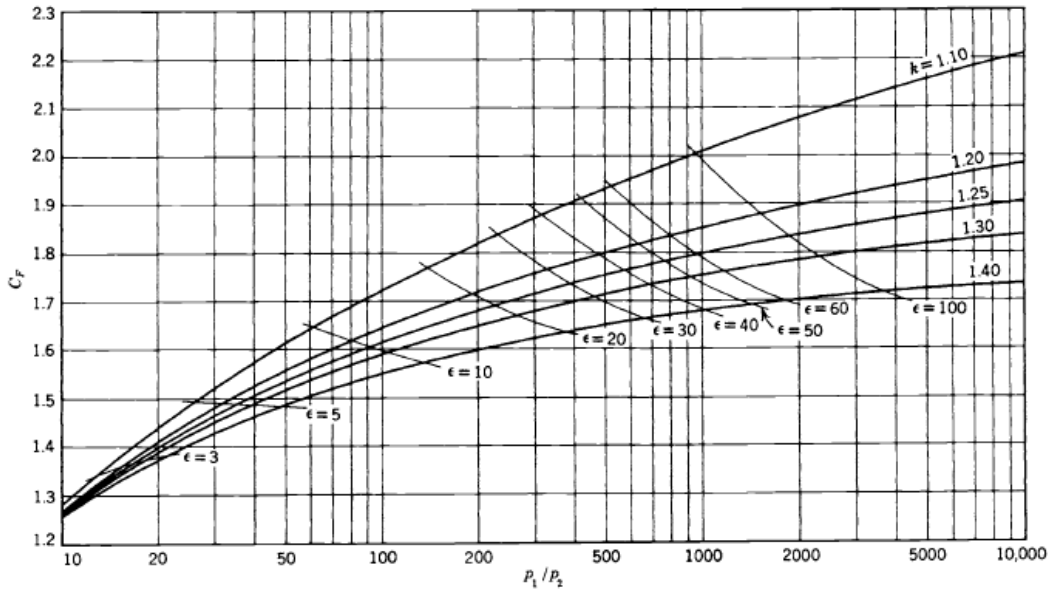

Figure 26: Thrust coefficient C_F as a function of pressure ratio, nozzle area ratio and ratio of specific heats.[66]

Additional use of advanced nozzle materials might help reduce the increased weight of the now larger expanded nozzles, but the performance gains would make up for such shortcomings and allow

additional weight margin for structural growth and thrust vector control additions. More advanced nozzle designs, such as extendible segmented nozzles or aerospike nozzles[54] could be used as well, increasing the thrust coefficient dramatically for the upper stages. For the purposes of the dissertation, to remain conservative, the total impulse was assumed constant when changing the nozzles. For the following examples, the nozzles have remained at roughly their same expansion ratio, with stage Isp's of 270 seconds. This could likely be driven higher (280+) with optimized nozzle replacement but we will remain at these conservative values.

The examples given in this section have shown that a simple change in nozzle configuration, keeping the motor grain intact and unchanged, can result in decreased chamber pressures. These decreased pressures in turn drive lower regression rates which limit the thrust and increase burn time. The former is good as it will reduce aerothermal heating, drag and large thrust to weight ratios which would require more structural margin to withstand. The latter is beneficial as it greatly mitigates the propensity for aged propellants to crack and subsequently burst. In addition there is a viable performance increase if the new nozzles are optimized properly to the new higher altitude mission. Nozzle changes are therefore required for the success of this mission profile to LEO.

Earth Escape Capable Performance Evaluation

A primary consideration of this rocket architecture was the potential for direct escape velocity such that the rocket could loft small payloads, on the order of 50 kilograms to Earth's Moon. From the previous example it is also shown that the rocket could not be launched in its current configuration; the rocket would not survive such excessive Mach numbers and thrust to weight ratios in such thick parts of the lower atmosphere. Using the methodologies listed above, the rocket nozzles, specifically the Mk70 booster nozzles, were redesigned to provide a lower chamber pressure thus a higher burn time, more than twice the previous value of 6.2 seconds.

Table 6: Operating Characteristics of Direct Escape Rocket

Stage #	**Type**	**m_o** [kg]	**m_p** [kg]	**t_b** [s]	**I_{sp}** [s]	**Thrust** [N]
Stage 0	2 x Mk70	1,909	1636	15	270	288,863
Stage 1	Mk70	991	818	15	270	144,431
Stage 2	Mk30	373	296	32	270	24,448
Stage 3	Mk30	373	296	32	270	24,448
Kick Stage	liquid	200	150	60	350	8,581
Total:	–	3,846	3,196	–	– –	-

As will be shown, a new requirement is born to meet the conditions of escape velocity, namely that the eccentricity value is over 1. This new problem reveals the need for an additional high performance stage, more akin to a liquid rocket engine specific impulse. However the stage does not need to be large, it will just act as a kick stage to place the final

payload, set at m*=50 kilograms, on a hyperbolic orbit. Again launching from a flight path angle of 90°, the velocity plot is shown in Figure 27.

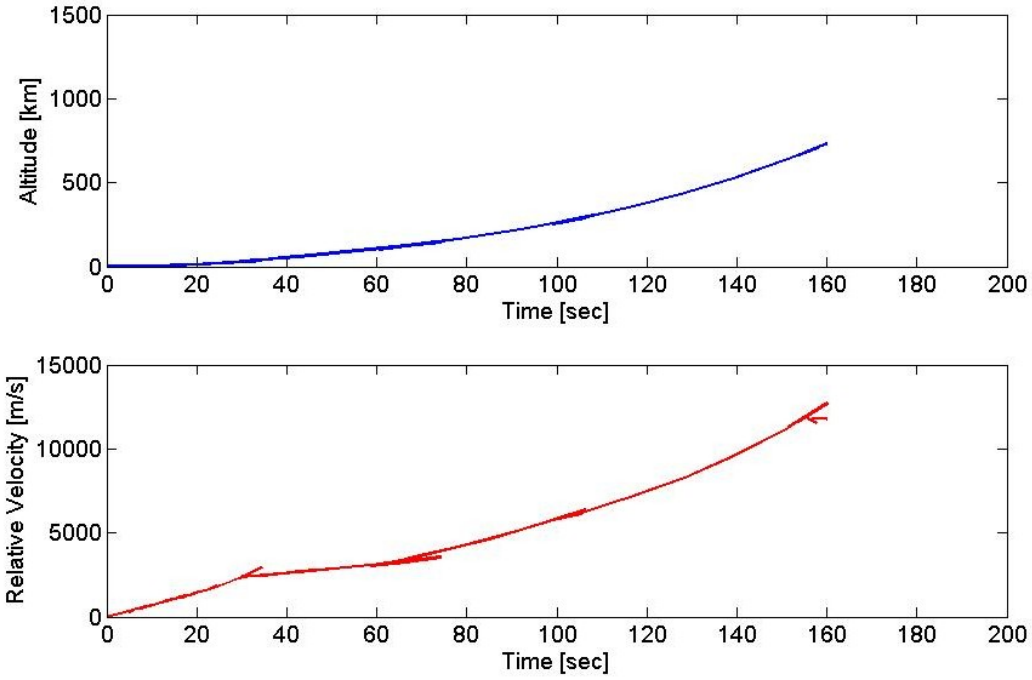

Figure 27: Altitude and relative velocity for escape capable launch vehicle configuration.

The above plot illustrates a relative velocity of 11.43 km/sec, well over the escape velocity requirement of approximately 11.2 km/sec from Earth's gravity, but at the expense of significant drag losses of 1,650 m/s. Though, as illustrated, a change in initial flight path angle could have more profound effects on the losses endured through the flight. The results of changing these values are collated in the below table.

Table 7: Changing Δv losses for different initial flight path angles.

Φ_i	Δv_T	Δv_{grav}	Δv_{drag}
90°	$11.43\ \mathrm{km/s}$	$1{,}650\mathrm{m/s}$	$212\mathrm{m/s}$
80°	$11.64\ km/s$	$1{,}500\mathrm{m/s}$	$280\mathrm{m/s}$
70°	$11.81\ \mathrm{km/s}$	$1{,}290\mathrm{m/s}$	$390\mathrm{m/s}$

These values illustrate that launching at a smaller flight path angle will result in more total velocity attained at the end of the final burn time. This is at the expense of more drag losses due to longer flight times through the atmosphere, but substantially reduced gravity losses. These gravity losses make up the bulk of the Δv losses and should therefore be minimized at all costs by gravity turn and linear-tangent steering methods. The final inertial values for the 70° launch case are an eccentricity of 1.14, an inertial flight path angle of 62.5°, an inertial velocity of 12 km/sec (above the escape velocity) and an inclination of orbit of 33° which was the same as the launch latitude.

With the excess velocity attained, it would be possible to either (1) carry more payload weight, about 20 kilograms, or (b) reduce the specific impulse for a more simple propulsion system. The later is chosen for several reasons, the most important of which are simplicity, maintainability and responsive launch capability. For a final stage specific impulse of 285 seconds, close to that of a hydrazine monopropellant, the rocket's inertial velocity is 10.53 km/sec, which is very close to the escape velocity at that altitude of 10.65 km/sec. The eccentricity attained is 0.993, which is

actually sufficient for a free-return lunar trajectory once the three-body interaction forces are accounted for.

For this same configuration, and a suitable change in launch trajectory to attain a circular orbit (i.e. gravity turn maneuver then linear tangent steering), the launch vehicle can loft about 110kg of payload to 250km. This is a respectable payload mass fraction of 2.86% using conservative values for the stage specific impulses used.

Figure 28 shows the diminished Mach numbers and thrust to weight ratios to more manageable levels for the new configuration with enhanced nozzles. At 60 seconds the rocket is already 100 kilometers above the Earth's surface.

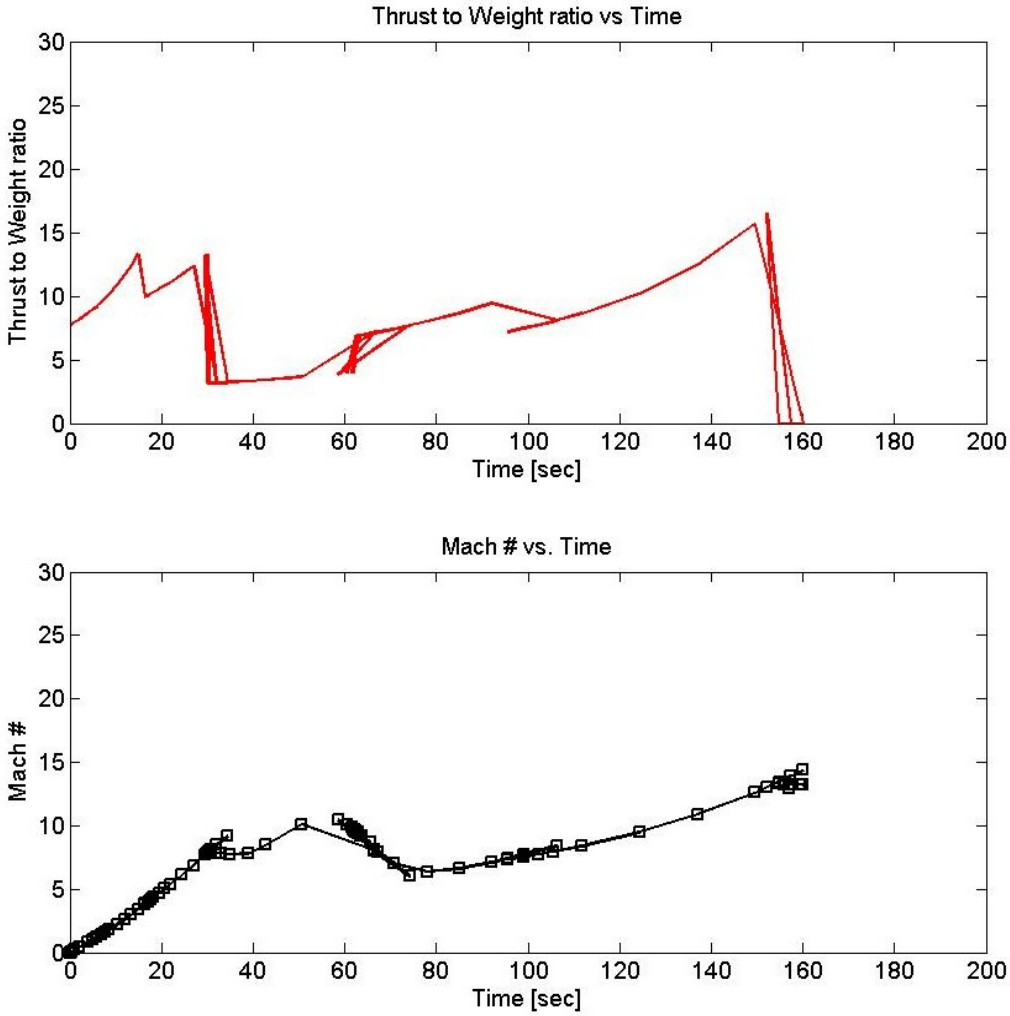

Figure 28: Thrust to weight ratio and Mach number for new direct-escape rocket configuration.

4. Performance-Mass-Cost Optimization Tool

Parameters such as mass ratio, specific impulses, technology factors, engine technology and trajectory for each stage are just a few of the hundreds of competing variables that represent a launch vehicle design. The interaction effects of these variables represent a very complicated response behavior which can only be modeled computationally. One such method, the calculus of variations, was described in a preceding chapter but tends towards unrealistic results as it omits key interaction effects. Other more sophisticated methods include genetic algorithms, neural networks, simulated annealing, and ant colony optimization schemes.[25] The problem with these is that as the design space is expanded the number of combinatorial designs grows factorially with the addition of variables and is very difficult to explore in its totality.[55]

Recent studies have suggested that "starting fresh and designing to cost rather than for performance would lead to significant reduction in the costs of launch operations."[25] Prior to this decade the overwhelming focus on launch vehicle development was for performance-driven designs, a residual from the 1950's era of ICBMs. Most modern day rockets follow the tradition of large very efficient engines used to loft a maximum of payload with the minimal amount of propellant. In 2004 the Space Propulsion Synergy Team made the statement that life cycle costs must be the primary metric, coequal with weight and performance, addressing

both launch operational costs and development.[56] Such a design has not yet been realized.

The purpose of this section is to introduce a performance-mass-cost optimization tool to evaluate different performance and weight variations and their effects on the life cycle costs (LCC). The underlying premise behind the proposed optimization scheme is an understanding between an improvement in performance and its associated LCC. An operationally responsive vehicle is unique amongst other launch vehicles in that LCC should be the defining metric, even more so than performance and weight. This is due mainly to the fact that the service life of this vehicle will be measured in years, if not a decade, without major requalification and refurbishment effort. It is therefore vitally important to choose subsystems that will reduce the LCC but still have an appreciable payload capability.

Because the design discussed herein is limited to off-the-shelf tactical missiles refurbished to serve a new purpose, the primary specific cost of the system, pound per pound, will come from the final stage development. This is a well known trait of launch vehicles whereas higher specific impulse engines are reserved for the final stages. This tool lends insight into the preliminary design of the upperstage portion of responsive space vehicles. To characterize the performance-mass-cost interaction a model based on life cycle cost, performance, weight, and mission type is sought. To this end the following assumptions are introduced:

- A high-end mission is chosen, Δv=3,400 m/s, which represents the extreme direct hyperbolic trajectory at which the upperstage must perform. Different monopropellants are evaluated for this mission.
- The inherent parameters of the propellant (density, range of specific impulse, etc.) are used with parametric weight equations for engine, pressurant, nosecone and subassembly masses for the mission. Remaining mass is considered useable payload mass.
- Cost estimating relationships (CERs) are calculated for total life cycle costs (LCC) including Design Development Testing and evaluation (DDT&E), Theoretical First Unit (TFU) and Operation & Maintenance (O&M) costs. Note: project administrative and management (PAM) and launch segment cost (LSC) are not included; instead they would be rolled up into higher design configuration costs.

Parametric Evaluation of Monopropellants

Monopropellants are considered for the purpose of this baseline analysis. Use of a monopropellant propulsive system is desirable because of its inherent low cost, simple operation and reliability. Liquid rocket engines were not evaluated because their elevated cost, complexity, and use of cryogenic oxidizers would not well suit the needs of an ORS capable vehicle. Solid rocket motors could be used as well but their lower

specific impulse and lack of maneuvering capability would greatly reduce the functionality of the proposed vehicle. As the next section will explain in more detail the propellants chosen represent only high performing, storable, high density monopropellant combinations. The following three propellants were selected as the most promising candidates that would be well suited to the needs of an operationally responsive spacecraft: the often-used Hydrazine, rocket grade high percentage Hydrogen Peroxide (H2O2), and the relatively new Hydroxylammonium Nitrate (HAN) blends.

Firstly a grouping of parametric weight equations, also known as mass estimating relationships (MERs), was collated and cross-checked from Refs. 32, 57, and 60 for evaluation of the system mass for each propellant. System weights are driven mostly by the density of the propellant: 1000, 1450, and 1700 kg/m^3 for Hydrazine, H2O2 and HAN, respectively. For brevity the entirety of these equations will not be listed, but they include parametric equations for engine weight, pressurant mass, nosecone and fairing mass, and subassemblies for a monopropellant space thruster. This thruster relies on a blowdown pressurization system and common space material selections. These MERs are each linked to the propellant selection at hand and other defining variables. For example, the mass of the nose in the following equation is influenced by max dynamic pressure, q_{max}, diameter of the nose, D_n, and the nose surface area, S_n. The latter two are direct functions of the density of the propellant, e.g. a smaller density would require a larger volume for a given amount of

propellant (based on the specific impulse of the thruster) and hence surface area for a given diameter.

$$M_{nose} = S_n[2.499e^{-4}q_{max} + 1.7008 + (3.695e^{-5}q_{max} - 3.252e^{-3})D_{nose}] \quad (37)$$

Secondly, a group of parametric cost estimating relationships is established to solve for the LCC as a function of engine mass, M_{eng}. These are obtained from Ref. 32 and were originally developed by the U.S. Air Force and NASA.

$$DDT\&E = 464 \cdot M^{0.867} \quad \text{(FY00\$K)} \quad (38)$$

$$TFU = 293 \cdot M^{0.777} \quad \text{(FY00\$K)} \quad (39)$$

The Design, Development, Testing and Evaluation (DDT&E) represents the largest cost of the initial LCC for the first year. Operation and Maintenance (O&M) is a function of the Theoretical First Unit (TFU): 10, 20 and 30 percent for HAN, H202 and hydrazine, respectively, to account for factors including storage life, toxicity and associated handling precautions and expenses. The total life cycle cost, for the first year in operation, is a function of these three values: LCC = DDT&E + TFU + O&M. This TFF is inflated considering economies of scale would certainly reduce the TFU cost as the number of units is increased and the DDT&E initial expenditure would be distributed accordingly. This TFF only includes the cost of the final stage which is a percentage of the total LCC and O&M cost, albeit an expectedly large percentage. It also does not include the cost of the payload, which parametrically costs upwards of 40% of the total cost of the spacecraft.[32] Additional O&M annual costs throughout the

lifetime of the launch vehicle would soon match the total DDT&E, in some case in less than a decade of ORS operation. Regardless, this method establishes a baseline in which to compare different propellants in terms of performance, mass and cost.

The results for this model are shown below as Figure 29. The figure of merit was chosen as life cycle costs per kilogram of payload. The primary variables are density-specific impulse, ρI_{sp} and inert mass fraction, both of which were found to be the key drivers in terms of both cost and performance. The solid lines represent the baseline configuration for each monopropellant propellant choice as a function of the range of allowable specific impulses attainable by the propellant: Hydrazine: 200 to 250secs; H2O2: 200 to 250secs; HAN blends: 200 to 270. The outlying lines represent a 20% increase or decrease in inert mass fraction. Decreasing the inert mass fraction increases useable payload mass and therefore decreases cost per kilogram put to orbit, but in a competing fashion raises costs due to the elevated DDT&E and TFU costs.

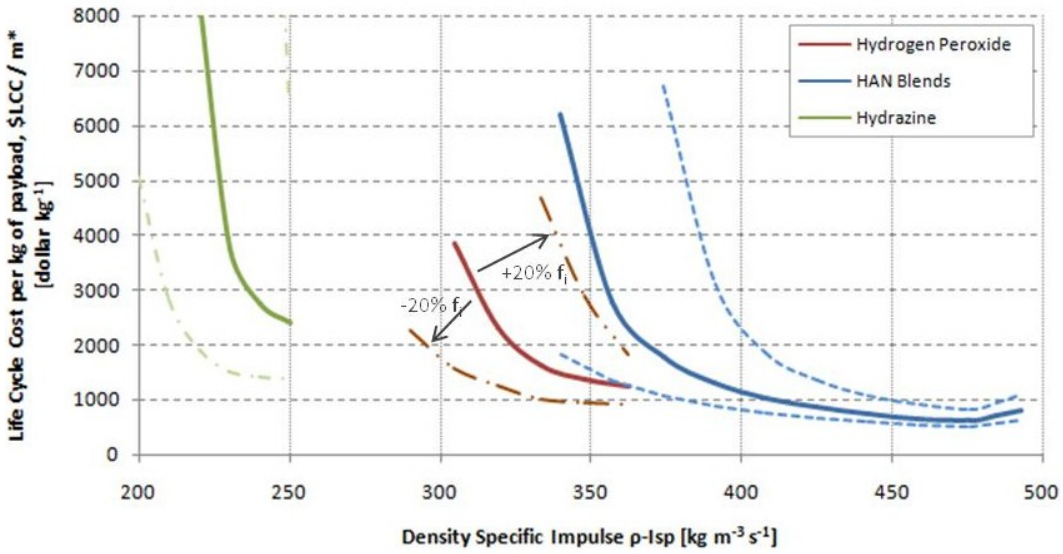

Figure 29: Life cycle costs per kilogram of payload as a function of density specific impulse for different monopropellants.

The plot illustrates that HAN blend monopropellants are ideal propellants for many reasons, most notably with its lower O&M expenses and greatly increased ρI_{sp}. This higher ρI_{sp} value results in a lower propellant tank mass and consequently additional payload to orbit for a lower cost. It is also noteworthy that HAN represents the lowest cost per unit payload for a large range of density specific impulses. As an example, HAN operating at only 230 seconds of specific impulse is comparable to H2O2 at its theoretical maximum of 250 seconds of I_{sp}, and is superior to hydrazine operating at 250 seconds inclusive of a 20% decrease in inert mass fraction. Moreover, the slope of the HAN line quickly flattens out under the range of $1,000 per kilogram of payload. This can be translated in two ways: (1) additional costs spent towards improving the specific impulse of HAN has a diminishing margin of return in terms of decreased

cost per unit payload, or (2) additional density specific impulse improvement can be used to increase usable payload mass without a large raise in cost.

Response Surface Methodology

A more in-depth analysis is required to investigate the trend of performance-mass-cost relationship beyond what is shown in Figure 29. For instance, what variables are best optimized to lower the cost per unit payload? It is shown that generally increasing the specific impulse will decrease this dollar amount, but only to a certain limit. The change in inert mass fraction, i.e. structural technology, is also a key variable and is intrinsically linked to this performance and should likewise be optimized. This section proposes the use of response surface methodology to show these interactions and reveal optimal solutions.

Response surface methodology (RSM) is a statistical technique used to model, analyze and optimize a problem in which a response is influenced by several or more parameters.[58] It provides the designer valuable insight into the behavior of complex phenomena over a range of parameter values[32], and is used here to evaluate the interaction effects of Figure 29. An excellent example of RSM used in aerospace applications are well documented in Ref. 59 where a parametric assessment of launch vehicles are calculated for modeling payload as a function of orbital altitude and inclination. For this assessment a second order model is used to represent the exponential curvature in the response:

$$y = \beta_0 + \sum_{i=1}^{k} \beta_i x_i + \sum_{i=1}^{k} \beta_{ii} x_i^2 + \sum \sum_{i<j} \beta_{ij} x_i x_j + \epsilon \quad (40)$$

Where β_0 is the intercept, $\beta_{i\&k}$ the partial regression coefficients and $x_{i\&k}$ are the predictor variables or regressors. This second-order response surface equation takes the form of the following equation to give an analytical expression for the figure of merit (LCC dollars per kilogram of payload) as a function of the two dominant variables: ρI_{sp} and inert mass fraction, f_i.

$$\frac{LCC\ \$}{m^*} = \beta_0 + \beta_1(\rho I_{SP}) + \beta_2 f_i + \beta_{11}(\rho I_{SP})^2 + \beta_{22}(f_i)^2 + \beta_{12}(\rho I_{SP}) f_i \quad (41)$$

A custom Matlab script was written to fit the data of Figure 29 to the above equation using the polynomial method of least squares. The partial regression coefficients for each propellant were found to be:

Table 8: Partial Regression Coefficients for Performance/Mass/Cost Response Surface Equations of Monopropellants

Propellant	β_o	β_1	β_2	β_{11}	β_{22}	β_{12}
H2O2	2.9474e+004	-279.6547	2.5743e+005	0.7573	9.1855e+005	-1.5756e+003
HAN Blends	3.2066e+004	-230.6029	2.2855e+005	0.3914	3.2350e+005	-725.1924
Hydrazine	1.3819e+004	-383.0074	4.7330e+005	4.6194	5.7530e+006	-1.0635e+004

Now that an analytical closed-form solution exists for each propellant, we can in turn examine the interaction effects individually as they influence the performance measure. This response behavior or

sensitivity analysis is found by taking the partial derivative with respect to each predictor variable:

$$\left[\delta\left(\frac{LCC\ \$}{m^*}\right)/\delta(\rho Isp)\right]_{Propellant} = \beta_1 + 2\beta_{11}(\rho I_{SP}) + \beta_{12} f_i \quad (42)$$

$$\left[\delta\left(\frac{LCC\ \$}{m^*}\right)/\delta(f_i)\right]_{Propellant} = \beta_2 + 2\beta_{22} f_i + \beta_{12}(\rho I_{SP}) \quad (43)$$

Such equations can be plotted as linear contour lines against the two predictor variables. For example, Figure 30 is the partial derivative with respect to the density specific impulse of HAN.

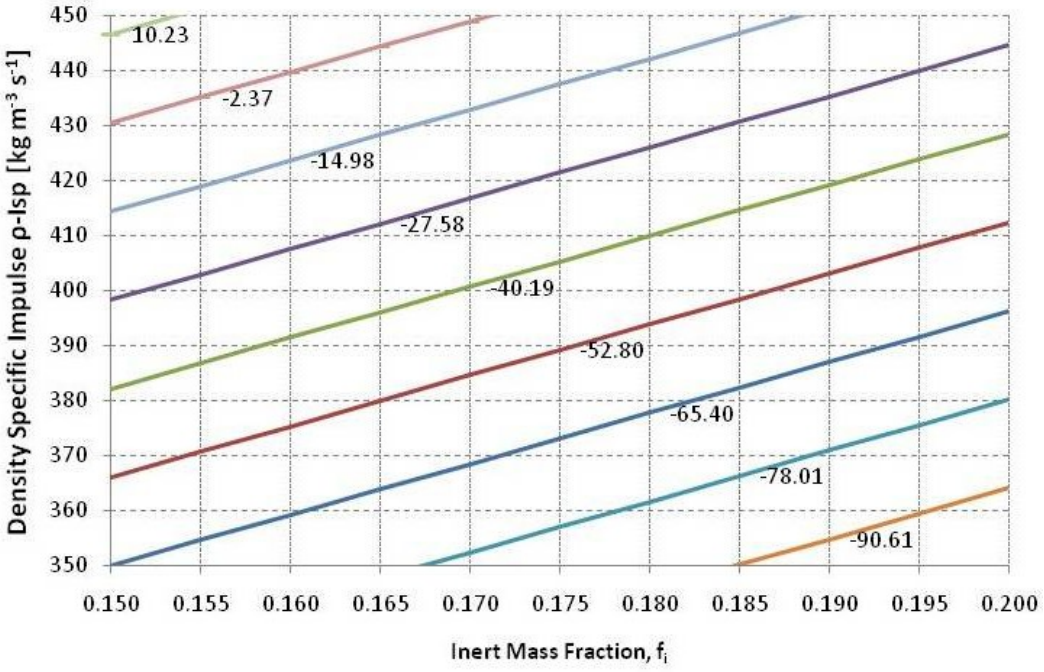

Figure 30: Partial derivative of LCC/m* with inert mass fraction held constant illustrates density specific impulse sensitivity for HAN.

The contours show the density-specific impulse sensitivity. Over the span of 100 ρI_{SP} and 0.05 f_i the ρI_{SP} sensitivity ranges from -102 to 12.88 \$/kg / ρI_{SP}. In other words for every ρI_{SP} that is added, the max gain in

$/kg of payload is 102 and actually reduces to -10.23 if the chosen Isp (technology level) is too high. Therefore, as expected, the optimal value lies above 430 ρI_{SP} (corresponding to ~260 seconds I_{sp}) in the range of lower mass fractions, 0.15 to 0.175.

Such plots can be made for each propellant type for comparison purposes. As an example, consider if the specific impulse of H2O2 and HAN is held at a constant 250 seconds or a density specific impulse of 363 and 425, respectively. A specific impulse of 250 seconds represents a high technology factor for H2O2 and a median one for HAN. Referring to Figure 29 these values both equate to just over $1,000 per kilogram of payload mass. Held at a conservative inert mass fraction of 0.16, the RSM shows that the max gain in $/kg of payload for HAN is +60 for each ρI_{SP} that is added and -14 for H2O2 as shown by Figure 30 and Figure 31. This means H2O2 has reached its performance limit and that HAN has a higher margin for improvement. If future flexibility of payload capabilities is a driving factor then HAN would be the obvious selection.

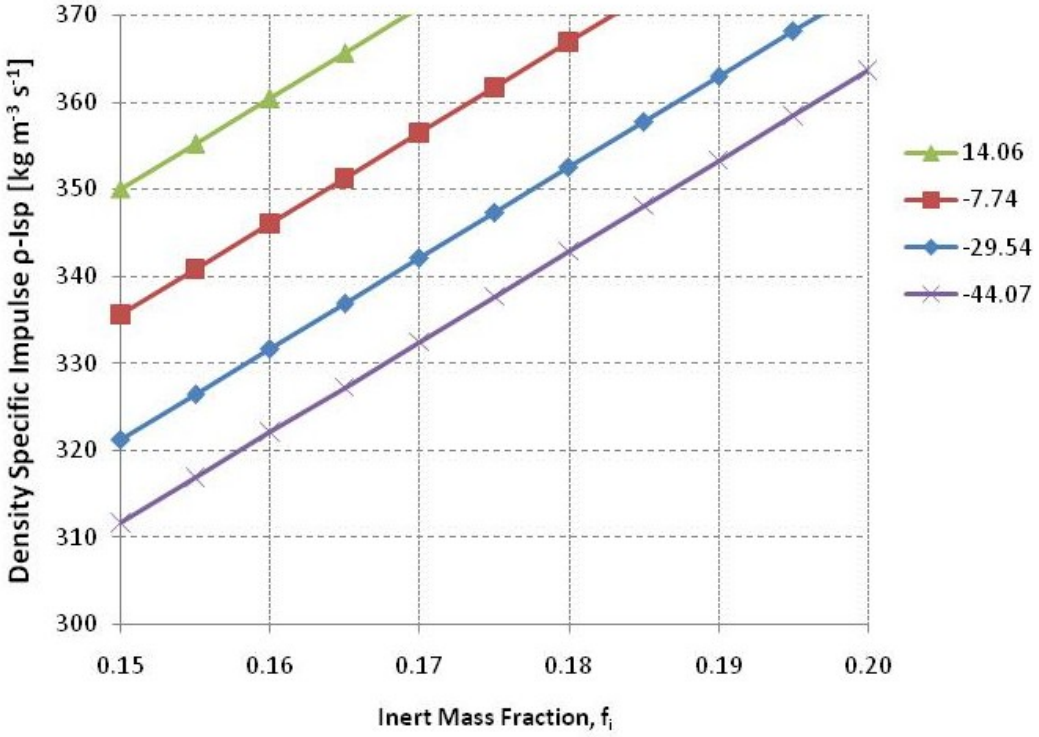

Figure 31: Partial derivative of LCC/m* with inert mass fraction held constant illustrates density specific impulse sensitivity for H2O2.

A similar plot to Figure 30 but with respect to inert mass fraction illustrates the effects of inert mass fraction with density specific impulse held constant. Continuing with the same example from the previous paragraph, we can evaluate what a change in mass fraction yields on the total LCC per unit payload mass.

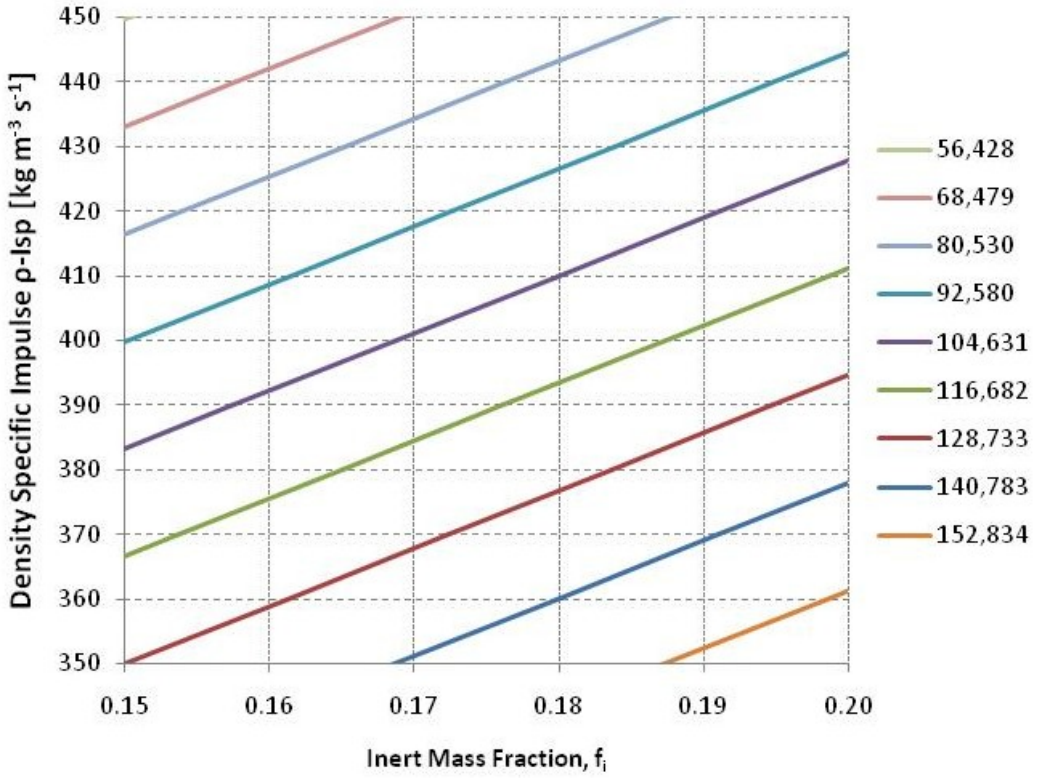

Figure 32: Partial derivative of LCC/m* with density specific impulse held constant illustrates density inert mass fraction sensitivity for HAN.

Again, for an inert mass fraction of 0.16 and a density specific impulse of 360 for HAN, the RSM contour for the inert mass fraction sensitivity plot (Figure 32) has a result of 128,000 $/kg per unit change in inert mass fraction. At first this seems high in comparison to the above stated values but recall that inert mass fractions are measured in fractions. These RSM values would aid greatly in the efforts of a mission designer looking to decrease launch costs or increase payload by either increasing engine efficiency or decreasing motor subsystem mass. The results state that a 5% increase in the ρI_{SP} of HAN would give a net reduction of $1,080 per unit payload mass, whereas a 5% reduction in inert mass fraction

would give $1,024 per unit payload mass. These values are nearly equal, so the final decision on which parameter to improve would be up to the discretion of the mission designer, i.e. which avenue would be the easier route. For this example, an inert mass fraction of 0.16 is conservatively high and would likely be the most promising variable for improvement. A similar comparison with H2O2 illustrates the opposite effect. Increasing the ρI_{SP} is too costly and does not reduce the LCC/m*, whereas a reduction in inert mass fraction does. In other words, the RSM dictates that for H2O2 it is instead more optimal (in terms of $/kg) to focus on improving weight savings than to improve performance past a certain point.

The RSM analysis shows that higher performance or reduced weight at any cost should not be the sole consideration, as is the case with conventional rockets. Rather there is an optimal solution for any unique mission once LCCs are considered. Similar analyses can be performed for the different variables of the mission, such as $/kg as a function of Δv, which shows which propellant, specific impulse and inert mass fraction would be best suited for a particular mission. This method aids in choosing a particular configuration by providing rule of thumb sensitivities and showing the interaction effects on the complicated response behavior modeled by the responsive surface equations for each propellant type. In short: it makes the mission designer's and planner's

jobs easier for parametric evaluation as a function of life cycle cost per useable kilogram of payload.

5. Upper Stage Engine Propellant Selection

Propulsive Requirements

The previous section has demonstrated that life cycle costs can be greatly reduced by appropriate selection of a simple monopropellant that meets mission performance requirements. Use of a monopropellant propulsive system is desirable because of its inherent low cost, simple operation and reliability. Moreover, a catalytic-based ignition is desirable for additional simplicity, throttleability and multiple restart capability. Such a system is ideal for ORS capable launch vehicles that would be required to wait for extended periods of time then launched at a moment's notice.

Despite these advantages monopropellants produce lower total specific impulse in comparison to liquid rocket engines, though high performance is not a prerequisite for an ORS capable upper stage. It has been shown through analysis of small satellite operations with high cost sensitivities that "propulsive performance is not the critical success factor".[27] That being said, monopropellants with higher inherent propulsive efficiencies are more desirable than low performing systems (such as cold or warm gas thrusters) for obvious reasons. For the purpose of this dissertation the specific impulse selection range for candidate monopropellants should be above 200 seconds at a minimum.

Monopropellant Selection

A select few monopropellants reach the above stated requirements for performance. An exhaustive comparison of such propellants is available in a great many studies and is beyond the scope of this dissertation. Several studies, including NASA Ref. 60 and Ref. 61 limit the discussion to high performing, Earth-storable, high density monopropellant combinations. The following three were selected as the most promising candidates that would be well suited to the needs of an operationally responsive spacecraft: the often-used Hydrazine, heritage rocket grade high percentage Hydrogen Peroxide, and the relatively new Hydroxlammonium Nitrate.

High concentration hydrogen peroxide was a popular choice for quite some time with use dating back to the 1930s.[62] It has a high density and auto-ignites with any standard precious metal catalyst bed, often with columns of silver screens. However high concentration hydrogen peroxide does not have favorable long term storage qualities and was mostly replaced by high-purity hydrazine in the 1960s for this reason.[63] A small but renewed interest in hydrogen peroxide has been reinvigorated[64] but its future remains uncertain with its low performance in comparison to hydrazine, storage issues and most of all its sensitivity to contamination.[65]

The use of hydrazine as a potential fourth stage kick booster was evaluated and initially chosen for a baseline. Hydrazine is a popular in-

space propulsion monopropellant due to its reaction with a catalyst, usually Shell-405, a high platinum content catalyst. It also has very good performance, upwards of 250 seconds of specific impulse. Despite its positive performance and storing capabilities, hydrazine is extremely hazardous to humans. An old musing of "if you smell it it's already too late" is not a stretch of truth. Figure 33 illustrates a representative picture of the Self-Contained Atmospheric Protective Ensemble, "SCAPE" protective gear complete with independent and explosion-proof breathing system. Such suits must be maintained and decontaminated after every use with hydrazine and represents only one line item required in the operations and maintenance (O&M) cost for hydrazine.

Figure 33: SCAPE suit for use with hydrazine monopropellant.[27]

For an ORS capable rocket the use of hydrazine would not be recommended due to required stringent handling of the propellant when stored in the launch vehicle for years at a time. This has been found to be

very costly in the past and significantly increases ground operations costs due to its toxicity, as reported by Ref. 27. This same study quantifies the potential for replacing hydrazine with a more benign non-toxic propellant to realize (1) recurring cost savings, (2) reduced duration and simplification of systems operations, and most importantly (3) reduced risk to personnel.

For these reasons and as a result of the parametric life cycle cost to total payload mass ratio analysis presented in the previous section, a relatively new non-toxic monopropellant was selected, one more ideal to the situation at hand. This propellant is called Hydroxylammonium Nitrate, or simply HAN, and is almost identical in performance values as hydrazine. Though HAN is in many ways advantageous to conventional hydrazine, it lacks a high Technology Readiness Level (TRL). The HAN development efforts discussed in the dissertation are first steps towards a remedy.

HAN is a very new addition to the space propellant market, having only been tested in small-scale prototype engines by NASA, Aerojet, and the Japanese space agency. HAN has yet to be adopted on any launch vehicle or spacecraft. Its benefits are derived not only for its high specific impulse, but more for its high density with a specific gravity as high as 1.84, i.e. 1.84 times the density of water, compared to 1.0 for hydrazine. Therefore it can be stored in comparably smaller and lightweight propellant tanks and still provide a generous amount of specific impulse,

approximately 200 to 260 seconds as a standalone monopropellant.[66] Such a large density specific impulse makes it an ideal propellant for tactical missiles or ORS spacecraft operations. Though the propellant is toxic it does not emit vapors nor is it a carcinogenic. HAN propellant has an indefinite storage lifetime and can potentially be released directly into the soil without adverse environmental effects which is ideal for demilitarized or end of shelf life disposal.[67]

A novel use of HAN propellant is proposed. HAN, still being researched thoroughly, is also known to be miscible with certain fuel liquids. One such fuel is methanol, and the HAN mixture (up to 95% aqueous solutions are available) can mixed with up to 15% of methanol by weight. A recent journal by Katsumi et al, 2009, Ref. 68, has shown that not only will methanol increase the specific impulse, but it tends to reduce the typically very high burning rates of HAN and improve overall combustion. To determine how this propellant combination will work, and what maximum efficiency it could provide, use of a thermochemical analysis is required.

HAN / Methanol – Thermochemistry and Performance

The software used for this study was the NASA-Lewis thermochemical *ProPEP* code which is based on minimizing the free energy and calculating the molecular mass, specific heats (thus the ratio of specific heat) and the temperature of the reaction for differing values of fuel and oxidizer. From these values calculations of the characteristic

exhaust velocity and other engine parameters can be found. Upon applying exit conditions the thrust coefficient and and specific impulse can be determined. Another comparable NASA code, called the NASA Glenn Chemical Equilibrium with Applications (CEA) is a suitable alternative for these calculations and has been used in the past to verify the results of *ProPEP*.

The specifics of the proposed engine are reserved for a later discussion, but for a monopropellant engine using 95% HAN operating at 1,000psi chamber pressure and a nozzle expansion ratio of 100, suitable to an advanced high-thrust monopropellant, the thermochemical code provides the following:

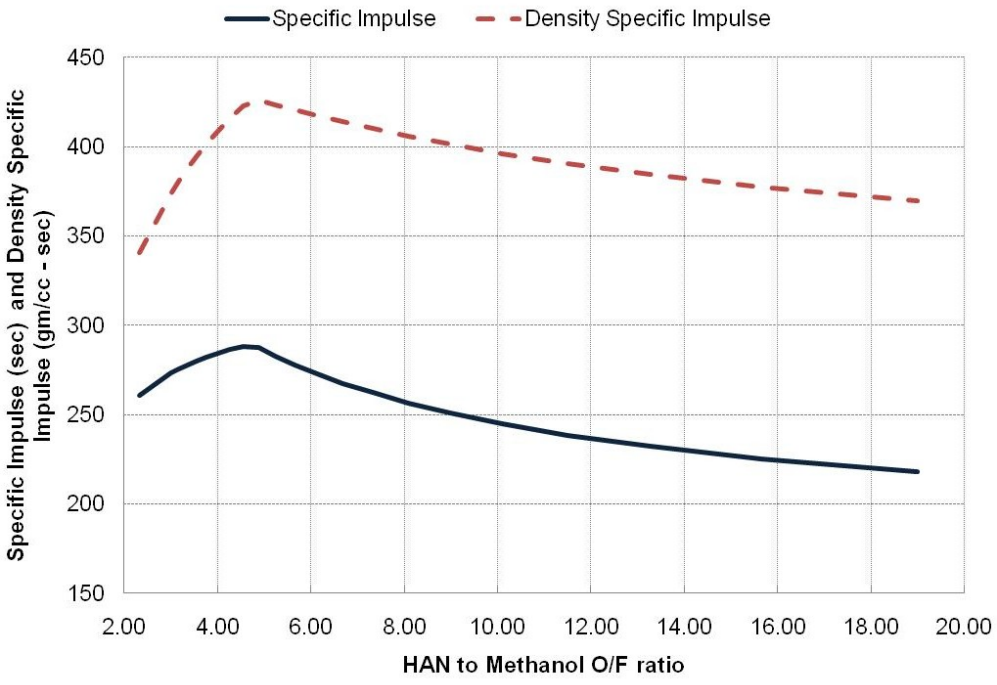

Figure 34: Specific impulse and density specific impulse for a range of O/F ratios. Motor operates at 1,000psi with an expansion ratio of 100.

It is shown that the optimum performance lies at a value of O/F = 4.6, which is 18% methanol by weight with a specific impulse value of 288 seconds and a remarkable density-impulse of 425 gm/cc-s. **This represents a density specific impulse increase over hydrazine of approximately 50%!** Such results are corroborated by Aerojet which calculated a maximum Isp of 269 using lower pressures (~200psi), lower expansion ratio (50:1) and different HAN percentage.[69] As a further example, the ever-popular LOX/LH2 liquid rocket engine has a specific impulse of over 450 seconds, but a density specific impulse of only 150 gm/cc-s because of the very low density of hydrogen.

The value for methanol percentage is slightly more than is allowed by miscible means, but post-injection of any amount exceeding 15% could be used. As Figure 35 demonstrates, the stagnation temperature of this propellant combination is quite high, commensurate with higher performing liquid engines. Heritage catalyst beds cannot withstand these extreme temperatures without some type of regenerative cooling apparatus.

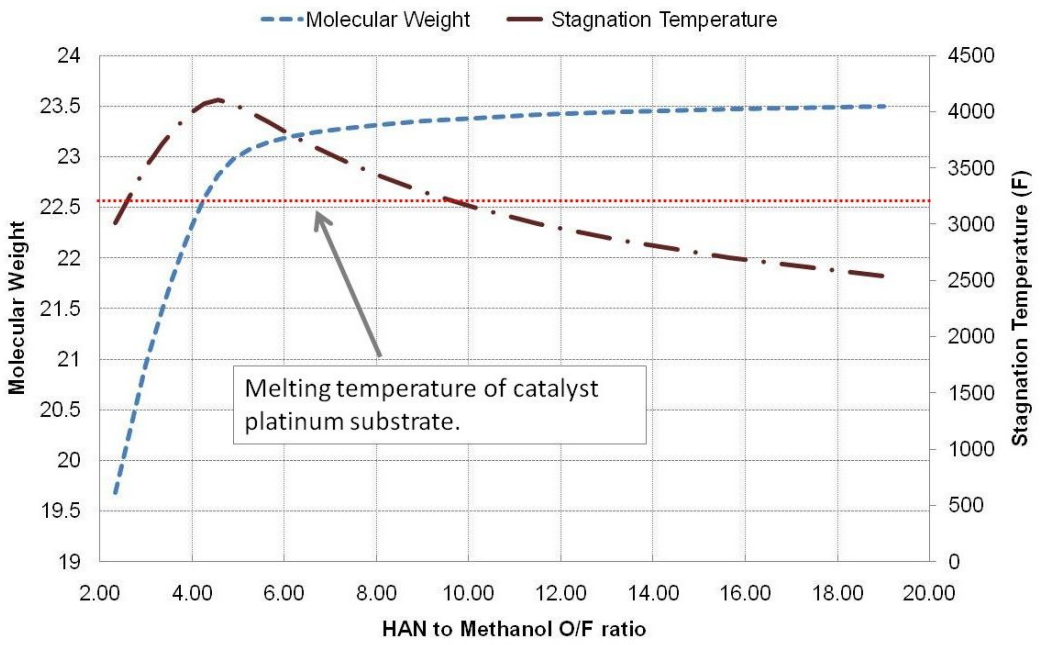

Figure 35: Combustion chamber temperature and molecular weight of HAN/methanol mixture for differing O/F ratios. Motor operates at 1,000psi with an expansion ratio of 100.

Values for the chosen catalyst bed (to be discussed later) have platinum substrate temperature limits of 3,200°F and an aluminum oxide catalyst structure with melting limits of approximately 4,000°F. These limits are common to many catalysts. Both substrate and catalyst substance temperature limits are below the expected stoichiometric temperature of the optimum mixture ratio of HAN and methanol. A reduction of stagnation temperature is of course not warranted as that will result in a decrease of total enthalpy and thusly an associated loss in performance. Therefore another means of injecting the propellant are required to limit abuse or melting of the catalyst bed. A full list of the thermochemical analysis with

95% HAN with varying amounts of methanol at an operating chamber pressure of 300psi is shown below:

Table 9: Thermochemical Evaluation of 95% HAN/Methanol at 300psi at 1atm exit pressure.

									specific impulse (s)		density Isp		c* (ft/s)		thrust coefficient		expansion ratio	
O/F	HAN/H20	*HAN %*	*water %*	Methanol	T_o (F)	gamma	MolWeight	density (gm/cc)	*frozen*	*shifting*	*frozen*	*shifting*	*frozen*	*shifting*	*frozen*	*shifting*	*frozen*	*shifting*
2.33	70	66.5	3.5	30	3007	1.227	19.684	1.3055	196.7	197.7	256.79	258.10	4484	4530.4	1.41	1.40	3.46	3.52
3.00	75	71.25	3.75	25	3506	1.2116	20.938	1.3684	205.6	206.3	281.34	282.30	4678.9	4716.6	1.41	1.41	3.55	3.57
3.17	76	72.2	3.8	24	3607	1.2087	21.206	1.3817	207.2	207.9	286.29	287.26	4713.5	4750.2	1.41	1.41	3.56	3.58
3.35	77	73.15	3.85	23	3707	1.2059	21.48	1.3953	208.7	209.4	291.20	292.18	4746.3	4782.3	1.41	1.41	3.58	3.59
3.55	78	74.1	3.9	22	3806	1.2032	21.757	1.4092	210.2	210.9	296.21	297.20	4776.7	4812.8	1.42	1.41	3.6	3.61
3.76	79	75.05	3.95	21	3901	1.2006	22.037	1.4233	211.4	212.3	300.89	302.17	4803.9	4841.1	1.42	1.41	3.61	3.62
4.00	80	76	4	20	3987	1.1983	22.313	1.4377	212.4	213.7	305.37	307.24	4825.6	4866.3	1.42	1.41	3.62	3.64
4.26	81	76.95	4.05	19	4052	1.1964	22.571	1.4524	213	214.9	309.36	312.12	4836.7	4885.5	1.42	1.42	3.64	3.67
4.56	82	77.9	4.1	18	4076	1.1954	22.785	1.4674	212.6	215.9	311.97	316.81	4828.4	4897	1.42	1.42	3.64	3.71
4.88	83	78.85	4.15	17	4047	1.1956	22.937	1.4827	211.2	214.8	313.15	318.48	4796.7	4870.3	1.42	1.42	3.64	3.73
5.25	84	79.8	4.2	16	3980	1.1966	23.043	1.4983	209.1	211.8	313.29	317.34	4747.8	4809.7	1.42	1.42	3.63	3.69
5.67	85	80.75	4.25	15	3890	1.1982	23.121	1.5143	206.4	208.5	312.55	315.73	4688.3	4742.8	1.42	1.41	3.62	3.66
6.14	86	81.7	4.3	14	3786	1.2002	23.182	1.5306	203.4	205.1	311.32	313.93	4621.7	4671.2	1.42	1.41	3.61	3.64
6.69	87	82.65	4.35	13	3672	1.2025	23.233	1.5473	200.2	201.5	309.77	311.78	4549.6	4595.6	1.42	1.41	3.6	3.61
7.33	88	83.6	4.4	12	3350	1.2051	23.277	1.5644	196.8	197.8	307.87	309.44	4472.8	4516.2	1.42	1.41	3.58	3.59
8.09	89	84.55	4.45	11	3422	1.2079	23.315	1.5818	193.1	194	305.45	306.87	4391.6	4433.1	1.41	1.41	3.57	3.57
9.00	90	85.5	4.5	10	3288	1.211	23.35	1.5996	189.3	190	302.80	303.92	4306.1	4346.2	1.41	1.41	3.55	3.54
10.11	91	86.45	4.55	9	3148	1.2145	23.382	1.6178	185.3	185.8	299.78	300.59	4216.3	4255.4	1.41	1.40	3.53	3.52
11.50	92	87.4	4.6	8	3004	1.2183	23.412	1.6364	181	181.5	296.19	297.01	4121.8	4160.3	1.41	1.40	3.51	3.49
13.29	93	88.35	4.65	7	2854	1.2224	23.44	1.6555	176.6	176.9	292.36	292.86	4022.6	4060.7	1.41	1.40	3.48	3.46
15.67	94	89.3	4.7	6	2700	1.2271	23.467	1.675	171.9	172.1	287.93	288.27	3918.2	3956.1	1.41	1.40	3.46	3.43
19.00	95	90.25	4.75	5	2540	1.2321	23.493	1.695	167	167.2	283.07	283.40	3808.2	3846	1.41	1.40	3.43	3.4

In addition, the following table completes the thermochemical analysis by including the specifications for a space-operable engine operating at 500psi and an expansion ratio of 100.

Table 10: Thermochemical evaluation of 95% HAN/Methanol at 500psia at nozzle expansion ratio of 100.

O/F	HAN/H20	*HAN %*	*water %*	Methanol	T_o (F)	gamma	MolWeight	density (gm/cc)	specific impulse (s)	density Isp	c* (ft/s) (frozen)	thrust coefficient	exit press. (atm)
2.33	70	66.5	3.5	30	3008	1.227	19.684	1.3055	260.8	340.47	4472.1	1.88	0.019
3.00	75	71.25	3.75	25	3508	1.2116	20.94	1.3684	273.1	373.71	4668.7	1.88	0.02
3.17	76	72.2	3.8	24	3610	1.2087	21.209	1.3817	275.4	380.52	4704	1.88	0.02
3.35	77	73.15	3.85	23	3711	1.2058	21.483	1.3953	277.7	387.47	4737.6	1.89	0.02
3.55	78	74.1	3.9	22	3811	1.2031	21.763	1.4092	279.9	394.44	4769.2	1.89	0.02
3.76	79	75.05	3.95	21	3909	1.2004	22.046	1.4233	282.1	401.51	4798	1.89	0.021
4.00	80	76	4	20	4000	1.198	22.327	1.4377	284.3	408.74	4822.1	1.90	0.021
4.26	81	76.95	4.05	19	4073	1.1959	22.595	1.4524	286.3	415.82	4836.9	1.90	0.021
4.56	82	77.9	4.1	18	4103	1.1948	22.818	1.4674	288.3	423.05	4831.9	1.92	0.022
4.88	83	78.85	4.15	17	4074	1.195	22.97	1.4827	287.3	425.98	4800	1.93	0.022
5.25	84	79.8	4.2	16	4002	1.1961	23.069	1.4983	282.6	423.42	4748.7	1.91	0.022
5.67	85	80.75	4.25	15	3907	1.1978	23.14	1.5143	277.7	420.52	4686.6	1.91	0.021
6.14	86	81.7	4.3	14	3798	1.1999	23.196	1.5306	272.7	417.39	4617.9	1.90	0.021
6.69	87	82.65	4.35	13	3681	1.2023	23.243	1.5473	267.5	413.90	4544.1	1.89	0.02
7.33	88	83.6	4.4	12	3556	1.2049	23.283	1.5644	262.1	410.03	4465.9	1.89	0.02
8.09	89	84.55	4.45	11	3426	1.2078	23.32	1.5818	256.5	405.73	4383.7	1.88	0.019
9.00	90	85.5	4.5	10	3291	1.211	23.353	1.5996	250.8	401.18	4297.3	1.88	0.019
10.11	91	86.45	4.55	9	3150	1.2144	23.384	1.6178	244.8	396.04	4206.8	1.87	0.018
11.50	92	87.4	4.6	8	3005	1.2182	23.413	1.6364	238.5	390.28	4111.8	1.87	0.018
13.29	93	88.35	4.65	7	2855	1.2224	23.441	1.6555	232.1	384.24	4012.3	1.86	0.017
15.67	94	89.3	4.7	6	2700	1.227	23.467	1.675	225.3	377.38	3907.7	1.86	0.017
19.00	95	90.25	4.75	5	2540	1.2321	23.493	1.695	218.2	369.85	3797.5	1.85	0.016

One such solution that will be proposed by this dissertation is the post-injection of all or most of the methanol directly into the combustion chamber. For example, an O/F of 11.5 (corresponding to 8% methanol which is still miscible with HAN) would reduce the stagnation temperature to a manageable 3,000°F. The remainder of the fuel could then be injected past the port of the catalyst bed and if mixed properly would still provide good combustion in the ideal range of performance. Several promising injection methods are proposed for later evaluation. The first is a coaxial injection of methanol through the catalyst bed where the hot decomposed HAN will serve to shear and atomize the incoming methanol similar to the LOX/LH2 Space Shuttle Main Engine coaxial injection scheme. The second involves a more conventional post-injection along the chamber walls past the catalyst region with an added benefit of some degree of chamber film cooling. Swirl injection would be favored for this purpose to give additional stay time of the methanol within the combustion chamber. Admittedly both concepts would ultimately increase the number of parts and tankage required and therefore reduces the simplicity of the monopropellant system. However the post injection of methanol will yield a substantial increase of approximately 50 seconds of specific impulse which is well worth the effort.

It remains to be shown that HAN can be properly injected, atomized and combusted at moderate pressures in a catalyst bed. Methods for improving performance thereafter can then follow.

6. Design and Testing of a HAN Thruster

"*One test is worth a thousand expert opinions*"

– Wernher von Braun (1912 – 1977), Rocket Engineer
& Lead Architect on V2 and Saturn V rockets

Thus far the study for a more promising ORS solution has pointed towards the development of an affordable, green, high density impulse upper stage engine to work in concert with heritage tactical missile solid rocket motors. This monopropellant engine, if proven, would be required to meet or exceed the performance of the historically chosen hydrazine. Several problems exist, the least of which is that a HAN thruster has never been developed past small scale (order of a few Newtons of thrust or less) prototypes. The remainder of this dissertation aims to empirically demonstrate a motor suitable for use as an upper stage space engine.

HAN Thruster Due Diligence

This discussion is not solely limited to progress with space thrusters using HAN. HAN and other similar combinations (e.g. mixtures with triethanolammonium nitrate or TEAN, etc.) were originally proposed for use in liquid gun applications. The findings of HAN for these purposes are well documented: Corner in 1976, Ref 70, Lee, et. al. in 1987, Ref. 71, among others. Many such analyses and experiments were directed by the Army Ballistic Research Laboratory at the Aberdeen Proving Grounds in Maryland during this period. Numerous conclusions from the liquid gun

efforts lend insight into the combustion characteristics of HAN in an appropriately designed thruster. Namely, it was shown that:

- HAN burning rates are considerably large (9 to 14+ cm/sec) verses usual liquid gun propellants.[72]
- It has been observed that many liquid monopropellants are very difficult to ignite below some critical pressure which is well above atmospheric pressure.[70]
- Difficult to ignite by pressure alone; HAN has a critical combustion pressure upwards of 250 MPa.[73] Also, it was found to be difficult to reliably ignite HAN below 3 MPa.[74]
- Burn rate has an abnormal, scattered dependence on pressure, with burning rates increasing dramatically past approximately 4 MPa, then largely pressure independent[68] until a certain high pressure range, 40 to 80mpa whereas the burning rate decreases with pressure.[72]

Common reported values for the burning rate of HAN solutions are approximately 10 to 20 mm/sec (Ref. 68) for the pressure range common to space monopropellant engines, < 4MPa. This is nearly an order of magnitude quicker than most other monopropellants at this pressure and could be exploited in regards to smaller, lightweight thrust chamber designs.

To date little research has been pursued into the formal application of working HAN monopropellant thrusters. Only two such thrusters, both

small-scale, have reported positive results. The first of which is Aerojet in a project sponsored by NASA Glenn Research Center. The thruster operated at fewer than 200 psi chamber pressure but produced over 250 seconds of specific impulse on a repeated basis. Aerojet's thermochemical analyses of their HAN/water/methanol blend predicted 269 seconds of specific impulse. The Aerojet thruster used an iridium coated catalyst that required 400C pre-heating to reliably ignite the HAN reactor. Test durations were up to 380 seconds with over 20 restarts resulting in smooth combustion, but with only Newtons of thrust.[69] A picture of the assembly is shown as Figure 36.

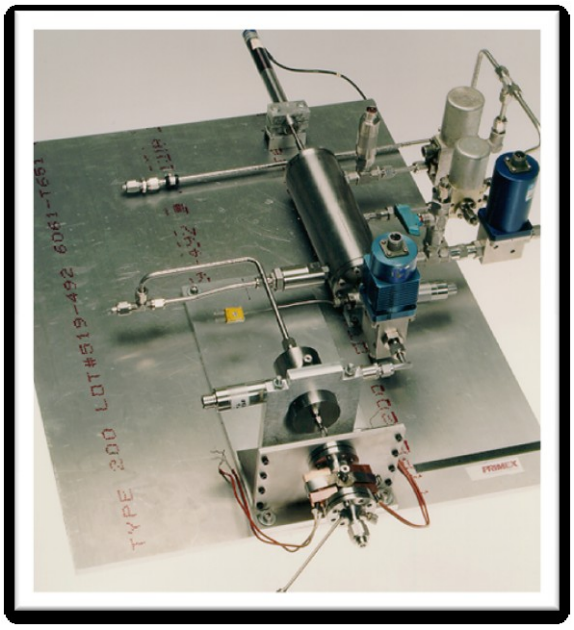

Figure 36: Test set-up of Aerojet HAN reactor.

The second HAN-based thruster development has been very recently pursued by researchers in Japan, Ref. 68 and Ref. 75. They report similar efficiencies for their tiny thruster, upwards of 240 second of

Isp with 90% efficiency for stable operations of 100 seconds. Moreover, research diving into the combustion mechanisms of HAN and methanol combinations has shown that not only will methanol increase the specific impulse, but it tends to reduce the typically very high burning rates of HAN and improve overall combustion. The linear burning rate in these experiments is greatly reduced which aids in long duration stable combustion.[68]

The aim of the remainder of the dissertation is to detail the design of a motor that surpasses these small-thrust pathfinder motors and will ultimately lead to development of appropriately sized final orbit insertion or reaction control system (RCS) thrusters. These motors will therefore need to provide thrust ranging several orders of magnitude: from less than one pound thrust up to several hundred pounds of thrust. The design of such a motor follows.

HAN-Solo v.1 Motor Design

The core methodology of the design of the HAN-Solo v.1 motor rests on a proof-of-concept motor with robustness, i.e. high factor of safety. This is a strict requirement for the motor because, as the name suggests, only one “solo” motor has been built due to time and financial limitations for development. Secondary to the robustness is a desire for modularity and quick turnaround time between motor tests. The rest of this section is devoted to the design of the proof-of-concept HAN-Solo v.1

motor; a concept drawing with major parts labeled is displayed as Figure 37.

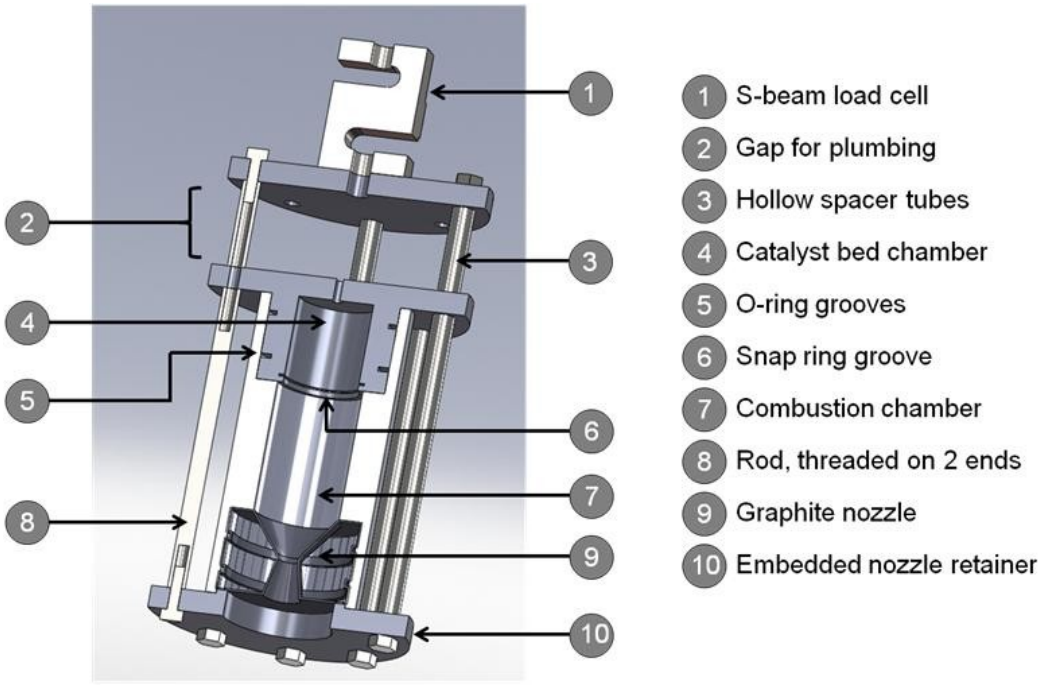

Figure 37: HAN-Solo v.1 motor design cutaway view.

The main objectives of the combustion chamber are to (a) effectively withstand the heat and pressure of the combusting gases and (b) provide positive retention of the remainder of the motor subsystems. The first is accomplished through an appropriate choice of chamber thickness dictated by a calculation of the maximum allowable hoop stress. The chamber was machined from 6061 stock aluminum for machinability which has yield strength of at least 8,000 psi and melts at approximately 1,200 degrees Fahrenheit. This melting temperature is not suited to the high stagnation temperatures that are seen by the motor though hardly

any metals are, including Molybdenum. This is a persistent problem in rocket motors but one that does not lack heat mitigation options. A common solution to the heating problem is an overdesign of the chamber wall to act as a heat sink, though this is only good for short duration hot-firings and where weight issues are not a factor. Typically such space monopropellants in this class, namely hydrazine, have electrodeposited high temperature-capable coatings and use refractory metals to rely on radiation cooling during operation. Other options such as active chamber wall cooling with embedded channels or even film cooling were evaluated but are not necessary as this motor will only burn for short durations, t_b< five seconds. Experience has shown that only thicker chamber walls and a sacrificial interior liner made of commercially available phenolic will be suitable for this application.

Firstly a chamber diameter must be chosen, i.e. an appropriate chamber volume must be calculated. The volume required must be of adequate size to allow complete mixing and combustion, requiring a sufficient “stay time” or “residence time”, t_s. Many factors contribute to this stay time, including the inherent propellant burning rate, injected conditions of the propellant, injector design, droplet sizes and combustor geometry, among others.[76] In turn this stay time relates to the required volume V_c and with a chosen chamber ratio the appropriate diameter can be found. Keeping with literature nomenclature, these values are often

written in terms of a unique parameter known as the characteristic length, L*.

$$L^* = {V_c}/{A_t} = {\dot{W}_{tc} \cdot V \cdot t_s}/{A_t} \quad (44)$$

The general trend is that an increase in L* will increase the characteristic velocity of the propellant up to an asymptotic limit. However, an increase in L* comes with the price of increased chamber weight, more surface area in need of cooling and increased frictional losses which tends to reduce stagnation pressure slightly. For adequate mixing purposes of future HAN/methanol-blends the L* was set to a conservatively high limit of 50 inches including the catalyst bed length which is based off of data for H2O2 and RP1 fuel.[76] The larger chamber volume promotes complete combustion and a lack of available data for this particular propellant suggests a conservative choice. Additional chamber volume only adds mass and some thermal losses, neither of which was of much concern in this present study.

For a monopropellant a great deal of the inherent residence time required for complete combustion is not based only on L*, as in a liquid engine design, but mostly on the catalyst geometry and reactivity. This is because most temperature activity is within the catalyst itself promoting a decomposition of the monopropellant into a hot gas, not within the subsequent combustion chamber volume. It is known that the nominal stay or residence time of a monopropellant through a catalyst bed is

directly proportional to the bed length L and inversely proportional to the bed loading, G [kg/s/m^2].[77] Longer residence times in the catalyst are advantageous as they allow for a more complete combustion, followed by additional combustion residence time in the L* provided by the combustion chamber. Higher pressures tend to increase the decomposition rates as shown in Figure 38 which would promote smaller combustion chambers but also require design margin for these higher pressures.

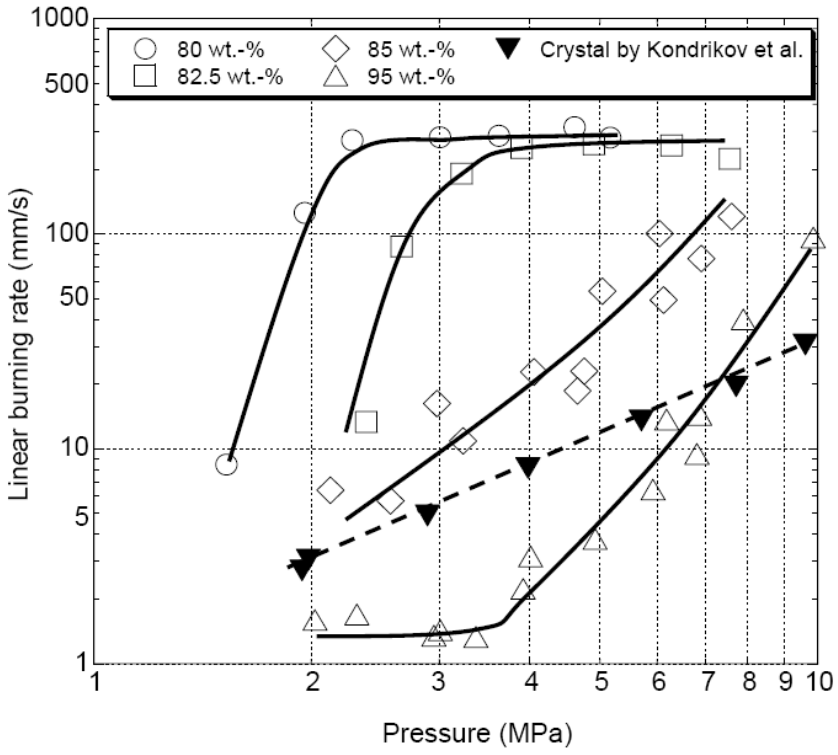

Figure 38: Linear burning rates of 80 to 95 wt% Aqueous Solution.[78]

Next a nozzle retention plate was designed to fit with a commercially available 76mm graphite nozzle available from Loki Research. Availability of such nozzles limited the nozzle throat size to 0.53 inches in diameter. This nozzle has a single o-ring and requires a

combustion chamber inner diameter of 2.725 inches for clearance. The nozzle retention plate also has an outer boss diameter to match this outside nozzle diameter, all of which was machined on a CNC mill, see Figure 39.

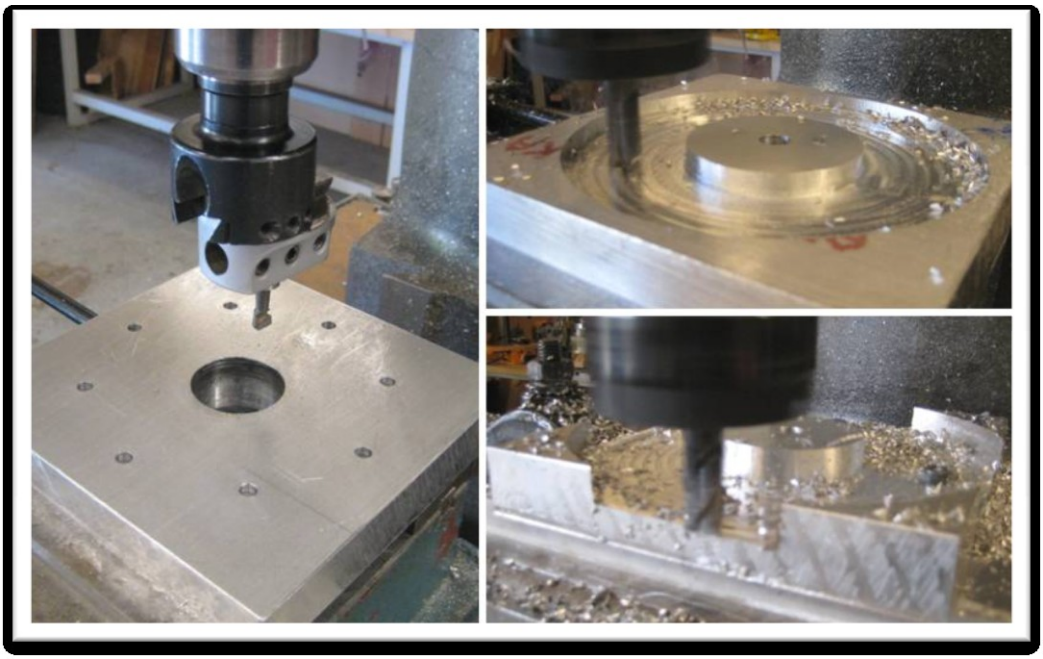

Figure 39: Collage of plate machining on CNC Mill at Arizona State University student machine shop.

The same design applies for the top side injector plate, Figure 40, whereas the outside diameter of the plate boss is machined to fit inside of the top combustion chamber opening with clearance for the o-ring groove and included Buna type o-ring. This plate must also hold an injector and was tapped with ¼ NPT female ports in both ends. Stainless steel adapters are used throughout to avoid material incompatibility with HAN blends. An inherent risk is adopted with use of SS plumbing connected to the injector plate. If a sum of propellant is ignited in these lines the result

could be an explosive burst of the lines, emitting small shards of braided stainless steel shards about the immediate area. Such accidents have occurred before in similar high pressure systems. As a mitigation step very high pressure hoses (2,000 max psi) were purchased for use in this system.

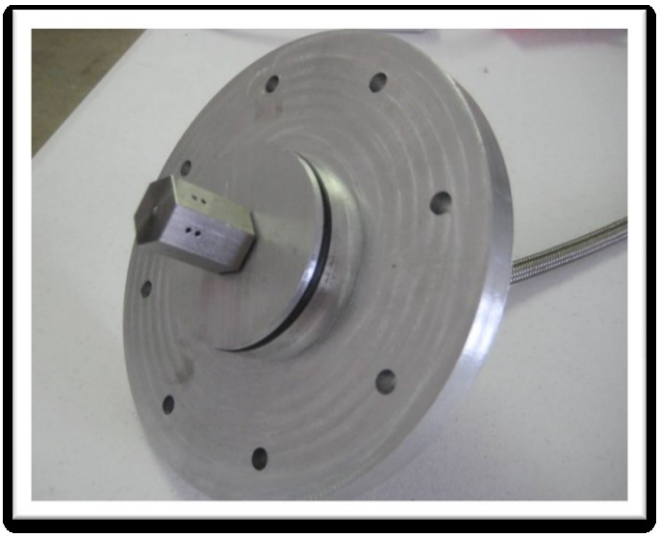

Figure 40: Injector plate with a custom stainless steel impingement injector.

Both end plates gripped the combustion chamber with the tension provided by eight (8) aluminum rods tapped for 1/4-20 high strength steel hex bolts with lock-wire head caps to prevent counter-rotation during operation. A final thrust plate was used to mate a compression load cell to the assembly and leave sufficient clearance for the propellant plumbing. The final assembly is shown as Figure 41.

Figure 41: Left: CAD model of HAN-Solo v.1, Right: Installed motor.

An exhaustive list of the inherent equations and calculation of the pertinent performance values will not be stated here. The motor was designed to operate at a maximum of 100lbf at a chamber pressure of 300psi and would provide a maximum of 177 second of I_{sp}. Table 11 lists a summary of these calculations.

Table 11: Pertinent design variables of HAN Solo v.1 motor design.

Chamber Pressure	300	*psia*
Thrust	100	*lbf*
Burn Time	30.00	*sec*
Design Exit Pressure	14.7	*psia*
Density of HAN/methanol mixture	94.53	lb/ft^3
Half angle of diverging nozzle	15	*degrees*
Half angle of converging nozzle	40	*degrees*
Exit Mach Number M_e	2.63	
Nozzle Expansion Ratio	2.65	
Stagnation Temp (R)	4299	*R*
Molecular Weight	23.121	*lb/mol*
Ratio of Specific Heats	1.5143	
C_F Thrust Coefficient	1.34	
Corrected c*	4247.45	*ft/sec*
Exhaust Velocity	5705.01	*ft/sec*
Actual Isp	177.32	*sec*
Propellant Flow Rate	0.56	*lb/sec*
Oxidizer tank volume (no ullage)	1.34	*gallons*
Throat Diameter	0.56	*in*
Exit Diameter	0.92	*in*

Injector and Catalyst Selection

It was determined through cold flow and hot fire operational testing (see next section) that injector sizing for this propellant is of the utmost importance. The reason for this was a necessity for small droplet or gasified particles such that they could be rapidly decomposed in the catalyst bed. A large droplet and/or non-uniform spray pattern can result in over-saturation of the catalyst bed and possibly end in an explosive situation. It was found that smaller particles react more quickly with the

chosen catalyst, whereas liquid pools would result in a “hang-fire”, i.e. a very long wait-time until ignition.

Several different injector options were investigated. The types included: commercially available 316 stainless steel spiral designed cone nozzles, two full-cone spray nozzles at several different mass flow rates (1 and 1.5 gallons per minute @ 40psi) and a series of custom-made injectors including fully axial, shower head and fully radial side-wall impingement. These injectors were compared on the basis of mass-flow rate and degree of atomization. Unfortunately, a lack of immediate access to high-speed video cameras or particle image velocimetry equipment for these tests limited the scope of analysis to visual comparatives. Figure 42 is a collage of cold flow tests for different injectors at different propellant tank pressures.

Figure 42: Clockwise from upper left: spiral flow valve, sidewall impingement on pre-catalyst bed chamber, cone spray with water, cone spray with HAN.

Equally important to the injector selection is the development of a catalyst able to react and decompose HAN. Literature has shown that HAN is particularly hard to ignite by pressure alone and would require pre-heating of a catalyst substrate made of platinum or iridium to ignite reliably. The latter method is used with hydrazine whereas the catalyst bed, namely a ceramic substrate of Shell 405, is pre-heated to hundreds of degrees prior to propellant introduction. Such a method would require 200-300°C for decomposition of HAN which would add to time-to-ignition, an unfavorable factor for operationally responsive vehicles.

As a result a different approach was pursued and eventually established as a sufficient method for ignition of a HAN monopropellant

engine. This advance was motivated by a need for a catalyst that would support auto-ignition upon contact with HAN. This substance was developed as a powder, approximately 50 microns in diameter, and is coated on a high-platinum catalyst substrate consisting of many small channels, see Figure 45. The purpose of said formula was to provide immediate decomposition of the HAN and thusly pre-heat the solid catalyst channeled substrate for further elongated reaction of the remaining of the HAN. The formula proposed is a proprietary blend of a HAN catalyst and several additives, developed originally by Rick Loehr of Raytheon Missile Systems and further modified for decreased reaction time. Figure 43 shows the mixture in a mortar bowl during particle refinement.

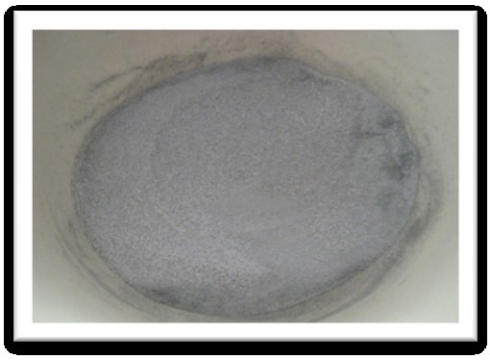

Figure 43: Consistency of catalytic mixture during particle grinding with mortar and pestle. Particle size is approximately 50 microns.

The primary ingredient of the mixture is known to react with water, methanol and HAN (all of which are present in the proposed motor configuration) and the additives complete the reaction with spectacular

results. Figure 44 is a video patchwork of such a reaction which takes place nearly instantly after introduction of HAN to the mixture.

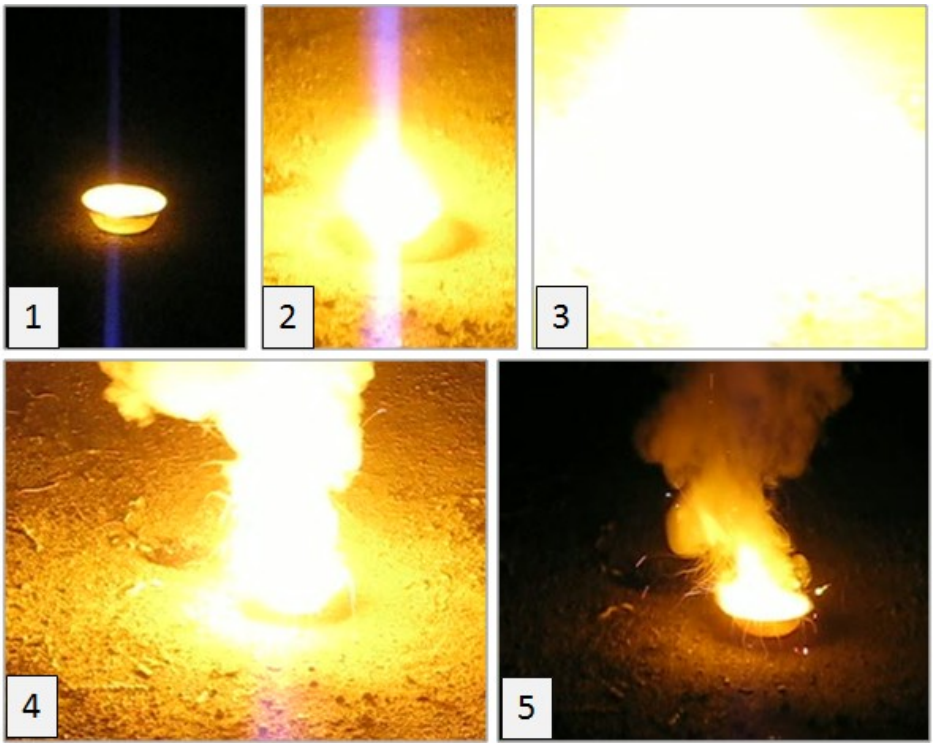

Figure 44: Fast reaction of approximately 1 tsp of liquid HAN and 1 gram of catalytic mixture.

As mentioned in the previous section: it is known that the nominal stay or residence time of a monopropellant through a catalyst bed is directly proportional to the bed length L and inversely proportional to the bed loading.[77] For this reason a long catalyst bed and low mass flow rate, ~0.239 lbs/sec or 0.1084 kg/sec, were initially chosen to support good initial decomposition without oversaturation, the results of which are listed below:

Table 12: Catalyst dimensions and values.

Variable	Value
L	5.08cm / 2.00in
Dia.	6.35cm / 2.50in
G_{max}	34.23kg/m^2 / 0.048698lb/in^2

The catalyst carrier is a solid catalyst bed supported with a high active metal platinum content, though it has been shown that an iridium based catalyst support is superior in performance for HAN.[75] As previously mentioned, the catalyst platinum doping substrate has a temperature limit of 3,200°F and the aluminum oxide catalyst structure has a melting limit of approximately 4,000°F. The channels of the catalyst bed are approximately 50 thousandth of an inch (0.050” or 1,270 microns) in width and height. As Figure 45 suggests the catalyst bed is reusable so long as the melting temperature of the aluminum oxide structure is not reached. It can simply be reloaded with a fresh coat of the mixture.

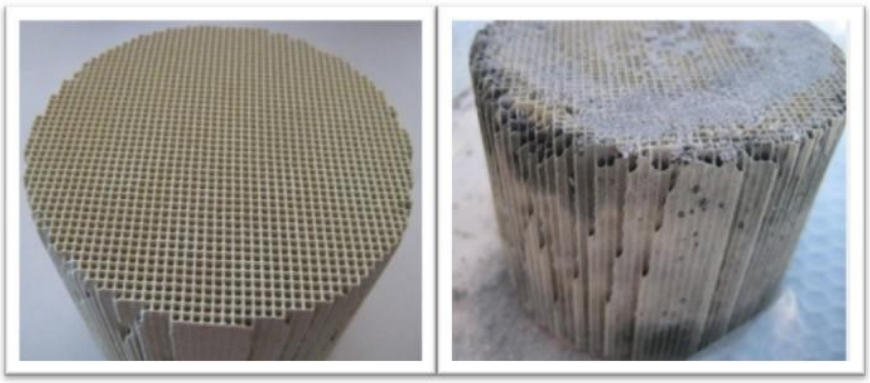

Figure 45: Left: Catalyst bed undoped with catalytic mixture. Right: Catalyst bed after several uses receiving fresh coat of mixture.

Setup of HAN Thruster, DAQ and Associated Hardware

The next step following the successful construction of the HAN-Solo v.1 thruster was a design for the monopropellant feed system and support hardware. This section briefly describes this test set-up and its major components.

A key consideration in this design was the capability for high and low flow operation. Low flow operation made use of a flow reducer to limit the mass flow rate during the start-up transient. High flow operation would be used once the catalyst bed was of sufficient temperature to support catalytic decomposition without the aid of the catalytic doping mixture. Higher mass flow rate through the catalyst bed is also found to reduce wear on the catalyst support material by convection. A low mass flow rate, hence a low bed loading, is desirable for complete combustion through the catalyst bed. The procedure was later amended to allow short pulse start-up operations to avoid oversaturation.

The tank used was an aluminum pressure vessel rated pass 1,000psi and measuring 19" long x 5.09" in diameter. This extra large ullage volume was advantageous as the system was designed as a “blow-down” tank with Helium used to provide the back pressure. Such large ullage volumes will help maintain a more uniform chamber pressure during a typical short duration test. Additional plumbing in the all-stainless steel system included manual valves for safety, check values to prevent backflow, and various NPT and AN hosing and fittings.

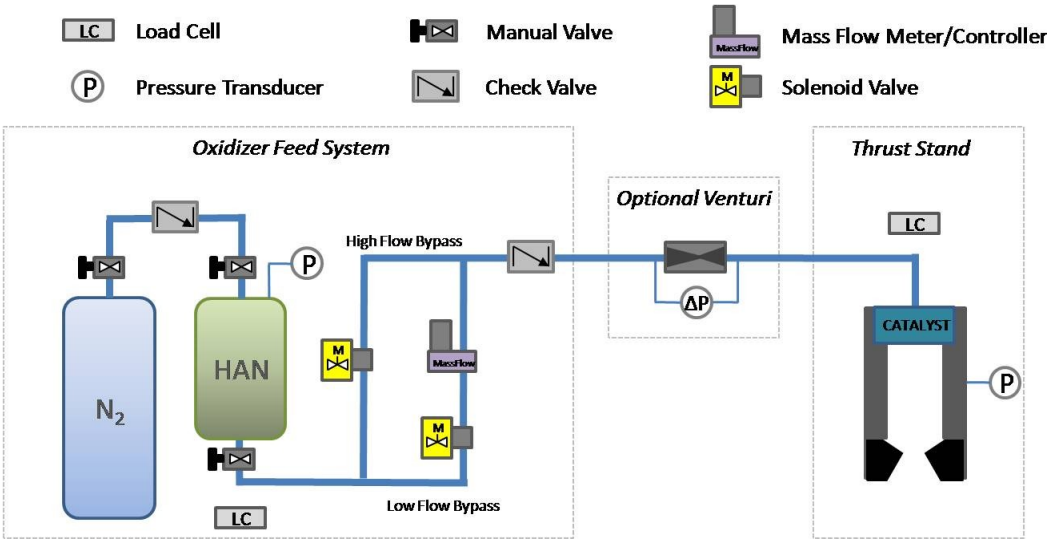

Figure 46: Flow diagram of HAN Solo v.1 plumbing.

Accurate measurement of thrust and stagnation pressure levels of the motor are required to evaluate the performance of the *HAN-Solo v.1* motor in both the initial low-flow motor ignition and the subsequent high-flow motor operation. The primary measurement devices and associated data acquisition system are described as follows:

- Thrust is measured by a tension-compression load cell: Omegadyne LC203 with 500 lbs limit. Excitation voltage is provided by a DI-8B signal conditioner and op-amp module that comes as an accessory module to the *DATAQ* DI-718B data acquisition system.
- Stagnation pressure of the motor is measured by an *Omega* PX309 pressure transducer with a range of 0 to 2,000psi connected to a ¼ NPT flow reducer connected directly into the side of the combustion chamber. An optional snubber is used as well to protect the

transducer from any drastic pressure spikes. The pressure transducer is packed with silicon grease prior to motor operation to deter any transient thermal inequilibrium that has in the past resulted in erroneous pressure measurements from the direct impingement of hot gas onto the sensing diaphragm.[79] The excitation voltage for these pressure transducers is supplied by an external dc source at 12VDC.

- Several *NOS Big Shot* nitrous vales are used to initiate propellant flow into the pre-catalyst bed chamber. These electric solenoids are powered by a custom made relay ignition box that provides a 12V source from a car battery whilst keeping the operator at a distance of up to 200 feet from the motor. Previous tests with this brand of electric solenoid supplies a mass flow rate of over 0.6 lbs/sec using a propellant of similar density and back pressure.
- The above set of data is measured and recorded by a *DATAQ* DI-718B data acquisition system. In addition to built-in modules for signal conditioning and op-amp excitation voltages, the data logger also displays the data real-time to a personal laptop at the test site through a Cat5 ethernet cable. The DI-718B has eight channels, each of which can be customized with the DI-8B modules, and supports sample rates up to 4,800 Hz.

A typical test fire consists of a set of rehearsed activities designed to maximize safety and also aims to produce repeatability between tests. A typical sequence for HAN motors was developed and is outlined below:

1. The motor is loaded with a new catalyst freshly coated with catalytic mixture.
2. Solenoid checks are initiated and cycled to show proper function.
3. The HAN tank is filled to an appropriate level and weighed.
4. HAN tank is kept in an upside down condition while helium is pressurized into the tank. The HAN tank, fully pressurized, is then secured in its holster in an upright gravity-feed position.
5. Valves are once again cycled to remove any excess helium pressurization from the feed lines and ensure that the values are fully closed.
6. Manual safety valves are opened and operators retreat to safe distance with ignition box.
7. Start data acquisition system recording.
8. Initiate low-flow solenoid to start pre-heating of catalyst chamber and initial combustion sequence.
9. Cycle low-flow solenoid to minimize excess propellant flow into chamber during transient.
10. After a short duration an additive in the catalyst mixture will be exhausted signaled by a change in the plume smokiness.
11. At this point the high-flow solenoid is initiated to start full flow.

12. After test fire the remaining HAN amount is weighed.
13. Known mass flow rate values for specific back pressures from previous tests are used to calculate performance from load cell and pressure transducers and measured propellant mass values.

7. Motor Testing and Future Variants

Following completion of cold-flow injector testing and many successful trials with the catalytic reaction mixture, full small-duration hot-fires could be attempted. The original purpose of the effort was to demonstrate and capture the performance qualities of HAN and other HAN blends (e.g. HAN/methanol). However, the effort quickly shifted towards demonstrating operability of the HAN propellant, as it was found that reliable ignition with the hypergolic catalyst mixture was a function of several variables. A solution was eventually established but future testing of the system is still warranted to further deduce the operation steps.

Static Hot-Fires of HAN-Solo v.1

Initial testing of the HAN-Solo v.1 motor was first carried out with cold-flow testing of the system to work out any plumbing issues and characterize the mass flow rate at the different flow levels. Multiple tests with water and then finally HAN were performed. Low-flow mass flow rate was approximately 0.1434 to 0.239 lbs/sec of HAN at 300psi tank pressure. The value carries a high degree of uncertainty because of the limited number of trials carried out and the inherent difficultly in recovering unused HAN from the system. Limited stores of HAN reduced the scope of testing to only a few pounds of propellant per cold flow trial. Future testing with water/glycerol blends that matches the viscosity of HAN is proposed

as a low cost solution for injector trials at different pressures to better determine HAN mass flow rates.

The first series of hot-fire tests were designed as proof-of-concept ignition tests and were limited to approximately 0.5 seconds in valve duration at very low tank pressures: 200 to 300 psi. The first several tests resulted in no-ignition pointing towards an issue with catalytic ignition. It was determined that the low-flow operation introduced too much liquid HAN into the cat bed chamber, thereby oversaturating the catalyst and allowing the propellant to exit the engine un-decomposed. One such trial eventually resulted in a “hang-fire” operation nearly a full minute after the propellant had been expended. The reason for this were small amounts of residual HAN left in the catalyst chamber eventually ignited with the remainder of the catalytic mixture. This created sparks and a sufficient heat source to ignite the HAN that was now occupying the ground below the test stand. The reddish-brown smoke seen in Figure 47, a tell-tale sign of incomplete nitrous dioxide combustion,[23] smoldered for over two minutes after the initial delayed reaction.

Figure 47: Hang-fire of motor during initial ignition trials.

Subsequent tests had more success once steps were taken to further reduce the initial propellant slug introduced into the motor. A higher back pressure was also used. This in turn increased the initial mass flow rate but shorter solenoid activation times were used to reduce the amount of propellant introduced. The elevated pressures were instead justified as a means to better atomize the incoming HAN and reduce over-saturation. This method soon became the winning combination and short pulse, $t < 0.3$ seconds, operations were now possible as shown in Figure 48.

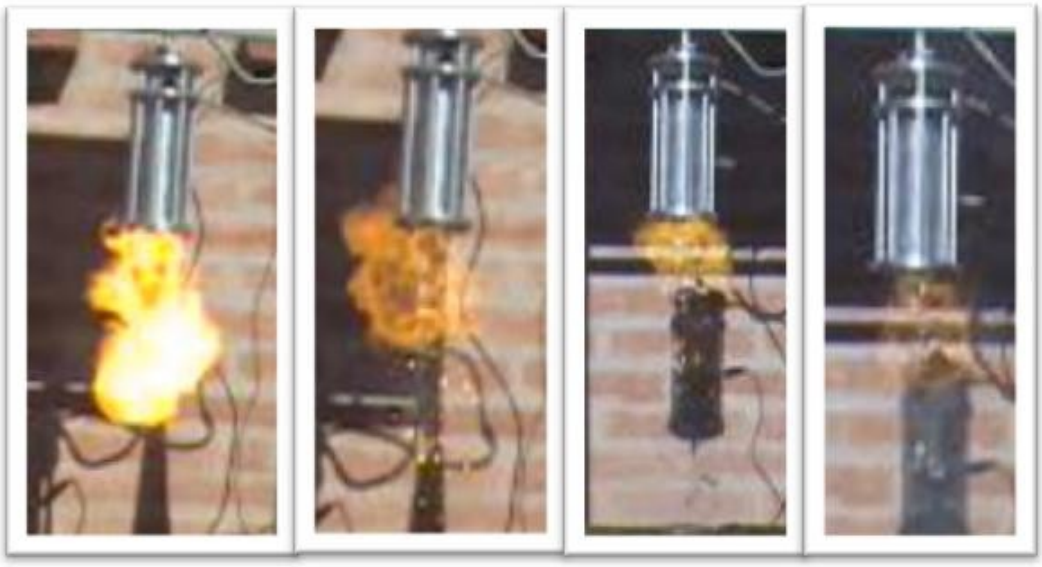

Figure 48: HAN Solo v.1 motor during short duration pulse fire operation.

The pulse operation method, now proven to reliably ignite the HAN, was eventually used to support longer duration testing. A few successive pulse operations were used to sufficiently heat the catalyst bed so that it could independently decompose incoming atomized HAN without the aid of the catalytic mixture. Again, higher pressures were used to (1) better atomize the propellant, (2) provide more engine thrust, but had the result of (3) increasing the burning rate of HAN. These tests were still limited to short burn times, $t < 0.5$ seconds, but included higher amounts of HAN flow and thusly more useable thrust and elevated chamber pressures.

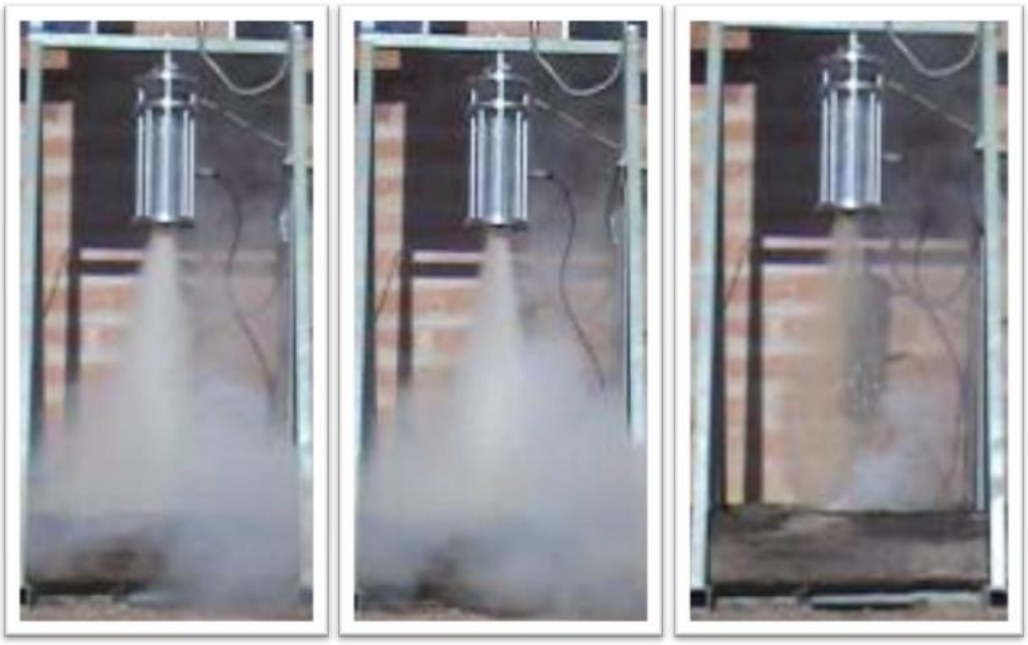

Figure 49: HAN Solo v.1 motor during longer sustained burn.

Above, Figure 49 shows a short thrust burn at a high tank pressure. The HAN plume should be clear for full combustion (far right) and the smokiness is residual magnesium additive to the cat bed which is extinguished in the very beginning of the burn. Upon closer inspection of the video feed and photographic evidence it is apparent that some un-combusted HAN is exiting the nozzle. This hints towards several likely culprits: (1) mass flow rate is set too high, (2) injector is not operating at a sufficient pressure to effectively atomize the propellant and (3) the characteristic length, L*, of the combustion chamber is set too small and not allowing sufficient stay time to fully combust the propellant. A solution of increasing the chamber pressure further was first tried, ending in disastrous results for the motor:

Figure 50: Left: Over-pressurization of HAN Solo v.1 following sustained thrust trial. Right: aftermath of over-pressurization.

As shown above in Figure 50, the case burst after approximately 0.3 seconds of operation in a subsequent trial. The difference between this test and preceding tests was the tank pressure, which was raised to over 600psi, resulting in a projected chamber pressure of approximately 400psi. Forensics of the motor post-fire showed that the over-pressurization occurred in the aft end of the motor along the combustion chamber seam where the graphite nozzle was located. This particular location was the thinnest section of the chamber, measuring only 0.1375” in thickness which was required to provide space for the graphite nozzle. The upper half of the chamber was blown upwards, shattering the catalyst bed. However, this piece of information clearly proves that the explosion was a result of over-pressurization in the combustion chamber. It was therefore not a violent reaction in the pre-combustion chamber which was

identified as a likely failure point due to over-saturation. This will be an important design point for subsequent test motors.

The likely cause for the failure is a runaway reaction rate that ignited much of the un-combusted liquid HAN in the chamber that was previously seen exiting the nozzle. As shown before in Figure 38, the reaction rates for HAN are unusually sensitive to pressure. At values approximately equal with the intended combustion chamber, 300 to 400psi, the reaction rate will increase rapidly, nearly an order of magnitude increase overall.

Concluding Remarks and Future Variants

Regardless of the final outcome of the HAN Solo v.1 monopropellant motor, many conclusions can be made. These include:

1. Development and testing of a new catalytic mixture that is hypergolic with HAN.
2. Developed a short-duration pulsing method to reliably ignite a HAN motor without the need for pre-heating the catalyst bed. Recommend reduced mass flow rates to get engine started and pre-heated.
3. Demonstrated short-duration sustained catalytic decomposition after ignition.
4. Have shown ease of handling operation with non-toxic HAN that has higher density and better storage qualities than both hydrazine and high percentage hydrogen peroxide.

5. Injection methods are vitally important to stable, sustained operation of HAN motor. Excess non-combusted liquid HAN can lead to rapid, unintended over-pressurization in the combustion chamber.
6. Figure 45 shows that the side-walls of the catalyst substrate witnessed more reaction than other parts. Care must be taken to avoid over-saturation at the edges, i.e. seal these edges or liquid HAN will pool and burn which might prove to be destructive to the motor.
7. High reaction rates at elevated pressures must be accounted for in the design of future motors. Any combustion instabilities in future motors could result in motor loss. However these decreased propellant stay times could lead to smaller, more lightweight combustion chamber designs.
8. HAN Solo v.1 represents the largest HAN monopropellant motor tested to date and further proves the concept as a viable replacement/upgrade for heritage hydrazine motor.

The unexpected loss of the HAN Solo v.1 motor unfortunately stopped short the additional planned test series for this motor. These included (1) performance calculations from a series of standardized HAN-only tests and finally (2) additional testing with HAN/methanol blends. The former would provide a baseline with which to compare the expected theoretical thermochemical analyses with empirical data. Such

comparisons are necessary to single out and identify the shortcomings and areas for improvement. The latter was an attempt to further improve the performance past that of hydrazine with the use of methanol blends which are miscible with HAN. Figure 51 illustrates some recent linear burning rate trials by Katsumi, et. al. showing that compositions with methanol added to the mixture will decrease the critical pressures and result in a more linear burning rate and markedly smoother combustion at higher pressures.[68]

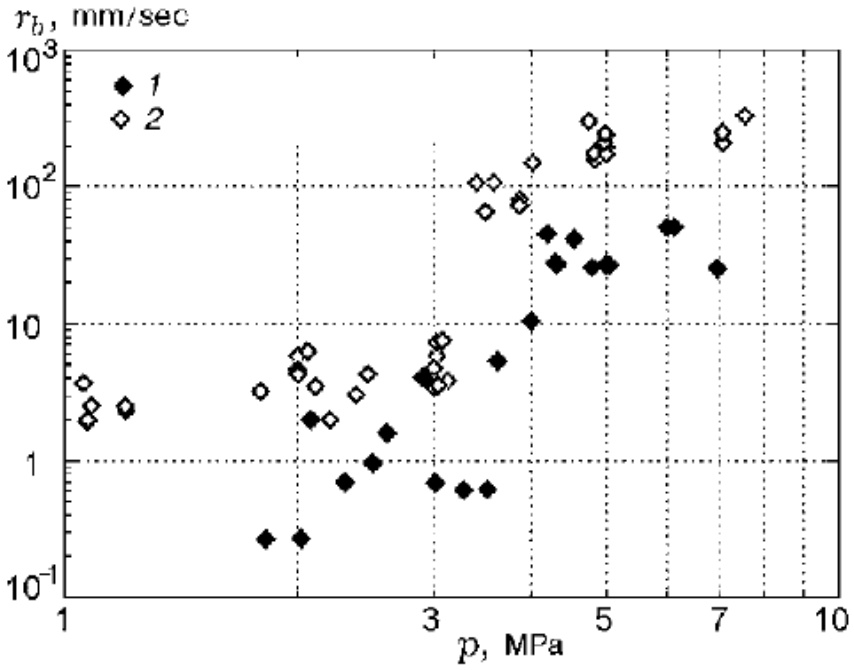

Figure 51: Burning rate of a HAN/AN/water/methanol mixture versus pressure: points 1 refer to a HAN/methanol composition and points 2 refer to HAN only.[68]

As discussed in the previous section this increase in performance comes at the cost of elevated temperature, past the temperature limit of

the catalyst platinum doping substrate at 3,200°F and the aluminum oxide catalyst structure temperature limit of 4,000°F. Current catalyst technology cannot withstand these temperatures for prolonged exposure, though it has been shown that higher mass flow rates through the catalyst tend to decrease the decease the temperature of the catalyst bed by convection.[68] Future motor designs should rely not on the stoichiometric addition of methanol, but rather reduce the amount of methanol in the HAN blend to limit the temperature through the catalyst bed to acceptable levels. If additional performance is required then a post-injection of the remainder of the methanol fuel can be directly injected in the combustion chamber. Additional trials would be required to set the optimum L* for this configuration.

Several promising injection methods are proposed for later evaluation. The first is a coaxial injection of methanol through the catalyst bed where the hot decomposed HAN will serve to shear and atomize the incoming methanol. This method is similar to the LOX/LH2 Space Shuttle Main Engine coaxial injection scheme. A preliminary CAD drawing of this scheme is shown below, the purpose of which was to use as much of the existing (and surviving) HAN Solo v.1 hardware as possible. This would limit combustion temperatures only to the face of the catalyst bed (where the decomposed HAN will serve as a barrier) and chamber walls. As a result the catalyst bed could be spared for recurring firings.

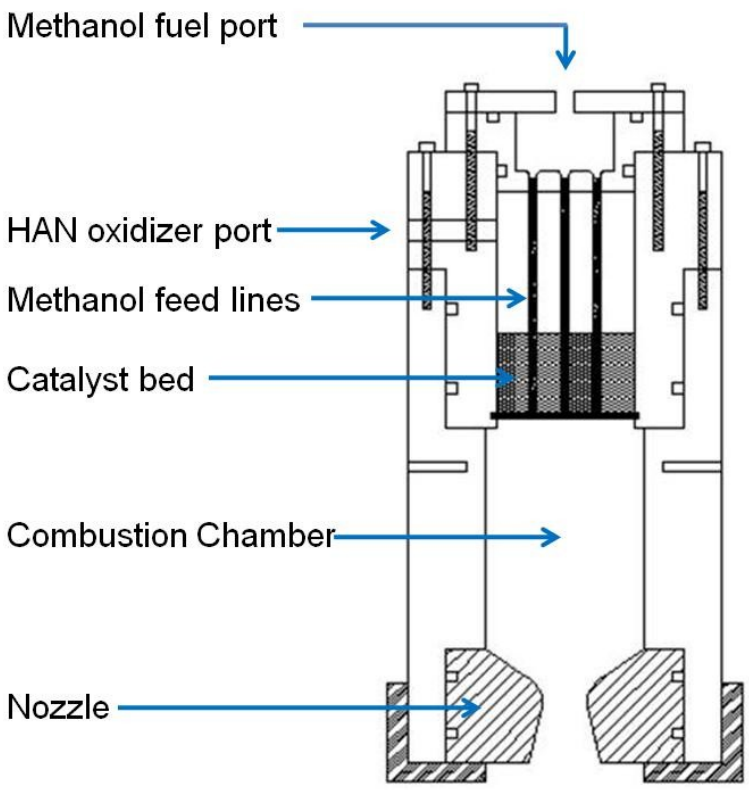

Figure 52: Coaxial injection of methanol through HAN catalyst bed.

The second method, shown in Figure 53, involves a more conventional post injection along the chamber walls past the catalyst region with an added benefit of some degree of chamber wall film cooling. Swirl injection would be favored for this purpose to give additional stay time of the methanol within the combustion chamber. This would reduce both chamber wall and catalyst temperatures to suitable values. But while both methods answer the HAN/methanol injection, they do not directly address the HAN injection prior to the catalyst bed. This should be a continuing focus area.

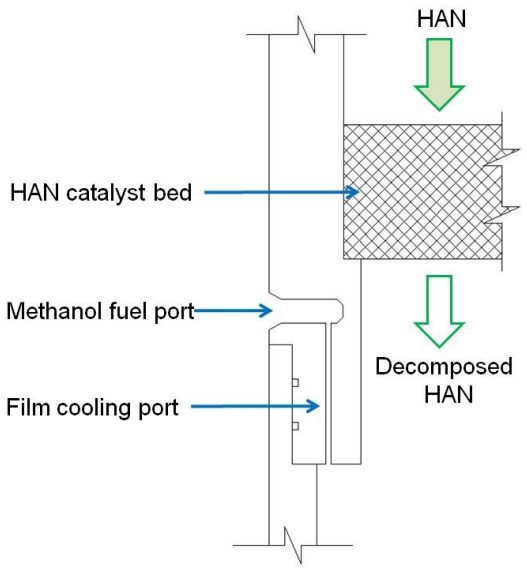

Figure 53: Fuel film cooling injection method.

The last method borrows heavily from liquid rocket engine injector designs. In the strictest terms any of these methods could be considered conversion from a monopropellant to a liquid rocket engine. This is not entirely appropriate since the vast majority of the propellant mass and volume would be HAN oxidizer, likely pre-loaded with miscible fuels. Thus the excess fuel is limited to very small tanks in comparison. In this case the preferred nomenclature would be “fuel augmented monopropellant”. Regardless, the likeness does afford the opportunity to use existing liquid engine designs to aid in the injection. As a result we are not limited to “shower head” designs but rather more complex and proven methods. This could include unlike-doublets, unlike-triplets, like-impinging-doublets, etc. Figure 54 shows an unlike impingement method of fuel and oxidizer. It should also again be reiterated that the large density and viscosity of HAN

was found to be difficult to atomize. A like-impingement method might work well to alleviate this ahead of the catalyst bed and thereafter a different scheme could be optimized to inject the now-decomposed HAN with the fuel. The catalyst bed in this configuration also does not have to be in line with the injector: it could be a standalone apparatus that decomposes the HAN in a separate small chamber then injects the remainder through injector plates as shown below.

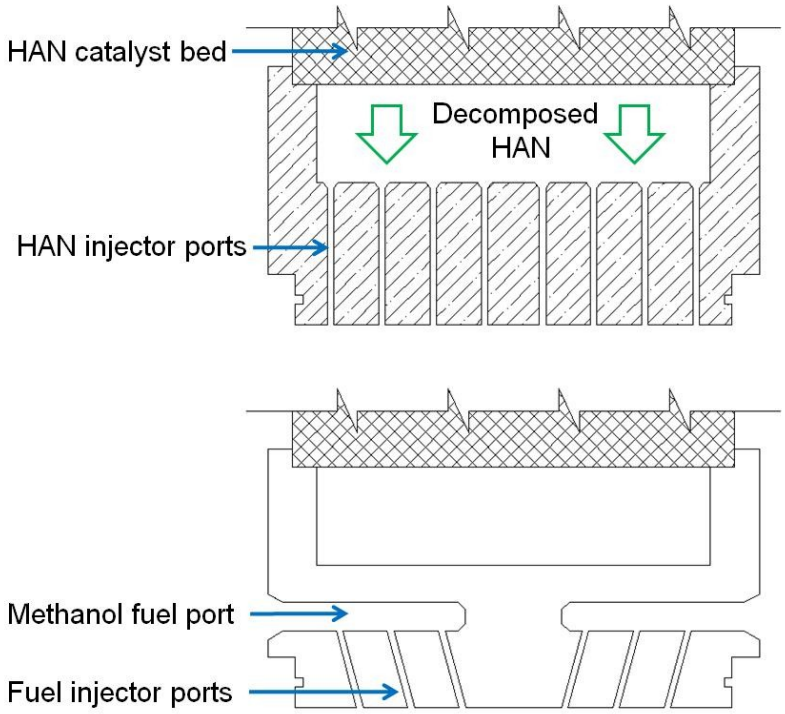

Figure 54: HAN/Methanol impinging injector plates. The views are rotated 45 degrees from each other. Top: HAN oxidizer feed. Bottom: Methanol injector ports.

Post injection of methanol by means of any configuration will yield a substantial increase of approximately 50 seconds of specific impulse. This would increase payload mass or ΔV capability at the cost of additional

complexity and structural mass. An additional cost-mass-performance analysis would be required to realize the benefits, if any, this proposed HAN/methanol motor will have on the life cycle cost of the intended launch vehicle.

The first question that would naturally arise would be “is it worth it?”. Such gains in specific impulse over the complexity of the addition of post injected methanol should be first quantified. There are several ways to answer this question, both in terms of cost, performance gain and physical changes to the system. At a first order look it is appropriate to compare the different methods versus the volume constraint, i.e. if the propellant selection will fit in the allotted structure. Density impulse plays a big role in this analysis, and while adding methanol will increase the specific impulse, it will also lower the density commensurate with the oxidizer to fuel ratio.

As a direct comparison an upper range ΔV mission of 3,000 m/s is used for the upper stage with a diameter of 0.35 meters. Following the examples in the dissertation a payload mass, m*, of 50 kilograms is chosen. A reasonable inert mass fraction, $f_i = m_s/(m_s+m_p)$, for an upper stage vehicle of 0.2 is also selected (values as low as 0.08 are possible), which is convenient because it is typically a function of only the propellant mass. Utilizing the ideal rocket equation from before, the mass of propellant can be arranged to:

$$m_p = \frac{m^* \cdot \left[e^{\frac{\Delta V}{Isp \cdot g_o}} - 1 \right] (1 - f_i)}{1 - f_i \cdot e^{\frac{\Delta V}{Isp \cdot g_o}}}$$

(45**)**

A number of propellant combinations are selected for comparison. The popular LOX/LH2 liquid engine is selected to show the large volume requirements for liquid hydrogen – note: even though the O/F ratio is six for this example, the LH2 fuel tank is nearly three times as long, though it carries one sixth the amount of mass as LOX. Following the examples from before, hydrazine and high percentage hydrogen peroxide are also included as a baseline. Lastly, different blends of HAN are incorporated. These are all summarized in the following table:

Table 13: Comparison of different propellant combinations and effect on tankage length.

	LOX/LH2	Hydrazine	H2O2	95% HAN	HAN Blend	HAN, 15% Methanol
Specific Impulse (sec)	430	250	250	230	250	280
Propellant Mass (kg)	149	425	425	620	425	295
Length of Ox Tank (m)	1.08	4.42	3.05	3.55	2.6	1.45
Length of Fuel Tank (m)	2.92	-	-	-	-	0.58
Total Length (m)	4	4.42	3.05	3.55	2.6	2.03

The differences are staggering; with the higher Isp (and thus lower propellant mass) LOX/LH2 combination, the combined tank length is nearly twice as long as the HAN blend with separate methanol tank. The use of heritage Hydrazine in this example is even poorer, while the overall propellant mass is commensurate with the HAN blend at the same Isp. Again, this is a function of the higher density specific impulse. Thus, even

though the extra methanol decreases the density of the propellant, the gain in Isp is enough to still drive smaller tanks.

It is also instructive to note that the length increases directly with the change in payload mass for this 3km/s ΔV mission. For every kilogram of m* added [or subtracted] the length will increase [or decrease] for each of the propellant combination by:

- 0.0798 [m/kg] for LOX/LH2 engine
- **0.0883** [m/kg] for Hydrazine
- 0.0609 [m/kg] for H2O2
- 0.0717 [m/kg] for HAN
- 0.0519 [m/kg] for HAN with 5% miscible methanol
- **0.0406** [m/kg] for HAN with 15% methanol (separate tank)

This again illustrates that HAN with small additions of fuel is much less sensitive to overt rocket length gain. These numbers provide a good rule of thumb for pre-designers to keep in mind through the design process. It is also known that a long and thin propulsion system geometry and a high-density propellant will help to reduce drag.[28] However, the length to diameter ratio (L/D) of the proposed architecture is already quite large so care must be taken to limit to the length gain on the upper stage. For instance the hydrazine solution would add an additional 12.6 L/D to the existing baseline which would increase the in-flight attitude control system requirements (thusly: weight and cost) to provide triaxial stabilization and control.[80]

This solution also opens up the opportunity to pre-load the HAN with a small amount of methanol (enough to keep the temperature below the critical value for the catalyst bed) then post-inject the remainder of the 15% by mass methanol into the combustion chamber. This affords the system more flexibility as it could also be co-utilized with other functions such as:

1. The small amount of excess methanol could be used for regenerative cooling (chamber and/or nozzle) until it is needed for combustion. Rocket fuels have an excellent heat capacity so it would be the favored medium over using HAN for this purpose.
2. Excess methanol could be loaded at a minimal change in structure mass to provide thrust vector control by liquid injection into the nozzle downstream of the throat. Methanol would be a reactive mass for liquid injection that would combust and increase the TVC angle. In this manner a weighty gimbal mechanism for the motor can be replaced, further reducing weight and cost.
3. As proposed before, the methanol can be post-injected in the form of film cooling along the chamber walls. This would cool the case somewhat while still increasing the chamber temperature with minimal change to molecular mass, thus more total specific impulse.

4. The methanol could be saved along with a sum of HAN to be used for later mission high-Isp maneuvers. For ORS needs, the HAN will have to auto-combust with the proprietary mixture. For restart capability, where startup time is no longer a prime factor, catalyst bed electric warmers could be used for engine restart and thrust shaping capabilities for in-space use.
5. Inject the methanol at a rate consistent with an optimum Isp to further increase the ΔV.

The latter is an interesting concept explored by the author with Dr. Mark Langhenry. Past literature regarding rocket propulsive efficiencies have remarked that an optimum is reached when the exhaust velocity is equal to that of the instantaneous velocity (Ref. 66) and also that there is an optimum mass ratio at m_f/m_o = 0.2032 when exhaust velocity is held constant (Ref. 81). For the first case, which neglects drag and gravity, it is not feasible to change the exhaust velocity in that manner. The rocket engine would be required to throttle from an Isp of zero to an Isp of approximately 780 seconds for a trip to LEO. No such engine is capable of that feat, and only nuclear thermal rockets or electric propulsion (both with low T/W) could achieve such high end Isp values.

However, when examining unexplained specific impulse losses on the Titan IV SRMs, Langhenry and Parks (Ref. 82), deduced that these Isp losses were attributed to nozzle losses (both efficiency and erosion)

and changes in operating pressures (c* is a function of p_o). Specifically for nozzles the Isp is expected to decrease throughout the burn because of erosion of the throat which leads to changes in the fixed area ratio. Subsequently they found that if the Isp were to decrease (or increase) at a linear rate, then the following equation could be derived to show the net reduction in ∆V.

$$\Delta V = -g_o I_{SP_o} \cdot \left[\left(1 - \frac{1 + {M_f}/{M_o}}{1 - {M_f}/{M_o}} \alpha \right) ln \left({M_f}/{M_o} \right) - 2\alpha \right]$$

(46**)**

Where "α" is the rate at which the initial specific impulse, Isp_o, changes linearly with respect to mass expelled.

Langhenry and Villarreal (Ref. 83) have since shown generalized cases with chemical propulsion systems that increase ∆V further by judicious use of the total propellant energy. It is shown that a net efficiency increase can be expected by diverting from the constant exhaust velocity operation. For many systems, such as solid rocket motors, the Isp is generally fixed. But for liquid engines or the augmented monopropellant presented herein, the exhaust can be changed in flight. This flexibility is not often used, only for means for mass flow rate control to increase or decrease thrust. It has been shown that several simple methods to change Isp in-flight can be employed for net gains in ∆.

A linear change in Isp or O/F is one such method, and though it is not the most efficient, it is still a good fit to the optimum. The optimum, as shown in Reference 83, is an exponential function that modifies the specific impulse throughout the burn. It has been shown that increases of ΔV on the order of a few percent or more can be obtained. Recall: the ideal rocket equation is an exponential function with regards to both Isp and ΔV, so even a small increase in effective Isp can have large impacts on the mass ratio. The following scenario calculates if these increases are worth the additional mass of a post-injected fuel system.

Under the assumption of equal amounts of propellant constituents (i.e. mass of both stay the same), we can derive an optimum linear function for the O/F ratio throughout the course of the burn that will maximize the ΔV gain. This means changing the O/F ratio from a set value to one which changes over time. As a preliminary example, consider a single tank of HAN with 10% methanol by weight added. This is documented as the higher end of the miscibility allowed for the mixture, though values upwards of 15% have been reported. The corresponding O/F ratio for this combination would be O/F = 9. Note: the optimum mixture ratio is approximately 19% methanol by weight (O/F=4.26), which corresponds to a c* of 4,837 ft/sec. A function with good accuracy that represents this O/F vs c* is $c^* = 6{,}228*(O/F)^{-0.17}$, in units of ft/sec. Both of these cases are displayed as constant O/F cases as a function of normalized c^*/c^*_{max} in Figure 55.

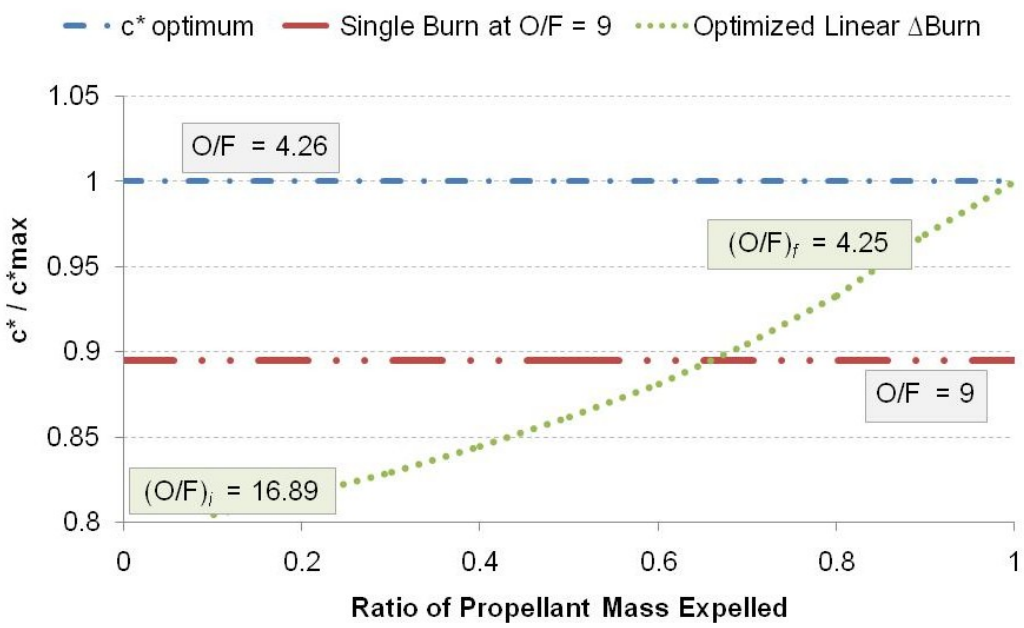

Figure 55: Normalized characteristic velocity versus propellant mass expelled for three cases of propellant expenditure methods.

Next we assume an appropriate range from O/F=4.25 (20% methanol by weight) to O/F=20 (just less than 5% by weight). A mass fraction of 0.2 is used and a thrust coefficient of 1.8 is selected which is appropriate for a space mission nozzle. As shown, there is an optimum linear range of O/F change that will maximize ΔV over the constant O/F case without any change to the propellant tank volumes. To do this, a generalized reduced gradient nonlinear optimization code is used in Microsoft Excel (or other suitable code) to vary the initial and final O/F whilst maintaining the same propellant masses. For this case, the initial and final O/F ratios turn out to be 16.89 and 4.25, respectively. This leads to an increase in ΔV of 2.462% over the baseline ΔV! Note that in Figure

55 the c* is not linear. Again, this is a function of the fact that O/F is being modified which has a nonlinear effect on c*.

It is shown in Reference 83 that a linear change in O/F is suitable, though the real optimum exists as an exponential function of specific impulse. However, to maintain the same propellant tank volumes and thrust, it is more prudent in this case to modify the O/F ratio.

This same exercise is expanded to include additional mass ratios (MR = 0.1, 0.2, & 0.3) as a function of their respective single burn O/F equivalences. Figure 56, in other words, shows the percent increase in ΔV attainable for any constant O/F HAN/Methanol system if they are instead designed to expend their propellant (fuel + oxidizer) in a linear O/F method. An interesting result to note from the embedded table in Figure 56 is that the optimized start and finish O/F ratio are the same for this propellant combination regardless of the mass fraction.

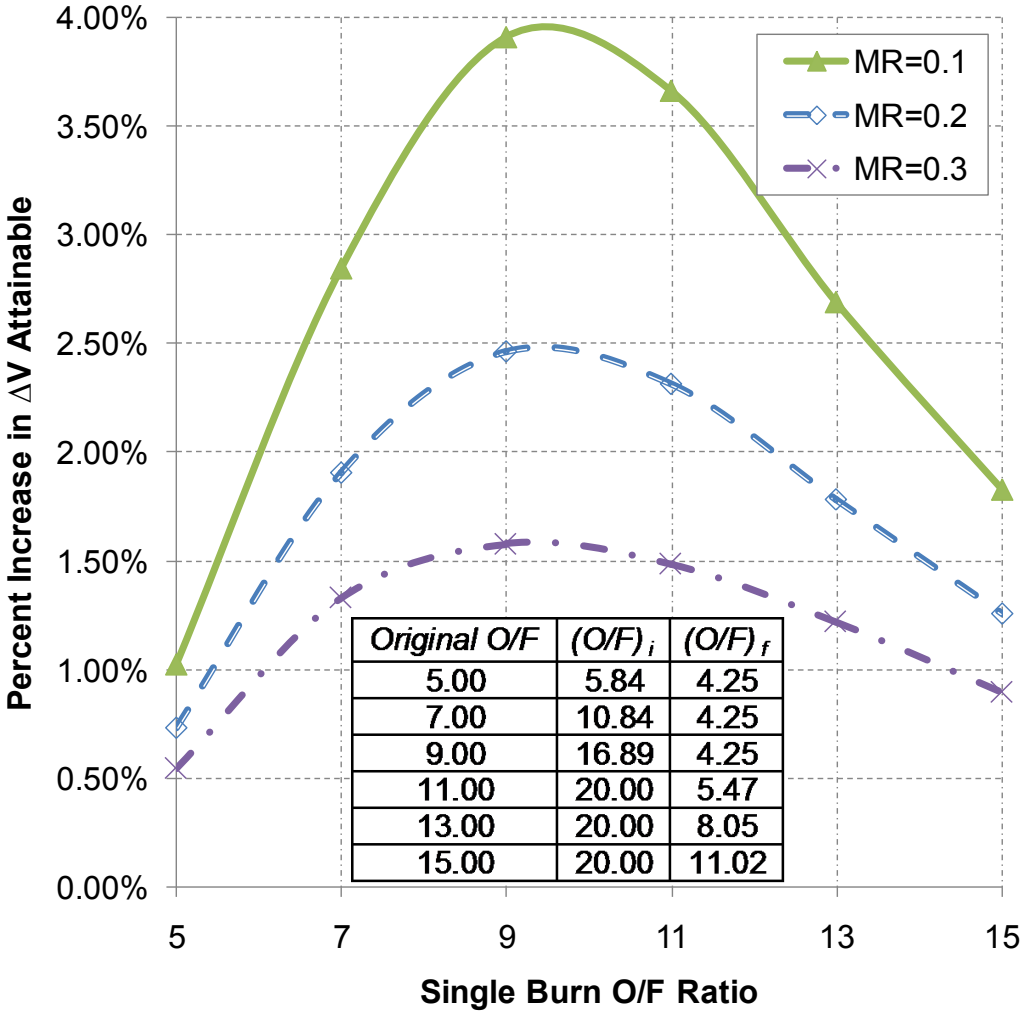

Figure 56: Percentage of increase of ΔV attainable for each O/F ratio vehicle with different Mass Ratios. Inset Table: Optimized initial and final O/F ratios to attain ΔV increase.

The final results from this exercise are very promising. Compared to cases with LOX/LH2, which represents the highest Isp liquid system in use, the HAN/Methanol with linear changing O/F has a drastically higher attainable ΔV gain. Upwards of 4% gains are noted for the lower mass fractions, whereas the LOX/LH2 system peaks at less than 2%. Again, an

optimized exponential function for ΔIsp exists, but the increases over the linear O/F method are marginal. Maintaining O/F also maintains thrust and total propellant percentages (thusly mass and volume), so existing liquid engine systems could be modified with no change to vehicle propellant tank structure. These ΔV gains must be tempered with that fact that additional mass would have to be allocated for the valves and control systems to drive changes to the O/F throughout the flight. However, using the ideal rocket equation, it is easy to show the gains in ΔV more than make up for this additional mass. Using a 4km/sec mission as an example, the mass ratio increase assuming a 4% increase in ΔV would be 6.5%. Larger ΔV missions amplify this MR increase further; 8km/sec yields an additional +12.6% ΔMR.

This section concludes with the statement that HAN, or other high density green propellants, are particularly well suited to the needs of ORS. The high density specific impulse propellants not only lower overall system support mass, but offer start/stop/restart capability plus throttleability. The latter is particularly noteworthy as it has been shown that post injection of methanol through a number of means could increase specific impulse significantly. Coupled with the time dependant linear O/F injection scheme described above, this propellant combination shows significant promise to reduce life cycle costs and increase total payload capacity over other conventional monopropellants.

8. Conclusions

"It is difficult to say what is impossible, for the dream of yesterday is the hope of today and the reality of tomorrow."

-Robert Goddard (1882-1945),

Physicist & Pioneer Rocket Engineer

The present work has explored a new design philosophy for a novel breed of affordable space launch vehicle capable of lofting small-satellites to orbit. The underlying premise focuses on the use of slightly refurbished demilitarized surplus tactical solid rocket motors. Such assets would be ideal for operationally responsive space missions whilst reducing overall system complexity, cost and operational risk over other conventional solutions. Concurrently, a parametric cost-mass-performance response surface methodology is used as an optimization tool to minimize life cycle costs of the proposed vehicle. Lastly, a new monopropellant, ideally suited to this design for a number of factors, was evaluated and test fired with good results.

The dissertation composes the following insights and general guidelines for the design of an operationally responsive vehicle:

(1) An extensive literature review reveals a great need for the successful development and introduction of a space vehicle that displays operational flexibility to achieve a range of orbits with very short notice. No such capability exists at the current time.

USSTRATCOM has mandated the following three essential desires:

- to rapidly exploit and infuse space technological or operational innovations,
- to rapidly adapt or augment existing space capabilities when needed to expand operational capability and
- to rapidly reconstitute or replenish critical space capabilities to preserve operational capability.[3]

Moreover it was discovered that the recent emergence of small satellites, driven by the high cost per pound to LEO, obviates the need for an affordable space launch vehicle platform for military or commercial satellites.

(2) Demilitarized surplus solid rocket motors, specifically Mk70 boosters and Mk30 sustainers, exist in great quantities. Such motors can be configured and used to meet the above stated ORS requirements. The choice in tactical motor selection differs sharply from the current launch vehicle market as tactical motors are:

- Produced in mass quantities for volume of purchase at low cost with superb quality control,
- engineered for long shelf-lives with no servicing required,
- make use of solid rocket motors which do not require fueling prior to launch,

- can be launched from existing military platforms around the world,
- are designed to be ready to launch within minutes of need,
- are readily available at little to no cost from the U.S. military surplus,
- require only minimal extra support equipment and services,
- can be easily shipped and stored,
- are very easily serviceable and augmented, and
- can be arranged to meet the requirements of different mission profiles.

(3) Use of a custom trajectory code explored the interdependence of the many variables required to arrive at a launch vehicle capable of delivering appreciable payload masses to orbit. This high fidelity modeling program incorporated modules for calculation of drag, gravity, time-dependant mass changes to the vehicle during propulsive boost, and the rotational effects of Earth. This program numerically integrates the equations of motions, which do not have a closed-form solution. This 3DOF program revealed required refurbishments for the proposed solid rocket motors, specifically for the nozzles, to reduce the high velocities, g-loading and dynamic pressures seen during boost through the lower atmosphere. The code also illustrated the need for an efficient final stage to deliver the large final amount of Δv required to attain orbit.

(4) A cost-mass-performance analysis shows that higher performance or reduced weight at any cost should not be the sole consideration for the design of an operationally responsive vehicle, as is the case with conventional launch vehicles. Cost estimating relationships are calculated for total life cycle costs including Design Development Testing and Evaluation, Theoretical First Unit and Operation & Maintenance costs. Coupled with parametric equations for weight and performance, a response surface methodology displays the interaction effects on the complicated response behavior modeled by responsive surface equations. This acts as an optimization tool which lends insight into the preliminary design of the upperstage portion of responsive space vehicles.

(5) Finally, it was shown that a suitable replacement for hydrazine as an upperstage monopropellant is desirable to meet the stringent requirements of ORS. The non-toxic research-propellant hydroxylammonium nitrate (HAN) was chosen as the most promising candidate for its high density specific impulse which was found to lower overall system support mass. Matched with the simple operation, throttleability and start/stop/restart capability this propellant shows significant promise to reduce life cycle costs and increase total payload capacity over other conventional monopropellants. This

dissertation concludes with the design and testing of this novel breed of monopropellant. Demonstrative testing showed positive ignition with a proprietary catalytic mixture and subsequent pulse thrust operation with a high platinum content substrate. The test motor, HAN Solo v.1, represents the highest known thrust HAN monopropellant motor tested to date. It is recommended that future research into HAN motors concentrate on efficient injection schemes at low mass flow rates and low pressures, and HAN/methanol blends be more thoroughly investigated as a way to further increase specific impulse. Such an engine would complete the design for a new rocket capable of meeting ORS constraints to provide responsive and accessible access to low Earth orbit at markedly reduced costs.

9. References

1. U.S. Congress Office of Technology Assessment. *Big Dumb Boosters: A Low-Cost Space Transportation Option?* NTIS #PB89-155196. Feb. 1989.

2. Air Force, *The Aerospace Force: Defending America in the 21st Century*. White paper, 2001.

3. AFSPC (Air Force Space Command). 2001. *FINAL Mission Needs Statement* AFSPC 001-01, Operationally Responsive Spacelift, ACAT Level I. Colorado Springs, Colo.: AFSPC.

4. U.S. Department of Defense. *Plan for Operationally Responsive Space*. April 2007.

5. Dunningan, J.F., *How to Make War, 3rd Edition*. William Morrow and Company, Inc. 1993.

6. Levine, Adam. *In Today's Space Race, Watch Out for China*. CNN article, November 11th, 2009. Accessed Nov. 20th, 2009. [http://www.cnn.com/2009/TECH/space/11/18/china.space]

7. Butler, Amy. *ORS-1 on Track for 2010 Launch*. Aviation Week. Dec. 8th 2009.

8. Hambling, David. *Grunts Get Spy Sats of Their Own*. Wired.com, December 1st 2009. Accessed Dec. 2nd 2009. [http://www.wired.com/dangerroom/2009/12/grunts-get-spy-sats-of-their-own/]

9. Barbosa, Rui. *China Completes 2009 Schedule by Launching another Spy Satellite*. NASA Space Flight, Dec. 15th, 2009. Accessed Dec. 16th, 2009: [http://www.nsaspaceflight.com/2009/12/china-completes-2009-schedule-by-launching-another-spy-satellite/]

10. Ziraksaz, Mohammad. *Combining the Cruise and Pegasus Missiles for Spy Micro-Satellite Launch, Part I*. AIAA2003-5117. 39th AIAA Joint Propulsion Conference, 2003.

11. Smith, Cristin. *Leveraging COTS Hardware for Rapid Design and Development of Small Satellites at the USAF Academy*. RS2-2004-5004. AIAA 2nd Responsive Space Conference, 2003.

12. Hambling, David. *The Big Promise of Small Satellites*. Wired.com, July 2nd 2009. Accessed Dec. 2nd 2009.

[http://www.wired.co.uk/news/archive/2009-07/03/the-big-promise-of-small-satellites-.aspx]

13. Klamper, Amy. *Orbital Wins DARPA Contract for Spacecraft Clusters*. Space News. 12/18/2009.

14. Carpenter, et al. *Technology Development for Future Sparse Aperture Telescopes and Interferometers in Space*. A Technology Whitepaper submitted to the 2010 Decadal Survey. March 24th, 2009.

15. International Space Business Council. *2005 State of the Space Industry*. August, 2005.

16. Commercial Space Transportation Quarterly Launch Report. Special Report: *U.S. & International Small Launch Vehicles*. United States Department of Transportation, Federal Aviation Administration, 1998.

17. Kesner, Kenneth. *Company Tests Rocket Engine that may Launch Affordable Access to Orbit for Small Satellites*. Accessed Dec. 23rd, 2009. [http://blog.al.com/breaking/2009/12/new.html]

18. The White House, Office of the Press Secretary. *The President's Space Policy and Commercial Space Initiative to Begin the Next Century*. Fact Sheet, Feb. 11, 1988.

19. Baker, David. *The History and Development of Rocket and Missile Technology.* New Cavendish Books, Sept. 7, 1978.

20. Westlake, Michael. *Southeast Asia Reaches Toward Space*. Aerospace America, Oct. 2009.

21. Orbital Sciences. *GQM-163A Coyote Supersonic Sea Skimming Target Fact Sheet*. 2009. [http://www.orbital.com/NewsInfo/Publications/Coyote_Fact.pdf]

22. Fleming, Hurdle, Maikis, Naumann,, Shanholtz, Tappe, Tse and Waltz. *Industry Challenges for the Next Generation Tactical Missile Propulsion System*. AIAA Joint Propulsion Conference 2009 Panel. Denver, CO.

23. Personal Communications with Richard Loehr, Principle Propulsion Engineer, Raytheon Missile Systems.

24. Wertz, James R. and Conger, Robert. *Responsive Launch with the Scorpius Family of Low-Cost Expendable Launch Vehicles*. 1st Responsive Space Conference. Redondo Beach, CA. 2003.

25. Hammond, Walter. *Design Methodologies for Space Transportation Systems*. AIAA Education Series. 2001.

26. U.S. Congress Office of Technology Assessment. *Reducing Launch Operations Costs: New Technologies and Practices,* OTA-TM-ISC-28, U.S. Government Printing Office, Washington, DC, Feb. 1989.

27. Bombelli, Vittorio, et al. *Economic Benefits of the use of Non-toxic Mono-propellants for Spacecraft Applications*. AIAA 2003-4783. Proceedings of the AIAA Joint Propulsion Conference., 2003.

28. Humble, R., Henry, G. and Larson W., *Space Propulsion Analysis and Design*. McGraw-Hill, 1995.

29. Stiennon, P. and Hoerr, D. *The Rocket Company*. American Institute of Aeronautics and Astronautics. 2005.

30. Hill, Philip and Peterson, Carl., *Mechanics and Thermodynamics of Propulsion, 2nd Edition*. Addison-Wesley Publishing. 1992.

31. Tewari, Ashish. *Atmospheric and Space Flight Dynamics*, Modeling and Simulation with MATLAB® and Simulink®. Birkhauser Boston, 2007.

32. Wertz, J.R., and Larson, W.J. *Space Mission Analysis and Design, Third Edition*. Microcosm Press and Kluwer Academic Publishers. 1999.

33. Hammond, Walter. *Design Methodologies for Space Transportation Systems*. AIAA Education Series, 2001.

34. Fleeman, Eugene. *Tactical Missile Design, Second Edition.* American Institute of Aeronautics and Astronautics Education Series. 2006.

35. Nielsen, J. *Missile Aerodynamics*. McGraw-Hill, 1960.

36. Newell, Homer. *Sounding Rockets*. McGraw-Hill Book Company, Inc. 1959.

37. Committee on Extension to the Standard Atmosphere (COESA): *U.S. Standard Atmosphere 1976*. U.S. Government Printing Office, Washington D.C. 1976.

38. COESA: *U.S. Standard Atmosphere 1962*. U.S. Government Printing Office, Washington, D.C. 1962

39. Wie, Bong. *Space Vehicle Dynamics and Control*. AIAA Education Series, 1998.

40. MacKay, John and Weber, Richard. *Performance Charts for Multistage Rocket Boosters*. NASA Lewis Research Center, Technical Note D-582.

41. Nau, Evan. *The U.S. Navy's Standard Missile, Scale Data.* T minus 5, Vol. 5 #4.

42. Maurer, Andrew and Mavris, Dimitri. *Integrating an Advanced Missile Defense Interceptor with the Navy Vertical Launch System*. AIAA Unclassified, 2006.

43. O'Rourke, Ronald. *Navy Aegis Ballistic Missile Defense (BMD) Program: Background and Issues for Congress*. CRS Report for Congress. April, 2011.

44. Kaiser, M., Cruddace, R., Bock, J., and Kowalski, M. *Report of the SRWG Sub-committee on High Altitude Rockets to Increase Astrophysics and Solar Observing Time*. October, 2009.

45. Bills, K.W., DePree, D.O., McCamey. R.K., and Smith, R.M. *The Chemical Kinetic Approach to Service Life Prediction of Propellant Systems*. AIAA Joint Propulsion Conference. AIAA-1979-1243.

46. Christiansen, A.G., Layton, L.H., and Carpenter, R.L. *HTPB Propellant Aging*. AIAA Journal of Spacecraft and Rocketry. AIAA 80-1273R Vol. 18, No. 3. 1981.

47. Brouwer, G.H., Keizers, H., and Buswell, J. *Aging in Composite Propellant Grains.* AIAA Joint Propulsion Conference. AIAA 2004-4058.

48. Miller, M., Fortner, J., Buswell, J., Chelner, H., and Lossner, M. *Health Monitoring for Munitions for Mission Readiness*. 43rd AIAA Joint Propulsion Conference. AIAA 2007-5789.

49. Hyde, Scott. *A Solid Rocket Motor Manufacturer's View of Sensors and Aging Surveillance*. AIAA-2001-3285.

50. Chelner, H., Buswell, J., Evans, J. *Embedded Sensors for Monitoring Solid Propellant Grains*. AIAA Joint Propulsion Conference. AIAA 2005-4362.

51. Brouwer, G., Pfiffer, A., Bancallari, L. *Development and Deployment of Diagnostic Prognostic Tactical Solid Rocket Motor Demonstrator*. AIAA Joint Propulsion Conference. AIAA 2011-5957.

52. Goodman, B., and Villarreal, J. *Solid Rocket Propellant Characterization through Crawfod Strand Burner Regression Rate Testing*. AIAA International Astronautics Congress, South Korea, 2009.

53. Dennis, J., Shark, S., and Villarreal, J. *Experimental Investigation and Analysis of the Sol-Brid Tactical Rocket Motor Concept*. AIAA 46th Joint Propulsion Conference. AIAA 2010-6783.

54. Shark, S., Dennis, J., and Villarreal, J. *Experimental Performance Analysis of a Toroidal Aerospike Nozzle Integrated with a Hybrid Rocket Motor*. AIAA 46th Joint Propulsion Conference. AIAA 2010-6784.

55. Villeneuve, Frederic. *A Method for Concept and Technology Exploration of Aerospace Architectures*. Georgia Institute of Technology Dissertation, 2007.

56. Robinson, John. *Controlling Launch Vehicle Life-Cycle Costs*. Aerospace America, October 2010. Pg 40 to 43.

57. Rorhschneider, R. *Development of a Mass Estimating Relationship Database for Launch Vehicle Conceptual Design*. Georgia Tech Report, 2002.

58. Montgomery, D. *Design and Analysis of Experiments*, 7th Edition. John Wiley & Sons, Inc. 2009.

59. Fleming, E., Lafleur, J., and Saleh, J. *Response Surface Equations for Expendable Launch Vehicle Payload Capability*. AIAA Space Conference 2009. AIAA2009-6656.

60. Schneider, S. *On-Board Propulsion System Analysis of High Density Propellants*. NASA/TM-1998-208811

61. Wernimont, E., *System Trade Parameter Comparison of Monopropellants: Hydrogen Peroxide vs Hydrazine and Others.* 42nd AIAA Joint Propulsion Conference. AIAA-2006-5235.

62. Ventura M. and Garboden, G., *A Brief History of Concentrated Hydrogen Peroxide Uses*, 35th AIAA Joint Propulsion Conference, AIAA Paper 99-279

63. Wucherer, E. et al, *Hydrazine Catalyst Production-Sustaining S-405 Technology*. 39th AIAA Joint Propulsion Conference, AIAA Ppaer 03-5079

64. Torre, et al., *Performance of a Monopropellant Thruster Prototype Using Advanced Hydrogen Peroxide Catalytic Beds*. Journal of Propulsion and Power. Vol. 25, No. 6 Nov-Dec 2009

65. Joyner, et al. *Propulsion System Choices and Their Implications*, 46th AIAA Joint Propulsion Conference, July 2010

66. Sutton, George and Biblarz, Oscar. *Rocket Propulsion Elements, 7th Edition*. John Wiley & Sons, Inc. 2001.

67. Morrison, W. *The Application of Liquid Propellant Gun Technology to Field Artillery*. ADB090195, 1985.

68.Katsumi, T., et al. *Combustion Characteristics of a Hydroxylammonium Nitrate Based Liquid Propellant: Combustion Mechanism and Application to Thrusters*. Combustion, Explosion and Shock Waves, Vol. 45, No. 4, pp 442-453, 2009

69. Zube, D., Wucherer, E. and Reed, B. "Evaluation of HAN-Based Propellant Blends" 39th AIAA Joint Propulsion Conference. AIAA2003-4643

70. Comer, R., *Ignition and combustion of liquid monopropellants at high pressures*. Proceedings of 16th International Symposium on Combustion, 1976. Pgs. 1211-1219

71. Lee, T.W., et al. *Analysis of Combusting High-Pressure Monopropellant Sprays,* Combustion Science and Technology, Volume 57, Issue 4 - 6 February 1988 , pages 95 – 112

72. Kondrikov, B.N., et al. *Burning of Hydoxlammonium Nitrate*. Combustion, Explosion, and Shock Waves, Vol. 36, No. 1, 2000.

73. Kounalakis, M.E. and Faeth, G.M. *Combustion of HAN-based Liquid Monopropellants near the Thermodynamic Critical Point*. Combustion Flame, Vol. 74, Nov.1988, page 179-192

74. Lee, T.W., et al. *Separated-Flow Considerations for Pressure-Atomized Combusting Monopropellant Sprays*. AIAA 1990-0463

75. Hisatsune, K. *Development of HAN-Based Liquid Propellant Thruster*. Proceedings of 2nd International Conference on Green Propellants for Space Propulsion. Italy, 2004

76. Huzel, D. and Huang, D. *Modern Engineering for Design of Liquid-Propellant Rocket Engines*. Progress in Astronautics and Aeronautics, Volume 147, 1992.

77. Torre, et al. *Performance of a Monopropellant Thruster Prototype Using Advanced Hydrogen Peroxide Catalytic Beds*. Journal of Propulsion and Power. Vol. 25, No. 6 Nov-Dec 2009.

78. Katsumi, et al. *Combustion Wave Structure of Hydroxlyammonium Nitrate Aqueous Solution*. 46th AIAA Joint Propulsion Conference. AIAA2010-6900.

79. Bui, et al. *Flight Research of an Aerospike Nozzle Using High Power Solid Rockets*. Proceedings of the 41st AIAA JPC Conference. AIAA-2005-3797.

80. Wertz, J. *Spacecraft Attitude Determination and Control*. Kluwer Academic Publishers. 1978.

81. Leitmann, G. *Propulsive Efficiency of Rockets: Optimization Techniques with Applications to Aerospace Systems*. Academic Press, New York. 1962.

82. Langhenry, M.T., and Parks, J.M. *Reconstruction of Flight Specific Impulse for Solid Propellant Rocket Motors*. AIAA Joint Propulsion Conference, 1991. AIAA-91-2428.

83. Langhenry, M.T., and Villarreal, J.K. *A Review and Discussion of Rocket Vehicle Propulsion Efficiency*. Proceedings of AIAA 2012 Aerospace Sciences Meeting, Pending. Session 218-SEC-3.

APPENDIX A

SHOP DRAWINGS OF HAN-SOLO V.1

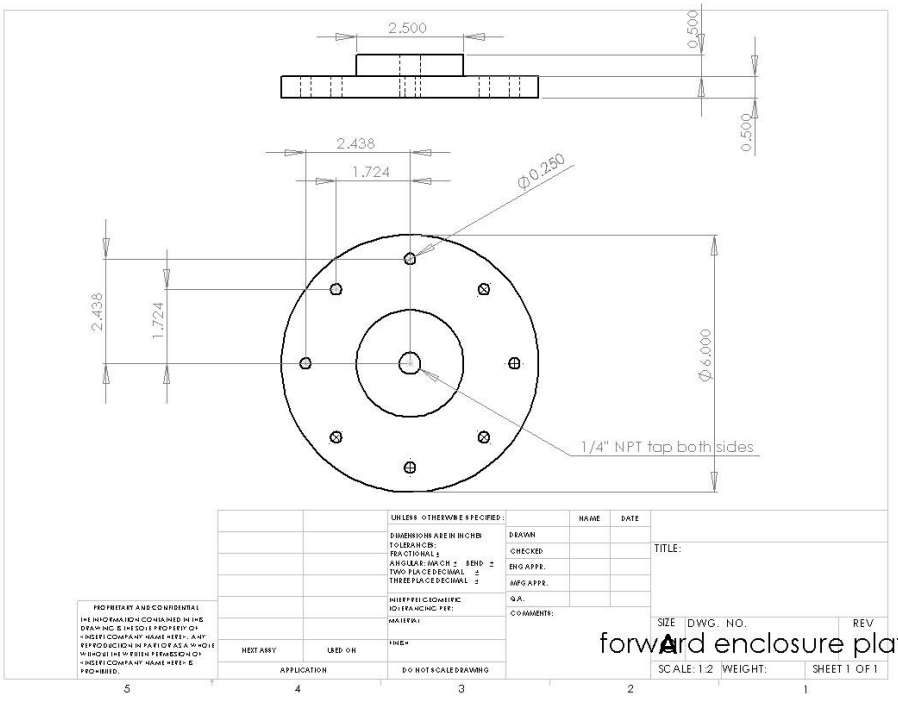

forward enclosure plate

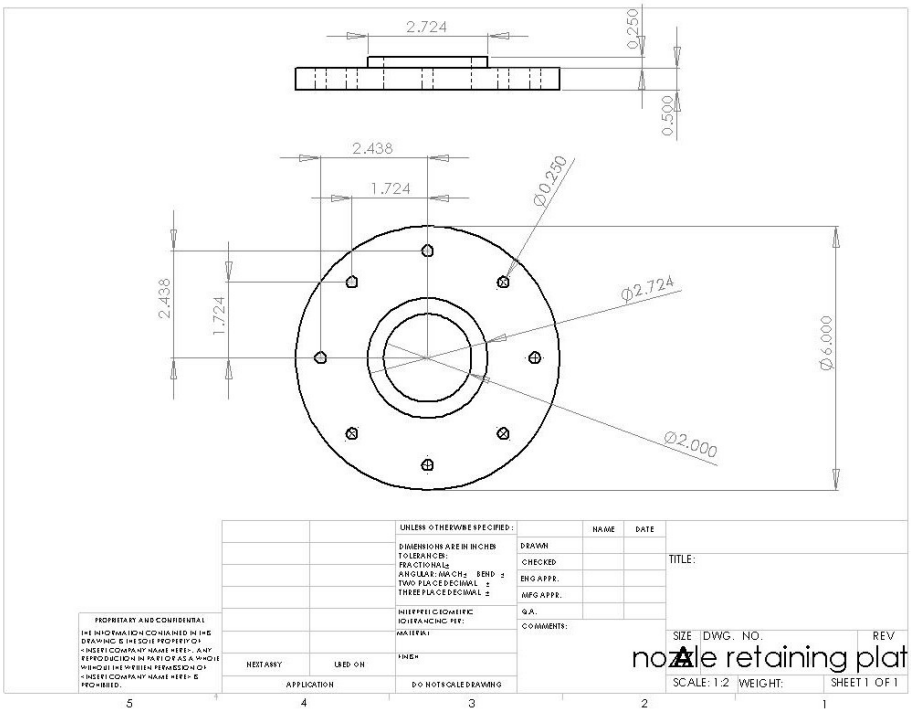

nozzle retaining plate

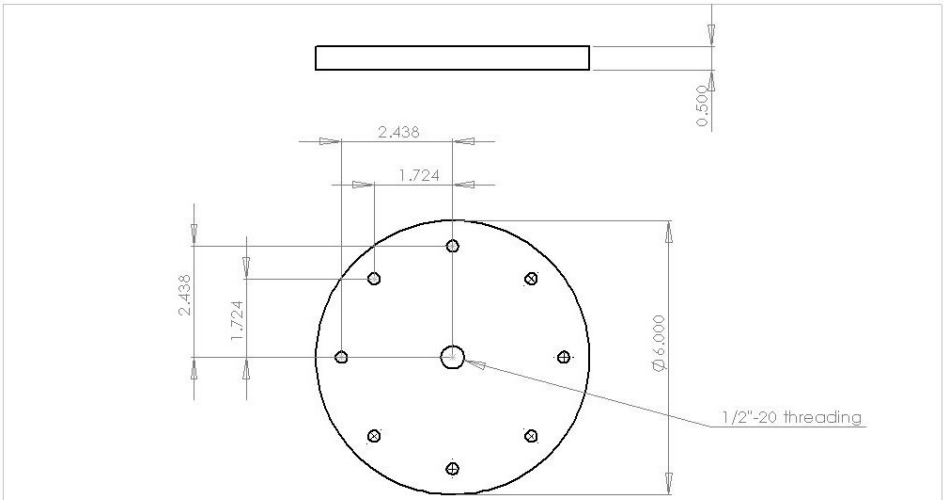

		UNLESS OTHERWISE SPECIFIED:		NAME	DATE
		DIMENSIONS ARE IN INCHES TOLERANCES: FRACTIONAL ± ANGULAR: MACH ± BEND ± TWO PLACE DECIMAL ± THREE PLACE DECIMAL ±	DRAWN		
			CHECKED		
			ENG APPR.		
			MFG APPR.		
		INTERPRET GEOMETRIC TOLERANCING PER:	Q.A.		
		MATERIAL	COMMENTS:		
NEXT ASSY	USED ON	FINISH			
APPLICATION		DO NOT SCALE DRAWING			

PROPRIETARY AND CONFIDENTIAL
THE INFORMATION CONTAINED IN THIS DRAWING IS THE SOLE PROPERTY OF <INSERT COMPANY NAME HERE>. ANY REPRODUCTION IN PART OR AS A WHOLE WITHOUT THE WRITTEN PERMISSION OF <INSERT COMPANY NAME HERE> IS PROHIBITED.

TITLE:

SIZE	DWG. NO.	REV
A	load cell plate	
SCALE: 1:2	WEIGHT:	SHEET 1 OF 1

5 4 3 2 1

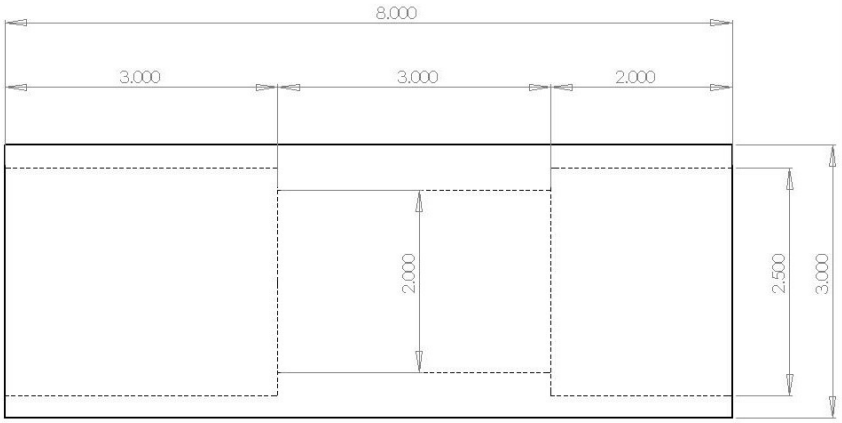

		UNLESS OTHERWISE SPECIFIED:		NAME	DATE
		DIMENSIONS ARE IN INCHES TOLERANCES: FRACTIONAL ± ANGULAR: MACH ± BEND ± TWO PLACE DECIMAL ± THREE PLACE DECIMAL ±	DRAWN		
			CHECKED		
			ENG APPR.		
			MFG APPR.		
		INTERPRET GEOMETRIC TOLERANCING PER:	Q.A.		
		MATERIAL	COMMENTS:		
NEXT ASSY	USED ON	FINISH			
APPLICATION		DO NOT SCALE DRAWING			

PROPRIETARY AND CONFIDENTIAL
THE INFORMATION CONTAINED IN THIS DRAWING IS THE SOLE PROPERTY OF <INSERT COMPANY NAME HERE>. ANY REPRODUCTION IN PART OR AS A WHOLE WITHOUT THE WRITTEN PERMISSION OF <INSERT COMPANY NAME HERE> IS PROHIBITED.

TITLE:

SIZE	DWG. NO.	REV
A	combustion chamber	
SCALE: 1:5	WEIGHT:	SHEET 1 OF 1

5 4 3 2 1

APPENDIX B

MATLAB 3DOF CODE

Runrocket.m

```
% made by james, 2009;

global grav_control;    grav_control = 1;                       %turn gravity on=1, off=0
global drag_control;    drag_control = 1;                       %turn drag on=1, off=0

global dtr;     dtr=pi/180;
global mu;      mu=3.986e14; %m3/s2
global omega;   omega=2*pi/(23*3600+56*60+4.0905);
global S1;      S1=pi*(0.23)^2;                                 %frontal surface area of a
Mk70
global S2;      S2=pi*(0.175)^2;                                %frontal surface area of a
Mk30
global c;       c=0.1;                                          %any number can be used;
necessary to run Tewari atmosphere model
global rm;      rm=6378140;                                     %radius of Earth [meters]
global Gamma;   Gamma= 1.4;                                     %ratio of specific heats for
air

%*****************************************************************
%               Stage 4 Variables
%           custom liquid rocket motor
%*****************************************************************

m_o_4 = 250;                %initial mass [kg]                 m_o_4 = 10; 20
m_f_4 = 249;                %final mass [kg]                   m_f_4 = 3.64; 10
Isp_4 = 285;                %specific impulse [sec]
t_b_4 = 60;                 %burn time [sec]

m_p_4 = m_o_4 - m_f_4;          %propellant mass [kg]
mdot_4 = m_p_4 / t_b_4;         %propellant mass flow rate [kg/sec]
f_4 = mdot_4*Isp_4*9.807;       %thrust [N]; assume ideal expansion

%*****************************************************************
%               Stage 3 Variables
%                 1 x Mk-30
%*****************************************************************

m_o_3 = 372.73;             %initial mass [kg]
m_f_3 = 77.27;              %final mass [kg]
Isp_3 = 270;                %specific impulse [sec]
t_b_3 = 32;                 %burn time [sec]

m_p_3 = m_o_3 - m_f_3;          %propellant mass [kg]
mdot_3 = m_p_3 / t_b_3;         %propellant mass flow rate [kg/sec]
f_3 = mdot_3*Isp_3*9.807;       %thrust [N]; assume ideal expansion

%*****************************************************************
%               Stage 2 Variables
%                 1 x Mk-30
%*****************************************************************
```

```
m_o_2 = 372.73;                 %initial mass [kg]
m_f_2 = 77.27;                  %final mass [kg]
Isp_2 = 270;                    %specific impulse [sec]
t_b_2 = 32;                     %burn time [sec]

m_p_2 = m_o_2 - m_f_2;          %propellant mass [kg]
mdot_2 = m_p_2 / t_b_2;         %propellant mass flow rate [kg/sec]
f_2 = mdot_2*Isp_2*9.807;       %thrust [N]; assume ideal expansion

%*****************************************************************
%                Stage 1 Variables
%                   1 x Mk-70
%*****************************************************************

m_o_1 = 990.91;                 %initial mass [kg]
m_f_1 = 172.72;                 %final mass [kg]
Isp_1 = 270;                    %specific impulse [sec]
t_b_1 = 15;                     %burn time [sec]

m_p_1 = m_o_1 - m_f_1;          %propellant mass [kg]
mdot_1 = m_p_1 / t_b_1;         %propellant mass flow rate [kg/sec]
f_1 = mdot_1*Isp_1*9.807;       %thrust [N]; assume ideal expansion

%*****************************************************************
%                Stage 0 Variables
%                   2 x Mk-70
%*****************************************************************
m_o_0 = 1909.10;                %initial mass [kg]
m_f_0 = 272.72;                 %final mass [kg]
Isp_0 = 270;                    %specific impulse [sec]
t_b_0 = 15;                     %burn time [sec]

m_p_0 = m_o_0 - m_f_0;          %propellant mass [kg]
mdot_0 = m_p_0 / t_b_0;         %propellant mass flow rate [kg/sec]
f_0 = mdot_0*Isp_0*9.807;       %thrust [N]; assume ideal expansion

global tb0;    tb0= t_b_0;
global tb1;    tb1= t_b_1;
global tb2;    tb2= t_b_2;
global tb3;    tb3= t_b_3;
global tb4;    tb4= t_b_4;

global fT0;    fT0= f_0;
global fT1;    fT1= f_1;
global fT2;    fT2= f_2;
global fT3;    fT3= f_3;
global fT4;    fT4= f_4;

global m00;    m00= m_o_0;
global m01;    m01= m_o_1;
global m02;    m02= m_o_2;
global m03;    m03= m_o_3;
```

```
global m04;     m04= m_o_4;

global mp0;     mp0= m_p_0;
global mp1;     mp1= m_p_1;
global mp2;     mp2= m_p_2;
global mp3;     mp3= m_p_3;
global mp4;     mp4= m_p_4;

global mL;      mL= m04-mp4;        %completely empty mass of stage 4

global f8;      f8=fopen('data.mat','a');

%-------------------------------------------------------------%           Initial flight parameters
(location, angles, etc.)
%-------------------------------------------------------------

long = -106.957397*dtr;
lat = 33.060241*dtr;
rad = rm;
vel = 0;
fpa = 35*dtr;
chi = 90*dtr;      %launch azimuth velocity, ~170 for due East?

%spaceport america: Coordinates ?33.060241°N  106.957397°W
%cape: long = -80.55*dtr;         lat = 28.5*dtr;

init = [long; lat; rad; vel; fpa; chi];

[t, o] = ode113('rocket',[0 350], init);% was using ode23, 45doesn't work well; 113 is good!
fclose('all');
```

Rocket.m

```
% "rocket.m" determines state space values
% Some callout functions and motions of equation
% based off of examples from Tewari
function deriv = rocket(t,o)

%DEFINE GLOBAL VARIABLES TO BE USED IN PROGRAM
global grav_control; global drag_control;
global dtr; global mu; global omega; global S1; global S2; global c;
global rm; global Gamma; global tb0; global tb1; global tb2; global tb3;
global tb4; global fT0; global fT1; global fT2; global fT3; global fT4;
global m00; global m01; global m02; global m03; global m04;
global mp0; global mp1; global mp2; global mp3; global mp4;
global mL; global f8;

%OPEN AND SET VARIABLES TO BE USED IN PROGRAM

if grav_control==1                                          %turn gravity on with
grav_control=1; gravity=0 otherwise
      [g,gn]=gravity(o(3),o(2));                            %gravity of oblate Earth at
current altitude and longitude
   else
      g=0;
      gn=0;
end

lo = o(1);la = o(2);                                        %call out for latitude and longitude
clo = cos(lo); slo = sin(lo); cla = cos(la); sla = sin(la);          %taking sine & cosines of
lat and long for ease of use later

fpa = o(5);                                                 %call out of flight path angle
chi = o(6);                                                 %call out for "A" - azimuth velocity
cfpa = cos(fpa); sfpa = sin(fpa); cchi = cos(chi); schi = sin(chi);      %taking sine &
cosines of FPA and A for ease of use later

   if o(3)<rm
      o(3)=rm;                                              %ensuring rocket height stays above
the ground!
   end

alt = o(3) - rm;                                            %altitude of rocket (location rel. to
center of Earth - radius of Earth)
v  = o(4);                                                  %call out velocity

   if v<0
      v=0;                                                  %ensuring rocket velocity stays positive
(magnitude of vel)
   end

%-------------------------------------------------------------
%            Atmosphere and Drag Calculations
```

```
%-------------------------------------------------------------

%CALL OUT PERTINENT VALUES BASED ON ALTITUDE OF ROCKET
if alt<=2000e3
   atmosp = atmosphere(alt,v,c);                          %multi-layer atmosphere
model by Tewari (c) 2006
   rho = atmosp(2);                                     %call out for density as a fn of
altitude
   Qinf = 0.5*rho*v^2;                                  %dynamic pressure Q_inf
   mach = atmosp(3);                                     %call out for Mach number

   CD = machtable(mach);                                  %call out drag coefficient
based on Mach number using "machtable.m"

   else
      rho=0;Qinf=0;CD=0;mach=0;                             %above 2,000km drag is
definately zero
end

%ASSIGNING THE VARIOUS FRONTAL SURFACE AREAS BASED ON STAGE #
if t<=tb0
      S = 3*S1;                                          %stage zero has three times the
surface area of a single Mk70
   elseif t<=(tb0+tb1)
      S = S1;                                           %stage one drops off 2 Mk70s,
leaving only one surface area
   else
      S = S2;                                           %all subsequent stages (2, 3, & 4)
have same smaller diameter
end

%FINAL DRAG CALCULATION

if drag_control==1                                       %turn drag on with
drag_control=1; drag=0 otherwise
      D=Qinf*S*CD;                                       %Drag calculation
   else
      D=0;
end

%-------------------------------------------------------------
%            Thrust and Mass Calculations of each Stage
%-------------------------------------------------------------

if t<=tb0
      fT = fT0;
      m = (m00+m01+m02+m03+m04) - mp0*t/tb0;

   elseif t<=(tb0+tb1)
      fT = fT1;
      m = (m01+m02+m03+m04) - mp1*t/(tb0+tb1);

   elseif t<=(tb0+tb1+tb2)
```

```
        fT = fT2;
        m = (m02+m03+m04) - mp2*t/(tb0+tb1+tb2);

    elseif t<=(tb0+tb1+tb2+tb3)
        fT = fT3;
        m = (m03+m04) - mp3*t/(tb0+tb1+tb2+tb3);

    elseif t<=(tb0+tb1+tb2+tb3+tb4)
        fT = fT4;
        m = (m04) - mp4*t/(tb0+tb1+tb2+tb3+tb4);

    else
        fT=0; m=mL;
end

[t alt m mach];

%-------------------------------------------------------------
%              Equations of Motion in relative frame
%-------------------------------------------------------------

Xfo = fT-D;                                          %assume force only in x-direction
Yfo = 0;  Zfo = 0;                                    %no force in y or z planes

longidot = o(4)*cfpa*schi/(o(3)*cla);
latidot =  o(4)*cfpa*cchi/o(3);
raddot = o(4)*sfpa;
veldot = -g*sfpa +gn*cchi*cfpa + Xfo/m + omega*omega*o(3)*cla*(sfpa*cla-cfpa*cchi*sla);
if t<=10;
    headdot=0; gammadot=0;
else
gammadot=(o(4)/o(3)-g/o(4))*cfpa-gn*cchi*sfpa/o(4)+Zfo/(o(4)*m)+
2*omega*schi*cla+omega*omega*o(3)*cla*(cfpa*cla+ sfpa*cchi*sla)/o(4);
    if abs(cfpa)>1e-6
    headdot=o(4)*schi*tan(o(2))*cfpa/o(3)-gn*schi/o(4)-Yfo/(o(4)*cfpa*m)-
2*omega*(tan(o(5))*cchi*cla - sla)+ omega*omega*o(3)*schi*sla*cla/(o(4)*cfpa);
    else
    headdot=0;
    end
end
deriv = [longidot; latidot; raddot; veldot; gammadot; headdot];

%CALCULATION OF INERTIAL VELOCITIES function in Plotty.m

 TtoW = fT/(m*g);        %thrust to weight ratio

if alt<=10000e3
    Qdot=Qinf*v*S*CD/20;
end

%printing to data.mat file for plotting and future calc purposes
```

```
fprintf(f8,'\t%1.5e\t%1.5e\t%1.5e\t%1.5e\t%1.5e\t%1.5e\t%1.5e\t%1.5e\t%1.5e\t%1.5e\t%
1.5e\t%1.5e\t%1.5e\n',...
        t,alt,m,v,veldot,lo,la,fpa,chi,TtoW,mach,fT,g);
```

atmosphere.m & gravity.n copyright Tewari, 2006 (see reference)

machtable.m

```
% "machtable.m" is a look-up table for a rocket drag coefficient
% based off of a reference Mach number.
%
% Values were tabulated from Wernher Von Braun's book:
% "The Mars Project", pg15 and is used in conjunction
% with the rockets frontal area in m^2.
%
% written by James Villarreal, 2009

function CD = machtable(mach)

mach_ref = [0; 0.8; 1; 1.4; 2; 3; 4; 5; 10; 99];

cd_ref = [0.40; 0.40; 0.80; 0.80; 0.69; 0.59; 0.57; 0.55; 0.55; 0.55];

CD = interp1(mach_ref, cd_ref, mach);
```

plotty.m

```
%plot function that calls out data.mat saved file
global mu;
global rm;
global omega;
close all;

dtr=pi/180;
%     t,alt,m,v,veldot,lo,la,fpa,chi,TtoW,mach,fT,g

load -ASCII data.mat

t = data(:,1);
alt = data(:,2);
m = data(:,3);

v = data(:,4);              %(relative)
vdot = data(:,5);           %(relative)
lo = data(:,6)*(1/dtr);     %(relative)
la = data(:,7)*(1/dtr);     %(relative)
phi = data(:,8)*(1/dtr);    %fpa or phi (relative)
A = data(:,9)*(1/dtr);      %chi or A (relative)

TtoW = data(:,10);
mach = data(:,11);
fT = data(:,12);
D = data(:,13);

LNGTH = length(data(:,1));

%-------------------------------------------------------------%             Converting relative to
inertial reference frame
%-------------------------------------------------------------blah = ((omega.*(alt+rm).*cos(la*dtr)) ./
(v.*cos(phi*dtr) ));
x=linspace(0,pi);

% plot(x,(1./cos(x)).*(sin(x)-blah(LNGTH)) - tan(A(LNGTH)*dtr))

FUN = @(x)(1./cos(x)).*(sin(x)-blah(LNGTH)) - tan(A(LNGTH)*dtr);    %defining function
for root finder method
Astar = fzero(FUN,A(LNGTH)*dtr)*(1/dtr)                          %root finder for A*_inertial
close to A_relative

%if Astar is HUGE then it has reached asymptotic solution. should instead
%be 90 degrees.

fpastar = abs( atan( tan(phi(LNGTH)*dtr)*( (cos(Astar*dtr))/(cos(A(LNGTH)*dtr)) ))*(1/dtr)
)  %FPA relative
velstar = v(LNGTH)*( (sin(phi(LNGTH)*dtr)) / (sin(fpastar*dtr)) )                    %V relative

%determining orbital parameters from last interial data points
```

```
lambda = (velstar^2) / (mu/(alt(LNGTH)+rm));                    %value equal to
twice the ratio of kinetic to potential energy
eccent = sqrt( ((lambda-1)^2)*(cos(fpastar*dtr)^2) + ((sin(fpastar*dtr)^2)) )
%eccentricity of orbit from last calculated positions

SpecE = ((velstar^2) / 2 ) - (mu/(alt(LNGTH)+rm));      %specific mechanical energy
a = -(mu/(2*SpecE));                                    %semimajor axis "a"
rp = a*(1-eccent);                                      %perigee distance "r_p"
inclin = acos( cos(la(LNGTH)*dtr)*sin(Astar*dtr)) * (1/dtr)

if rp>rm
   display('orbit does not intersect Earth')
else
   display('orbit is sounding rocket ... or ICBM')
end

if eccent>=1
   display('escape velocity!')
end

%---------------------------------------------------------------
%              Plotting!
%---------------------------------------------------------------

figure;
subplot(2,1,1)
plot(t,alt/1e3,'b-','LineWidth',2)
xlabel('Time [sec]')
ylabel('Altitude [km]')
axis([0 1000 0 3000])

subplot(2,1,2)
plot(t,v,'r-','LineWidth',2)
xlabel('Time [sec]')
ylabel('Relative Velocity [m/s]')
axis([0 1000 0 10000])

% figure;
% subplot(3,1,1)
% plot(t,alt/1e3,'b-','LineWidth',2)
% xlabel('Time [sec]')
% ylabel('Altitude [km]')
% axis([0 200 0 1500])
%
% subplot(3,1,2)
% plot(t,v,'r-','LineWidth',2)
% xlabel('Time [sec]')
% ylabel('Relative Velocity [m/s]')
% axis([0 200 0 15000])
%
% subplot(3,1,3)
% plot(t,m,'m--','LineWidth',2)
% xlabel('Time [sec]')
```

```
% ylabel('Mass [kg]')
% axis([0 200 0 4000])

% figure;
% plot(t,vdot)
% xlabel('time [sec]')
% ylabel('relative velocity dot [m/s]')
%
figure;
subplot(2,1,1)
plot(t,phi)
xlabel('time [sec]')
ylabel('Relative Flight Path Angle, FPA [deg]')
%
% subplot(2,1,2)
% plot(t,A)
% xlabel('time [sec]')
% ylabel('Relative Launch Azimuth Angle, A [deg]')
%
%
% % figure;
% % plot(t,eccent,'b-','LineWidth',2)
% % title('Eccentricity vs. Time')
% % xlabel('Time [sec]')
% % ylabel('Eccentricity')
% % axis([0 200 0 1.1])
% %
% figure;
% subplot(3,1,1)
% plot(t,Astar)
% xlabel('time [sec]')
% ylabel('astar [deg]')
%
% subplot(3,1,2)
% plot(t,fpastar)
% xlabel('time [sec]')
% ylabel('fpa star [deg]')
%
% subplot(3,1,3)
% plot(t,-velstar)
% xlabel('time [sec]')
% ylabel('vel star [m/s]')
% %
figure;
subplot(2,1,1)
plot(t,TtoW,'r-','LineWidth',2)
title('Thrust to Weight ratio vs Time')
xlabel('Time [sec]')
ylabel('Thrust to Weight ratio')
axis([0 200 0 30])

subplot(2,1,2)
plot(t,mach,'ks-','LineWidth',2)
title('Mach # vs. Time')
```

```
xlabel('Time [sec]')
ylabel('Mach #')
axis([0 200 0 30])
% %
% %
% figure;
% % subplot(2,1,1);
% plot3(lo,la,alt/1e3,'g-','LineWidth',2)
% title('Earth Relative Trajectory Trace')
% xlabel('Longitude')
% ylabel('Latitude')
% zlabel('Altitude [km]')
% % axis([-110 -105 30 35 0 10000])
% grid on

% subplot(2,1,2);
% plot(lo,la,'b--','LineWidth',2)
% xlabel('Longitude')
% ylabel('Latitude')
% axis([-110 -105 32 34])
% grid on
%
%
% figure;
% plot(t,fT,'ks-','LineWidth',2)
% title('Thrust  vs. Time')
% xlabel('Time [sec]')
% ylabel('Thrust')
% axis([0 200 0 300000])
%
% figure;
% plot(t,D,'ks-','LineWidth',2)
% title('Drag  vs. Time')
% xlabel('Time [sec]')
% ylabel('Drag #')
% axis([0 200 0 10])

% figure;
% plot(t,m,'m--','LineWidth',2)
% xlabel('Time [sec]')
% ylabel('Mass [kg]')
% axis([0 200 0 4000])


% YI = INTERP1(X,Y,XI)
```